The Regulatory Mechanisms of PIR-B and STARD7 in Inflammatory Bowel Disease

by

Jazib N. Uddin

A dissertation submitted in partial fulfillment
of the requirements for the degree of
Doctor of Philosophy
(Immunology)
in the University of Michigan
2022

Doctoral Committee:

Professor Simon P. Hogan, Chair
Professor Philip King
Professor Nicholas Lukacs
Professor Bethany Moore
Professor Charles Parkos

Jazib N. Uddin

jazib@umich.edu

ORCID iD: 0000-0001-5303-5213

DEDICATION

To my family for their unwavering support, my friends for their constant encouragement, and my colleagues for their continuous guidance. Your time and care have meant everything to me.

ACKNOWLEDGEMENTS

As I assembled this dissertation and reflected on my career to-date, I started to realize the impact that my mentor, Dr. Simon Hogan, has had on my life. I met Simon when I arrived in Cincinnati to pursue my master's degree. I was at a point in my life where I wasn't sure what I wanted to do next; Simon took me on in his lab and provided me with the resources and direction I needed, ultimately inspiring me to pursue this PhD. Since our first meeting, he has always gone above and beyond to help me become an independent scientist, emboldening me with the tools and autonomy I needed to confidently develop my own ideas. Simon's commitment to mentorship over the last six years has provided an invaluable foundation for me, which I know will serve me well going forward.

I have really enjoyed the comradery within the members of the Hogan Lab, who have all been extremely kind and generous with their time. Their commitment to assisting me as I attempted to learn new techniques or to develop new ideas was pivotal for all the work described within this dissertation. I want to give a special thank you to Sunil Tomar, Simone Vanoni, Varsha Ganesan, Lisa Waggoner, Ankit Sharma, Chang Zeng, Sahiti Marella, Amnah Yamani, Gila Idelman, Yanfen Yang, Andy Dang, and Taeko Noah. You all made coming to work such a pleasure and I cannot thank you enough for all your help and friendship.

I would like to also thank a few of the other mentors who I have had the opportunity to work with throughout my graduate career. To Drs. Philip King, Nicholas Lukacs, Bethany Moore, and Charles Parkos: Our meetings were incredibly valuable and provided me with

constructive feedback that greatly improved both my writing and oral presentations. I would like to especially thank the committee for their assistance with developing the mechanistic studies described in Chapter 2. And to Drs. Kasper Hoebe, Senad Divanovic, and Ariel Munitz: your input was indispensable early on for trying to understand the new direction of the project, and you continued to provide valuable guidance throughout my entire graduate career.

The faculty and staff of the University of Michigan's Graduate Program in Immunology welcomed me with open arms and have always been supportive of my scientific development and my wellbeing. Dr. Bethany Moore and Zarinah Aquil both were especially kind when I first moved to Michigan and made the transition as seamless and easy as possible. I am also very appreciative of the current directors of the program, Drs. Malini Raghavan and Durga Singer, as well as our program administrator, Molly Bannow, who have all been encouraging and helpful throughout this entire process.

I have been exceedingly lucky to have found loving and inspiring friends, who have each been an integral part of my graduate career. While in Ohio, Sara Abrahams, Melanie McKell, Jenny Shao, Alyssa Thomas, and Adri Wilburn together made up my support system, helping me to thrive in our first few years as students. Once I moved to Michigan, Luis Correa, Julie Ferrell-Olson, Monica Jurczyk, Gail Jurczyk, Ashley Munie, Remus Neagu, Mack Reynolds, Tammi Tu, and Emily Yarosz all provided friendships full of positivity and encouragement, which I am beyond grateful for. I want to especially extend my gratitude to Mike Haggadone and Eli Olson. Their friendship has been imperative as we all navigated the final years of graduate school together, and our evening chats have been an uplifting motivation, getting me through to this conclusion. The third community I would like to thank is the one built in my time before graduate school. Ines Acosta, Meaghan Cloherty, Ryan Cloherty, Andy Daugherty, Stephen

Mitchell, Alina Shafii, Bryan St. George, and Alex Kotlyanskiy have all been amazing companions and supporters. These communities mean the world to me, and I look forward to the many more adventures life will bring us.

The person I am today is a testament to the love and care I have received from my family. My parents, Shahana and Naseer Uddin, have always supported my scientific curiosity and have sacrificed so much to ensure I could get to where I am today. My brother, Ferzan Uddin, has been an incredibly valuable friend and is always available when I need him most. Ferzan and I have both been navigating our post-college careers simultaneously, and I couldn't think of anyone better to have on my side. I also want to thank my in-laws, Sandi and Jack Heda; I have known them for over a decade and their love and support has always been unwavering. My brother-in-law, Michael Heda, and sister-in-law, Elanna Heda, both deserve thank-yous as well, their kindness and friendships are very special to me.

Above all, I would like to thank my wife, Vicki, for her steadfast love and relentless support. Vicki is always there for me no matter what and has made countless sacrifices to help me throughout my graduate career. Vicki has helped keep me steady and has been my best friend and biggest advocate for the last decade. Without her, I doubt I would be where I am today.

TABLE OF CONTENTS

LIST OF TABLES

LIST OF FIGURES

ABSTRACT

Rationale: The inflammatory bowel diseases (IBD), Crohn's Disease (CD) and Ulcerative Colitis (UC) are chronic relapsing gastrointestinal (GI) inflammatory diseases that are driven by a breakdown of the intestinal epithelial barrier which permits an aberrant intestinal inflammatory response against microbial antigens**.** We have previously identified 1) the inhibitory receptor, paired immunoglobulin-like receptor (PIR-B) and 2) the lipid transfer protein, steroidogenic acute regulatory (StAR) protein-related lipid transfer (START) domain-containing protein 7, STARD7, to play critical roles in innate inflammatory signals and integrity of epithelial barrier respectively. The aim of this dissertation is to define the involvement of PIR-B in $CD4^+$ T-cell functionality and STARD7 in integrity of intestinal epithelial barrier and the role of these functions in susceptibility to colitis.

Results: We demonstrate that *Pirb*$^{-/-}$*Il10*$^{-/-}$ mice were protected from development of *Il10*$^{-/-}$ spontaneous colitis phenotype and αCD3-mediated intestinal enteropathy. The reduced disease phenotype was associated with fewer $CD4^+$ Th17 cells in the mesenteric lymph nodes and diminished systemic IL-17a levels. Employing a $CD4^+$ $CD45RB^{hi}$ T-cell transfer model of colitis we show that *Rag*$^{-/-}$ which received *Pirb*$^{-/-}$ naïve $CD4^+$ T-cells were protected from T-cell mediated colitis. In vitro polarization of naïve $CD4^+$ T-cells revealed an intrinsic deficiency of *Pirb*$^{-/-}$ Th17 cell survival and cell cycle progression due to hyperactivation of mTORC1 signaling. In silico analyses established upregulation of Th17 and tissue resident memory (TRM) transcriptional signatures in PIR-B^+ murine $CD4^+$ T cells and $LILRB3^+$ human $CD4^+$ T cells. Severe CD patients

marked with high LILRB3 expression were strongly associated with mucosal injury and a proinflammatory Th17-signature.

Additional In silico analyses identified significantly reduced expression of *Stard7* in UC patients which was strongly associated with impaired metabolic function and detrimental inflammatory outcomes. STARD7 knockdown in intestinal epithelial cells resulted in compromised mitochondrial architecture which severely impaired oxidative phosphorylation. Notably, loss of STARD7 directly impacted the formation of cristae and expression of respiratory Complex I mitochondrial energy generation which compromised intestinal epithelial barrier function. Activation of the energy sensor AMPK reconstituted the mitochondrial morphology, upregulated expression of tight junction proteins, and enhanced integrity of the barrier in STARD7 deficient epithelial cells. In vivo we demonstrate that *Stard7*^{Tg}*Il10*$^{-/-}$ mice were more susceptible to the development of DSS-induced and the *Il10*$^{-/-}$ spontaneous colitis phenotypes due to exaggerated activation of macrophage and CD4^{+} T cell compartments.

Conclusions: These data support the concept that 1) PIR-B regulates CD4^{+} Th17 differentiation and development of mucosal T cell memory responses and that 2) STARD7 is a crucial regulator for mitochondrial function and maintenance of the intestinal epithelial barrier. Collectively, this dissertation provides new insight into functions for inhibitory receptors and lipid transport proteins in regulating inflammatory responses and maintenance of intestinal homeostasis and identifies that loss of either molecule can impact susceptibility to IBD.

CHAPTER 1 - Introduction

Inflammatory bowel disease (IBD) is a progressive chronic relapsing disease characterized by inflammation of the mucosa within the gastrointestinal tract (GI). Intestinal microbiota, along with environmental and genetic factors, have been shown to impact IBD susceptibility, with disease ultimately resulting from a dysregulated immune response that occurs due to the breakdown of the intestinal epithelial barrier[1]. IBD encompasses two clinically defined diseases: Crohn's Disease (CD) and Ulcerative Colitis (UC).

The incidence of IBD is on the rise globally; however, the largest gains have been seen in industrialized regions[2]. In Europe, over 2.5 million individuals have been diagnosed with IBD, with a prevalence of CD estimated to be 213 cases per 100,000 and prevalence of UC estimated to be 294 per 100,000[3]. Congruently, in the United States, IBD currently impacts over 3 million Americans, with a prevalence of CD believed to be 274 cases per 100,000 and prevalence of UC estimated to be 286 per 100,000[4]. These cases of IBD are only expected to increase as the world continues to become more industrialized; current trends suggests that by 2030, IBD will impact over 4 million individuals in North America[4]. IBD patients have a disproportionally high financial burden with an estimated lifetime cost of $377 to $498 billion[5] in the USA; estimated lifetime costs for individual CD and UC patients is believed to range from $132,396 to $707,711[6]. The distribution of IBD between males and females is comparable within developed countries, with most new patients being diagnosed before 35 years of age[7]. Genetics alone cannot explain disease susceptibility; monozygotic twins display disease concordance of 50-75% for CD

but only 10-20% for UC. This highlights that IBD pathogenesis, both for CD and UC, is directly tied to social and environmental factors such as diet, access to health care, environment, and microbial exposure during early age[8].

CD and UC have unique clinical manifestations. CD is characterized with discontinuous areas of inflammation which usually involves the terminal ileum and colon but can occur anywhere within the GI tract[9]. Furthermore, the inflammation in CD can be transmural leading to complications such as the presence of strictures, fistulas, granulomas, and abscesses within the bowel wall[10]. In contrast UC is characterized with continuous mucosal inflammation that is exclusively confined to the colon[11]. Additionally, the inflammation in UC is usually restricted to the mucosa and submucosa, which results in superficial damage to the intestinal wall[12]. CD and UC also have divergent associations with various risk factors for disease development. Smoking, for example, has been shown to increase CD development by two-fold[13]. However, in UC, smoking has been shown to have protective effects; most UC patients are non-smokers[14]. Appendectomies have also been implicated in increasing risk for CD development but have been found to protect against UC development, especially in children[15,16]. This divergence is believed to be related to the role the appendix plays in controlling immune responses against the intestinal microflora[17]. While CD and UC are defined by these discrete characteristics, both diseases are characterized by symptoms which include periods of abdominal pain, weight loss, and bloody stool[18]. IBD is a complex disease and treatment of these symptoms requires an understanding of the immunological mechanisms that drive disease pathogenesis.

Immunopathology of IBD

Dysregulated immunological responses are critical for driving IBD pathogenesis. Multiple genome-wide association studies (GWAS) have identified over 200 single nucleotide polymorphisms (SNPs) associated with IBD, and a large number of these polymorphisms have been identified in cytokine receptors, immune signal transducers, chemokine, and chemokine receptor genes that control and mediate immune cell responses[19]. The risk variants associated with IBD are in genes that regulate immune cell function and compromise mucosal immunity, ultimately disrupting intestinal homeostasis. The intestinal epithelium serves as a mechanical barrier which segregates the mucosal immune system from foreign content that is present in the lumen of the intestine. Importantly, the epithelium expresses pattern recognition receptors (PRR) that can detect bacterial components and promote epithelial cells to secrete antimicrobial peptides; disruption in the signaling of these receptors has been linked to IBD. For example, mutations within the NOD2 locus have a strong association with IBD pathogenesis; NOD2 is an intracellular microbial sensor that is expressed on epithelial and innate immune cells and regulates inflammatory responses[20].

In IBD, genetic mutations and environmental factors will ultimately impair mucosal homeostasis and result in the breakdown of the epithelial barrier which allows for exaggerated translocation of microbial products into the lamina propria. This will lead to the activation of innate immune cells which contribute to the initiation of IBD pathogenesis. One of the early responders are neutrophils that mediate intestinal inflammation through the release of multiple inflammatory mediators, including TNF-α, IL-6, IL-1β, and GM-CSF[21]. Neutrophils will also promote the recruitment of monocytes into the intestine which will differentiate into

inflammatory macrophages that secrete cytokines, including TNF-α, IL-6, IL-1β, IL-12, and IL-23[22]. Alongside these innate immune cells, dendritic cells (DC) are present in the lamina propria which coordinate innate and adaptive immune responses. In addition to producing proinflammatory cytokines, DCs are professional antigen presenting cells (APC), which can capture the microbes that have entered the lamina propria and process them into a peptide which is presented on Major Histocompatibility Complex (MHC) class II molecules. Once these microbial antigens have been loaded onto MHC-II complexes, APCs will present antigen to $CD4^+$ T cells to initiate the adaptive arm of the intestinal inflammatory response.

$CD4^+$ T cells in the Pathogenesis of Inflammatory Bowel Disease

$CD4^+$ T cells are an essential component of the adaptive immune system; they are referred to as helper T cells due to their capacity to produce a wide milieu of cytokines and chemokines which aid cytotoxic $CD8^+$ T cells and support B cell-mediated antibody production. A crucial aspect of $CD4^+$ T cells is that each cell expresses a unique T cell receptor (TCR) that must recognize its cognate antigen peptide loaded on a MHC-II molecule. TCR engagement with the peptide-MHC-II complex alone is not sufficient to properly activate $CD4^+$ T cells. APCs express a wide variety of additional costimulatory or inhibitory receptors or ligands that interact with their respective counterparts expressed on the surface of $CD4^+$ T cells and ultimately determine cell fate. Cytokines, which are secreted by both APCs and T cells, provide a critical third signal that will influence $CD4^+$ T cell activation and modulate their differentiation. A few of the key cytokines that are involved in the development of helper $CD4^+$ T cells include: IL-12 which results in Th1 differentiation, IL-4 which results in Th2 differentiation, IL-4/ TGF-β

which results in Th9 differentiation, IL-6/ IL-23/ TGF-β and IL-1β which result in Th17 differentiation, IL-6/ TNF-α which results in Th22 differentiation, and IL-2/ TGF-β which will lead to regulatory T cell (Treg) differentiation[23,24]. Cytokine signaling allows for positive feedback regulation, where cytokines which are produced by differentiated T cells will also aid in the polarization of other T cells. For example, Th1 cells will secrete IFN-γ which will act upon naïve $CD4^+$ T cells and skew them toward Th1 differentiation. As indicated above, T cell differentiation is heavily influenced if there are more than one cytokine present in the environment. One unique example of this is the cytokine TGF-β, which can induce T cell differentiation into Th17 or Treg cells[25]. If IL-6 signaling occurs concurrently with TGF-β signaling, this will skew toward Th17 differentiation; but if TGF-β signaling occurs in the presence of IL-2, this will promote Treg differentiation [26]. Similarly, IL-23 in the presence of IL-6 and TGF-β will promote the production of Th17 cells[27]. Intriguingly, cytokine signaling has been directly linked to IBD pathogenesis; polymorphisms in IL-12 and IL-23 have been found to confer risk to both UC and CD[20,28].

Cytokine signaling ultimately results in the activation of transcription factors which are essential for T cell differentiation[29]. For helper $CD4^+$ T cell subsets, regulation occurs through the combination of two different transcription factors. The initial transcription factor which regulates differentiation is the signal transducer and activator of transcription (STAT) proteins.

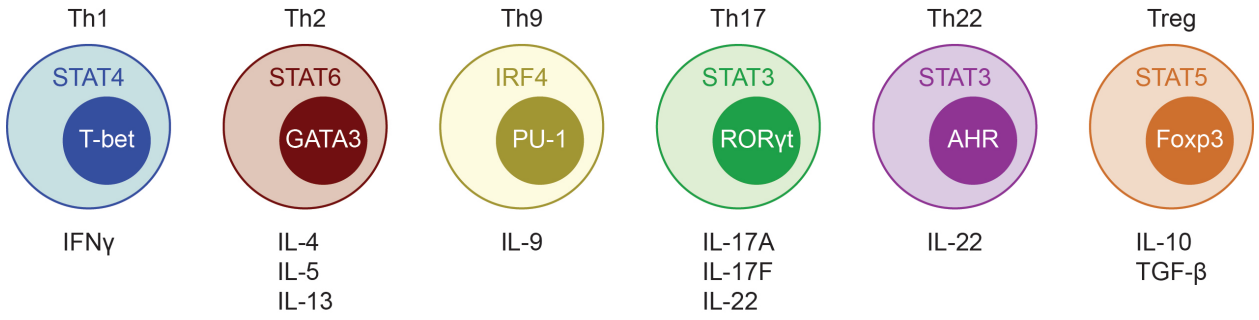

Figure 1-1 Overview of Helper T cell Subsets.

Cytokine signaling results in the activation of janus kinases which phosphorylate STAT proteins and promote their dimerization and activation. These STAT dimers translocate to the nucleus where they upregulate the expression of secondary transcription factors, which are essential for $CD4^+$ T cell differentiation[29]. The transcription factor pairings that regulate T cell differentiation are STAT4/TBET, STAT6/GATA3, IRF4/PU-1, STAT3/RORγt, STAT3/AHR, and STAT5/FOXP3 for Th1, Th2, Th9, Th17, Th22, and Treg differentiation, respectively[30-35] (Figure 1).

Today, it is well understood that a hallmark feature of IBD pathogenesis is the unrestrained immune response mediated by $CD4^+$ T cells, which is a key driver of the chronic inflammatory responses that exacerbates disease. Specifically, Th1 and Th17 cells have been implicated in CD while Th2 cells are believed to drive disease pathogenesis in UC[36-38]. Recently, Th9 cells have been implicated in UC pathogenesis; this subset secretes IL-9 which is believed to impact epithelial barrier integrity[39]. Furthermore, clinical and experimental studies have identified a critical role for IL-$17a^+$ $CD4^+$ T cells in the pathogenesis of IBD. Work utilizing the $CD4^+$ $CD45RB^{high}$ T cell transfer model of colitis revealed that IL-17–producing $CD4^+$ T cells exacerbated the colitic response [40]. Consistently, analyses of draining LN and colonic lamina propria from *Il10*$^{-/-}$ mice with spontaneous colitis revealed that exaggerated IL-17a is produced from $CD4^+$ T cells. UC patients have also been characterized by significantly reduced levels of Th22 cells within inflamed colonic tissue compared to healthy contols[41]. Th22 cells are regulated by the transcription factor AhR and produce potent amounts of IL-22, which has been shown to promote anti-inflammatory functions by enhancing antimicrobial defense in epithelial cells[42]. Current work has revealed that APCs will secrete an IL-22 binding protein (IL-22BP) which impairs IL-22 signaling and suggests that downregulating IL-22BP can enhance IL-

22 activity and limit colitis development[43]. CD and UC patients are often found to have reduced Tregs in the intestine relative to healthy control patients[44]. Mutations in *Il10* locus or the receptor IL10RA, which result in the failure of Tregs cells to suppress proinflammatory macrophages, has been associated with pediatric very early onset intestinal inflammation[45,46].

Recent work has identified a role for discrete memory T cell populations that reside within the GI and contribute to pathogenic IL-17a responses in IBD. Specifically, clinical studies have identified increased frequency of $CD4^+$ tissue resident memory (TRM) T cells with a proinflammatory Th17 phenotype in biopsy samples from active CD and UC patients compared with healthy control patients[47-50]. In line with this, elevated levels of $CD69^+CD103^+$ $CD4^+$ TRM T cells have been associated with clinical flares[48]. TRMs are notable for their lack of recirculation in the bloodstream. Because of this hallmark property, TRMs can be characterized by cell surface expression of CD69 and CD103. CD69 establishes tissue residency by counteracting the S1PR1 signaling which leads to egress into the blood[51]. CD103 interacts with E-cadherin, which is expressed on intestinal epithelial cells and retains the T cells within the tissue[52]. There are other subsets of memory $CD4^+$ T cells besides TRMs; central memory T cells (TCM) are a subset of memory T cells that reside in the secondary lymphoid organs, and effector memory T cells (TEM) are another subset of memory cells that circulate in blood and can reside in previously inflamed peripheral tissue[53]. These two memory T cell populations can be distinguished from each other based on their expression of various cell surface markers. TCMs express CD44, CCR7, and CD62L while TEMs also express CD44 but have lost expression of CCR7 and are heterogeneous for CD62L expression[54,55]. Memory $CD4^+$ T cells are long-lived cells generated from effector $CD4^+$ T cells that have mounted a successful immune response and survived the apoptotic contraction of the $CD4^+$ T cell compartment. Importantly, memory cells

can survive in the absence of antigen in a quiescent state; however, upon re-exposure to microbial antigens, memory $CD4^+$ T cells can rapidly proliferate and generate effector T cells which can produce robust levels of proinflammatory cytokine [53,56]. The generation of memory $CD4^+$ T cells is heavily dependent on the balance of activating and inhibiting signals. Notably, input from inhibitory receptors, such as CTLA-4 and LAG-3, control the development of memory $CD4^+$ T cells and modulate memory $CD4^+$ T cell responses through negative regulation of the TCR signaling[57,58].

The dysregulated intestinal immune response consists of a wide variety of immune cells interacting in a complicated axis. However, the $CD4^+$ T cell compartment is a highly heterogenous population of cells that has been implicated in contributing to different stages of IBD pathogenesis and thus offers a plethora of viable targets for developing therapeutics.

Current and Emerging Therapeutics for Treating IBD

To address quality of life improvements and to help manage disease complications, several therapeutic advances have been made as we have gained a better understanding of disease pathogenesis. For UC patients, anti-inflammatory drugs such as 5-aminosalicylates and corticosteroids have been used to induce disease remission[59,60]. Mechanistically, these drugs target proinflammatory pathways, such as NF-κβ signaling, which reduce the production of pathogenic cytokines. Immunosuppressive drugs have also been proven to be beneficial for both CD and UC patients. Drugs such as tacrolimus have been shown to block NFAT activation and control cytokine production from T cells[61]. Innate and adaptive immune responses have also been targeted by drugs such as methotrexate and azathioprine, which induce apoptosis in

pathogenic cells by inhibiting activating signaling pathways[62,63]. These classic therapeutics help control detrimental inflammatory processes but do not cure IBD; this has led to the development of biologics which have allowed for a more targeted approach to treat IBD patients.

αTNF agents have revolutionized our approaches for inducing remission and treating pathological complications in IBD[64]. These biologics are often used in combination with immunosuppressive agents, and this approach has been effective at limiting severe disease development and has even been found to prevent the formation of fistulas[65]. Despite the evolution of advanced medical therapy including biologics, the risk of surgery at 5 years is ~20% for UC and surgery rates are ~30-40% in CD, indicating a need for development of new therapeutic approaches for the treatment of disease[66]. The therapeutic approaches described above have broadly targeted the dysregulated immune cells or have targeted proinflammatory mediators produced by a wide variety of immune cells. However, emerging therapeutics have had a paradigm shift in that they have attempted to narrow the targets they suppress, including targeting lymphocyte recruitment to the intestine. $CD4^+$ T cells residing in the lymph nodes (LN) are activated by dendritic cells (DCs) loaded with cognate antigen. These primed $CD4^+$ T cells will then enter the bloodstream and are recruited to the intestine based on the expression of specific integrin and chemokine receptors on the cell surface. The integrin $\alpha_4\beta_7$ is expressed on the surface of $CD4^+$ T cells and binds to the MAdCAM-1 expressed on intestinal endothelial cells, which allows for T cells to egress from the bloodstream[67]. Biologics targeting $\alpha_4\beta_7$ have proven to be successful for treating both CD and UC in clinical trials and have been approved for therapy; additional monoclonal antibodies targeting MAdCAM-1 are currently in clinical trials for treating IBD patients[68,69].

Other approaches have successfully targeted the retention of T cells in the intestine. Specifically, T cells express $\alpha_E\beta_7$ (CD103) which interacts with E-cadherin expressed on intestinal epithelial cells[70]. Blocking $\alpha_E\beta_7$ significantly reduced the number of T cells which were retained in the gut[71]. Mucosal T cells that reside in the small and large intestine are also known to express CD69, which counteracts the effects mediated by S1PR1 and prevents tissue egress into the bloodstream[72]. A recent clinical trial treated UC patients with an S1PR1 agonist; the therapeutic retained immune cells within the lymphoid organs and ultimately reduced levels of intestinal inflammation[73]. Overall therapeutics targeting lymphocyte egress, recruitment, and retention have been successful for remission in IBD patients. Importantly these biologics have proven to be successful in patients who fail to respond to other treatments, including αTNF agents, and provide a viable new route for treating IBD[74].

The success of targeting TNF-α has led to the exploration of whether other proinflammatory cytokines can be targeted to impair the dysregulated intestinal inflammation associated with IBD. Unfortunately, early clinical trials have proven that singularly focusing on specific cytokines can lead to limited improvement[75,76]. Clinical trials conducted with the IL-13 neutralizing antibody in UC patients revealed no significant clinical improvement[75]. Similarly, clinical trials with αIFN-γ biologic demonstrated limited improvement in disease activity in CD patients[77]. Targeting IL-17a proved to be a bigger concern, as CD patients who received the IL-17a biologic demonstrated exaggerated adverse outcomes relative to patients who received placebo[78].

While targeting these proinflammatory mediators that are directly secreted by pathogenic $CD4^+$ T cell populations has been met with limited success, there have been viable therapeutics that target the activation or signal transduction of these T cells. For example, IL-6 is secreted by

myeloid cells and DCs and can act upon $CD4^+$ T cells to activate and differentiate them into a pathogenic Th17 subset[79]. Clinical remission in CD patients has been observed with a biologic that targets the soluble form of the IL-6R and can block IL-6 signaling. Additionally, this treatment was found to be effective in severe CD patients who were resistant to αTNF therapy[80,81]. Therapeutic success has also been observed with biologics that target the IL-12 and IL-23 cytokines; IL-12 and IL-23 are heterodimers that both contain the p40 subunit and are cytokines involved with the differentiation of Th1 and Th17 cells respectively. α-p40 blockers have already been approved for treating CD patients, and antibodies that specially block IL-23 signaling by targeting the p19 subunit are currently under investigation[82,83]. The therapies discussed thus far have used a narrow approach to limit the cytokines that the drugs target; however, other investigators have utilized a broad therapeutic strategy that blocks the signal transduction of several cytokines[84]. In UC, for example, blocking Jak1, Jak2, Jak3, and Tyk2 signaling has been shown to successfully limit intestinal inflammation[84]. In line with this, specifically targeting Jak1 signaling was found to improve clinical outcomes in CD patients[85]. Cumulatively, the success and failures of these clinical trials emphasize how important it is to continue targeting these inflammatory pathways, which are mediated by various cytokines, and how essential it is to expand our approaches to focus on novel signal transduction pathways, which can impact excessive mucosal inflammation.

The pathogenic inflammatory response in IBD is driven by a wide variety of immune cell subsets. However, the most successful modern therapeutics have homed in on specifically regulating the $CD4^+$ T cell compartment, whether it be targeting the recruitment of these T cells from the lymphoid organs, bloodstream, and the intestine or targeting the proinflammatory mediators produced by these adaptive immune cells. We know that differentiated $CD4^+$ T cells

accumulate in the intestine over time in IBD patients, and furthermore, we know that increased retention of these T cells is associated with the clinical flare ups which are observed in IBD[86]. These therapeutic advancements have just begun to show the new avenues for treatment of IBD, and further understanding of how these pathogenic T cells are regulated is desperately needed for the development of future therapeutics.

Inhibitory Receptors

The human genome contains over 300 genes that encode for immune inhibitory receptors[87]. These inhibitory receptors are characterized by an intracellular cytoplasmic domain which contains immunoreceptor tyrosine-based inhibitory motifs (V/L/I/SxYxxV/L/I ; ITIM). The ITIM domain acts as a docking site for intracellular phosphatases that dephosphorylate various activating phosphorylation events that are mediated by kinases[88,89]. ITIM domains interact with either tyrosine phosphatases (SHP-1, SHP-2) or phosphatidylinositol phosphatases (SHIP-1, SHIP-2) to localize and guide these phosphatases to their respective kinases to counteract activating receptors that contain immunoreceptor tyrosine-based activating motifs (Yxx(L/I)x6-8Yxx(L/I); ITAM). ITAM domains are located on the hallmark receptors of the adaptive immune system such as T cell and B cell antigen receptors (TCR, BCR) as well as on Fc receptors (FcR), which are found on innate immune cells[90]; these immune cells also express ITIM-bearing receptors which inhibit activation signaling by dephosphorylating a variety of proteins involved in TCR, BCR, and co-stimulatory signaling cascades[91]. Thus, inhibitory receptors serve as a rheostat that can modulate the activation signal that is given to an immune cell to impact the strength of an inflammatory response.

Overview of Murine Paired Immunoglobulin-Like Receptors

Paired receptors refer to two receptors that possess highly homologous extracellular domains and often interact with similar ligands but possess opposing ITAM-domain containing activating and ITIM-domain containing inhibitory motifs that confer different types of signal transduction[92]. The activating and inhibitory members of paired receptors are characterized by high sequence identity[93]. Intriguingly, the expression pattern of these paired receptors is highly variable, leading to unique repertoires of these proteins being present across different cellular compartments. Thus, paired receptors are believed to be crucial regulators of the immune system that temper activating or inhibitory signaling to regulate effector function[94].

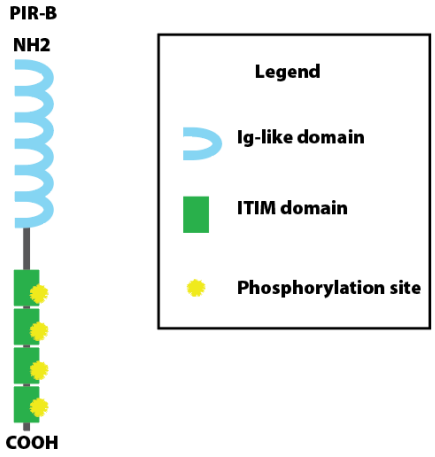

Figure 1-2 Structure of PIR-B.

Paired immunoglobulin-like receptors (PIR) are a family of genes that were identified in BALB/c mice[95]. The PIR family encompasses a set of receptors: the activating receptor, known as paired immunoglobulin-like receptor type A (PIR-A), and the inhibitory receptor, which is referred to as paired immunoglobulin-like receptor type B (PIR-B). Genomic studies found that

Pir genes are located on the terminal region of chromosome 7 in mice, with six genes encoding for *Pira* isoforms and a single gene for *Pirb*[96]. The *Pirb* locus contains a total of 15 exons, where exons 1-8 encode the extracellular domain, exons 9-10 encode the transmembrane region, and exons 11-15 encode an extended intracellular cytoplasmic domain[97]. PIR-B is a 120 kDa type I transmembrane glycoprotein which contains six extracellular immunoglobulin-like domains, followed by a hydrophobic region and a cytoplasmic domain that possesses four ITIM domains, which can interact and signal via SH2 domain-containing phosphatases (Fig. 2). In contrast, the *Pira* locus contains 10 exons where exons 1-8 encode the extracellular domain and exons 9-10 encode the transmembrane region alongside a short cytoplasmic domain[97]. Structurally PIR-A is an 85 kDa receptor which is characterized with six immunoglobulin-like domains in the extracellular domain followed by a transmembrane domain and a short intracellular domain that possesses no signaling capacity. PIR-A possesses an arginine residue within the transmembrane region that permits binding with the common FcγR[98]. The FcγR contains an ITAM domain that performs the signal transduction for PIR-A[99]. PIR-A and PIR-B are expressed on a wide variety of hematopoietic cells including macrophages, monocytes, DCs, mast cells, neutrophils, basophils, and eosinophils[100-103]. While PIR-A and PIR-B were originally believed to be expressed in similar levels in a pairwise fashion, recent studies identified dominant PIR-B expression on plasmacytoid dendritic cells (pDC), B cells, and neurons[104-106]. Interestingly PIR-A and PIR-B seem to be highly modular, with expression levels of these paired receptors becoming highly upregulated during activation and differentiation[107].

The extracellular domain of PIR-A and PIR-B is highly homologous, with a shared sequence identity of over 90%, and indicates that the activating and inhibitory receptors share the same ligand. Initial studies identified that PIR-B interacted with MHC-I molecules; PIR-B

activation was diminished by nearly 50% in *B2m*$^{-/-}$ mice; β2- microglobulin is a critical component of MHC-I molecules[108]. This interaction was confirmed using surface plasmon resonance analysis, where a recombinant protein of the extracellular domain of PIR-B was shown to bind to various murine MHC-I alleles; specifically it was shown that PIR-B interacted with H-2L^{d}, H-2D^{d}, H-2K^{b}, H-2K^{k}, and H-2K^{d} with binding affinities ranging from K_d = 190–560 nM[109]. Furthermore, this group used a H-2L^{d} tetramer and confirmed the MHC-I molecule colocalized with PIR-B on the surface of splenic B cells. Additionally, they demonstrated the tetramer was binding to PIR-A on *Pirb*$^{-/-}$ macrophages with confocal microscopy[109].

While early studies revealed that these receptors interact with MHC molecules, recent studies have demonstrated an expanded library of ligands which are capable of binding with the extracellular domains of PIR-A and PIR-B. For example, *Staphylococcus aureus* (*S. aureus*) was shown to bind to the extracellular domain of both PIR-B and PIR-A; PIR-B was shown to recognize lipoteichoic acid (LTA), a negatively charged cell wall component of gram-positive bacteria[110]. Interestingly, *S. aureus* interacted with a unique epitope on PIR-A and PIR-B as an α-PIR monoclonal antibody that blocked the PIR-bacteria interaction did not impact PIR-MHC interaction[109]. Notably, there is a level of bacterial specificity with respect to binding PIR-A and PIR-B, as other gram positive bacteria such as *Listeria monocytogenes* did not interact with the PIR's[110]. Furthermore, gram negative bacteria including *Helicobacter pylori* and *Escherichia coli* (*E. coli*) but not *Pseudomonas aeruginosa* interacted with PIR-B[110]. Interestingly *Pirb*$^{-/-}$ mice have enhanced susceptibility to *Salmonella enterica* (*S. enterica*) infection and in vitro studies with *Pirb*$^{-/-}$ macrophages found these cells were unable to control intracellular bacterial growth. It remains unclear whether *S. enterica* directly binds to PIR-B to invade macrophages[111].

Recent studies have demonstrated that PIR-B is also expressed on neurons [106,112]. PIR-B was shown to interact with unique ligands in the central nervous system (CNS) including nogo, myelin-associated glycoprotein (MAG), and oligodendrocyte myelin glycoprotein (MAG)[113]. PIR-B functions alongside the nogo receptor by interacting with myelin-associated inhibitors and impairing axonal regeneration[114]. Notably, PIR-B binding affinity for nogo protein is higher than for MHC-I molecules (K_d = 0.57 μM vs K_d = 4 μM), and nogo binds to the same domains on the extracellular region of PIR-B as MHC-I molecules[114]. Thus, unlike the bacterial ligands, these CNS derived ligands may represent a unique competitive mechanism for signal transduction in PIR-B. PIR-B was shown to be capable of binding to other CNS ligands, β-amyloid[115]. Soluble β-amyloid oligomers have been implicated in Alzheimer's disease (AD) by mediating synaptic defects and PIR-B deficiency rescued synaptic plasticity in murine models of AD[115].

Overview of Human Leukocyte Immunoglobulin-Like Receptors

Probing of a human splenocyte cDNA library with the murine PIR probe led to the discovery of human orthologs of PIR, human Ig-like transcripts (ILT)/leukocyte immunoglobulin-like receptor (LILR). In contrast to mice, the human genome encodes for five inhibitory receptors and six activating receptors, all of which are located on the human chromosome 19q13.4[116]. The inhibitory receptors are referred to as LILRBs (LILRB1-LILRB5), and like their murine counterpart, PIR-B, their cytoplasmic region contains ITIM domains. The extracellular domains for all LILRBs are characterized by four immunoglobulin-like domains with the exception of LILRB4 and LILRB5, which contain two immunoglobulin-like domains[116]. LILRBs have been shown to be expressed on myeloid and lymphoid cells, with LILRB1 and

LILRB5 being highly expressed on T cells[117-119]. Likewise, the activating receptors are referred to as LILRAs (LILRA1-6) and associate with FcγR and signal via ITAM domains in the Fc receptor[117]. The human receptors differ from their murine counterparts in the ectodomains; most LILRAs are characterized by four immunoglobulin-like domains within the extracellular domain with the exception of LILRA1 and LILRA5 which contain two immunoglobulin-like domains[116]. LILRAs have also been shown to be expressed on a wide variety of myeloid and lymphoid cells; LILRA3 is highly upregulated on pDCs[119]. The expanded number of these stimulatory and inhibitory receptors, which contain unique extracellular domains, suggests a more robust system is required in humans to fine tune immune responses and allows for unique regulatory mechanisms.

Consistent to the mouse orthologues, human LILRA and LILRB have been shown to have multiple ligands, including MHC-I molecules. In humans LILRB1 and LILRB2 have been shown to bind to MHC-I alleles. X-ray crystallography revealed that the immunoglobulin-like domain of LILRB1 and LILRB2 specifically binds the β2-microglobulin domain of the MHC molecules. Notably, this interaction is independent of the antigenic peptide that is loaded in the MHC-I molecules and provides a wider range of flexibility to activate these inhibitory molecules[120,121]. LILRB3 has also been described as a novel inhibitory MHC class I receptor expressed by NK, myeloid and dendritic cells[122]. LILRB1 and LILRB3 can interact with MHC-I molecules in cis and trans fashion[123-125]. Inhibitory receptors in humans can also interact with non-classical MHC-I proteins. LILRB2 was found to interact with the CD1d receptor and deterred the loading of lipid antigens into the binding groove of CD1d, ultimately preventing the activation of CD1d restricted NKT cells[126]. LILRBs can bind to innate immune antigens; specifically, LILRB1 binds to *E. coli* and LILRB3 binds to *S. aureus*[110]. Structural studies

confirmed that LILRB1 can also recognize variant surface antigens on cells that have been infected with *Plasmodium* parasites[127,128]. Furthermore, LILRB2 was shown to be capable of binding to the CNS ligand, β-amyloid, with an estimated k_d of 206 nM[115].

The identification of a diverse range of ligands ranging from MHC-I molecules to bacterial ligands and CNS ligands highlights the complex nature of PIR-B and LILRB negative signaling in the modulation of immune responses. PIR-B and LILRB3 regulatory effects have already been linked to wide-ranging biological processes, including osteoclastogenesis, pulmonary fibrosis, myeloid cell regulation, and $CD8^+$ T cell proliferation[129-131]. Furthermore, the demonstration that these inhibitory receptors can act in either cis or trans fashion and the idea that these ligands can either compete for or bind to separate domains in the extracellular region of the receptor compounds the regulatory mechanisms that influence the inhibitory signal transduction mediated by these receptors. Altogether, these discoveries emphasize the importance of developing our understanding of how these inhibitory receptors function in different compartments of the immune system.

The Impact of PIRs in Transplantation

Transplantation is a crucial, potentially lifesaving medical procedure that can assist patients with failing tissues and organs. Unfortunately, moving an organ from a donor to a recipient often results in an immune mediated rejection of the transplant. Naïve T cells are trained in the thymus to recognize a variety of foreign antigen peptides that have been loaded onto a specific MHC allele[132]. However, there is a high degree of diversity in human MHC molecules, and thus MHC matching between donor and recipient patients in transplantation

procedures is extremely challenging[133]. This often leads to an allogenic transplantation where there is an MHC mismatch between the donor's tissue and recipient's immune compartment, ultimately leading to a severe immune response against the donor tissue, which can result in complete rejection of the graft.

Immunological targets are believed to be a viable therapeutic approach for controlling the activation of alloreactive T cells, which mediate detrimental transplant rejection. This has led to studies that questioned whether PIR-A and PIR-B interactions with MHC molecules could alter transplantation outcomes. Intravenous administration of splenocytes isolated from a BALB/c mouse to sub lethally irradiated C57BL/6 mouse induced graft versus host disease (GVHD) where 50% of the mice died by 20 days after transplantation[109]. In contrast, *Pirb*$^{-/-}$ C57BL/6 mice administered splenocytes from a BALB/c mouse exhibited enhanced susceptibility to GVHD where all of the mice died by 20 days after transplantation[109]. Furthermore, the *Pirb*$^{-/-}$ mice had increased numbers of donor IFN-γ^+ CD4$^+$ and CD8$^+$ T cells which were localized to the recipient's spleen. Congruent with the exaggerated T cell population, DCs in the *Pirb*$^{-/-}$ mice were found to be hyperactivated with enhanced expression of CD40, CD80, CD86, MHC-I, and PIR-A[109]. Recent work built on these findings by identifying a role for PIR molecules in contributing to immunological memory responses, which led to the rejection of allograft-transplanted tissue[134]. Specifically, PIR-A expression on macrophages was found to be responsible for mediating trained immunity responses to allogenic MHC-I molecules[134]. Notably, the macrophage memory-like response to allogenic tissues were abrogated in host mice treated with a fusion protein that specifically blocked PIR-A signaling, ultimately preventing acute allograft rejection[134]. Altogether these studies implicate PIRs as crucial regulators for cell

activation, and given their ability to broadly recognize MHC molecules, suggests they can be key targets for regulating allogenic immune responses.

The Impact of PIR-B in Innate Immune-Mediated Colitis

The inflammatory bowel diseases (IBD) are chronic relapsing inflammatory disorders. While CD and UC are recognized to be $CD4^+$ T cell dependent diseases, recent advances in our understanding of the role of commensal bacteria and pattern recognition receptors (e.g toll-like receptor 4 (TLR-4) and caspase recruitment domain 15 (CARD15) polymorphisms) in IBD pathogenesis indicate a key role for innate immunity in colonic inflammation[135]. Consistent with this, activated macrophages are a prominent constituent of the inflammatory infiltrate in CD and UC[136]. Macrophage depletion protects against onset of colitis in the *Il10*$^{-/-}$ spontaneous model of colitis[137]. Furthermore, M-CSF deficient (op/op) mice, which are not able to develop mature macrophages, or wild type (WT) mice administered neutralizing anti-CSF-1 antibody, demonstrate decreased susceptibility to dextran sulfate sodium (DSS)-induced colitis[138,139].

Given that PIR-B expression is highly upregulated on activated macrophages[140], investigators evaluated the role of PIR-B in regulating macrophages and their contribution to the development of innate immune mediated colitis[141]. *Pirb*$^{-/-}$ mice were found to be more susceptible to DSS-induced colitis relative to WT mice. Notably, the increased susceptibility to disease was associated with increased secretion of the IL-6 and IL-1β, suggesting that PIR-B deficiency was generating hyper-inflammatory macrophages[141]. Consistent with this, peritoneal inflammatory macrophages from *Pirb*$^{-/-}$ mice produced enhanced levels of TNF-α, IL-6, and IL-1β in response to *E. coli* stimulation[141]. Mechanistically, *E. coli* stimulation of *Pirb*$^{-/-}$

inflammatory macrophages resulted in enhanced phosphorylation of ERK-1/2 and p38. It also altered regulation of downstream transcription factors, increased FosB activation, and impaired c-Jun expression. Cumulatively, these studies identified that PIR-B-SHP-1/2 axis negatively regulates both MAPK and NFκβ signaling pathways in activated macrophages (Fig. 3)[141].

Adoptive transfer of *Pirb*$^{-/-}$ bone marrow derived macrophages into WT mice led to earlier onset of DSS-induced colitis, and this was associated with exaggerated production of IL-6 and GM-CSF[141]. Thus, this body of work identified PIR-B as a unique target for suppressing macrophage function and a receptor that could potentially be utilized to abrogate detrimental inflammatory responses in IBD. In **Chapter 2** of this dissertation, we will expand on these findings by determining if PIR-B regulates the $CD4^+$ T cell compartment and if PIR-B is required for the onset and sustainment of T cell dependent colitis.

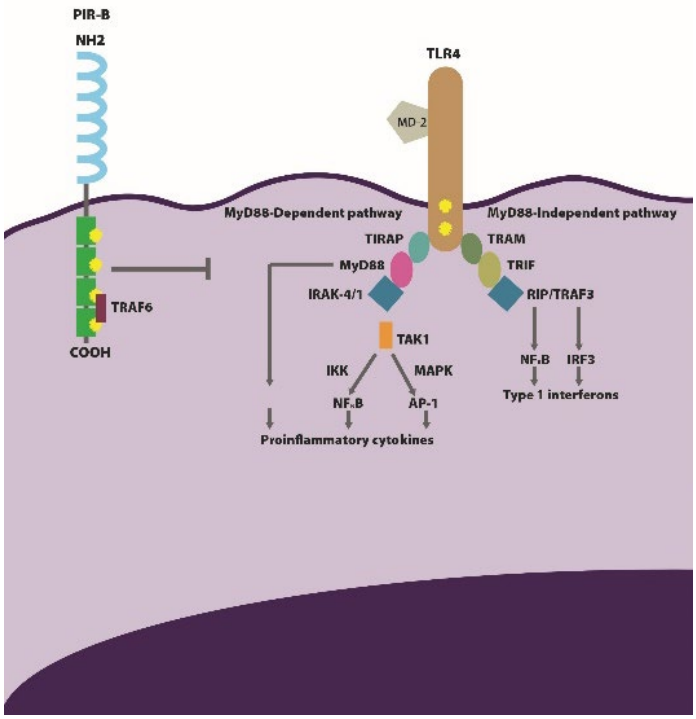

Figure 1-3 Overview of PIR-B Signaling.

Overview of Steroidogenic Acute Regulatory Proteins

Steroidogenic acute regulatory (StAR) proteins belong to the StAR protein-related lipid transfer (START) domain superfamily; these proteins possess a START domain that consists of 210 amino acid residues that bind to specific lipids and are known to be critical regulators of lipid transport across various cell types[142]. These START domains have been identified in 15 different proteins, STARD1-STARD15. The ligands for the majority of these STARD proteins are currently unknown. STARD2 is known to bind to phosphatidylcholine (PC) while STARD10 and STARD11 bind to ceramide, and these proteins have been shown to be important for transport of these newly synthesized lipids between different organelles within a cell[143,144]. Lipids are a critical component of the plasma membrane and cellular organelles; the synthesis of lipids, however, is limited to the endoplasmic reticulum, golgi complex, and mitochondria[145]. Therefore, these lipid-binding proteins are thought to play a vital role in lipid membrane trafficking to facilitate organelle formation and function. Thus, our understanding of the members of the START family of proteins is important for building on our knowledge of how proteins engage in lipid binding and mediate lipid exchange across different cellular membranes to maintain cell homeostasis and survival.

The Role of STARD7 in Intracellular Lipid Trafficking

Stard7 mRNA was originally identified to be highly expressed in the choriocarcinoma cell line JEG-3[146]. The *Stard7* gene is located on chromosome 2 and shown to possess 8 exons. *Stard7* encodes a 370 amino acid precursor protein, STARD7-I, which has an approximate

molecular weight of 43.1 kDa and contains an N-terminal mitochondrial targeting sequence (MTS)[146,147]. Importantly, the MTS can be cleaved to generate a truncated form, STARD7-II which is a 295 amino acid protein with a molecular weight of 34.7 kDa. STARD7-I is processed in the mitochondria to give rise to the mature protein, STARD7-II, which resides in the cytoplasm. Recent mechanistic studies demonstrated that STARD7-I traffics across translocase of the outer membrane (TOM) complexes expressed on the outer mitochondrial membrane and is proteolytically processed in two consecutive steps within the mitochondrial inner membrane. Matrix-localized mitochondrial processing peptidase (MPP) initially cleave the MTS of STARD7-I and is further processed by presenilin-associated rhomboid-like (PARL) protease in the transmembrane domain which ultimately generates the mature form of STARD7[148]. Interestingly this work also found that only 40% of STARD7-II reaches the cytosol; 60% of mature STARD7 resides within the mitochondrial intermembrane space where it presumably facilitates PC transfer between the outer and inner mitochondrial membrane[148].

Additional studies utilizing radiolabeled lipid vesicles and fluorescence resonance energy transfer assays found that both STARD7-I and STARD7-II preferentially bind to phosphatidylcholine (PC) with limited lipid binding to phosphatidylserine, phosphatidylethanolamine, and sphingomyelin[147]. Confocal microscopy revealed that STARD7 shunts PC from the ER and facilitates integration of this lipid into the mitochondria of HEPA-1 cells[147]. Previous studies have demonstrated that loss of STARD7 induces significant alterations in mitochondrial morphology that is marked by loss of mitochondrial PC content and loss of respiratory function[149]. Specifically, STARD7 knockdown HEPA-1 cells displayed disorganized cristae structure, and activity of the mitochondrial respiration was compromised, resulting in diminished ATP generation and cell proliferation[149]. Altogether, these bodies of work establish

STARD7 as a regulator of energy dynamics in hepatic cells and suggests a role for STARD7 in inflammatory diseases that are associated with altered metabolism and mitochondrial dysfunction.

The Impact of STARD7 in Epithelial Cell Homeostasis and Inflammatory Disease

Utilizing *Stard7*^{Tg} (*Stard7*$^{+/-}$) mice, investigators have demonstrated that intraperitoneal sensitization and intratracheal challenges with ovalbumin (OVA) induced an exaggerated airway inflammatory response in *Stard7*^{Tg} mice relative to WT mice; notably, the increased disease phenotype was associated with significantly increased IL-13^{+} CD4^{+} T cells and eosinophils in the lungs of the *Stard7*^{Tg} mice[150]. Mechanistic analyses revealed that STARD7 deficiency was associated with increased permeability of the lung epithelial barrier[150]. Consistent with this, the authors observed that older *Stard7*^{Tg} mice developed spontaneous dermatitis; loss of *Stard7* resulted in defects in the basal cell layer of the epidermis which was leading to an exaggerated Th2 immune response[150]. Cumulatively, this body of work identifies STARD7 as a critical regulator of epithelial barrier function in the lung and skin and sets the foundation for investigating how STARD7 may play a protective role in mucosal tissues by maintaining the compartmentalization of pathogenic immune cells from the local antigens that can activate them.

Previous studies have established that STARD7 plays a critical role in mitochondria PC trafficking, mitochondria homeostasis, and epithelial barrier function. Additional work has also reported an important role for epithelial barrier dysfunction and exacerbation of the IBD phenotype. In **Chapter 3** this dissertation will determine whether STARD7 influences the

integrity of the intestinal epithelial barrier and if it can impact the development of acute and chronic colitis.

Dissertation Objectives

This dissertation aims to identify the mechanisms behind how immune responses are controlled in the intestine and how changes in the regulators of these networks can lead to detrimental disease outcomes. In **Chapter 2** this dissertation will identify an important role for PIR-B in the regulation of $CD4^+$ Th17 effector cells and colitis development and provide insight into divergent functions for inhibitory receptors in regulating innate and adaptive inflammatory responses. In **Chapter 3**, this dissertation will reveal how STARD7 is essential for maintaining the integrity of the intestinal epithelial barrier and preventing the development of detrimental inflammatory responses that mediate colitis.

<u>Gaps in Knowledge (Chapter 2):</u>

1. Can PIR-B impact the development of colitis by regulating the $CD4^+$ T cell compartment?
2. Is PIR-B expressed on $CD4^+$ T cells, and can it intrinsically regulate pathogenic effector functions mediated by this compartment?
3. What are the molecular processes by which PIR-B impacts $CD4^+$ T cell signaling pathways, and is it restricted to different helper T cell subsets?

Central Hypothesis: PIR-B regulates $CD4^+$ Th17 development and is required for the $CD4^+$ Th17 pathogenic immune responses and induction of T-cell dependent colitis.

The specific aims of this hypothesis are:

1. Define the requirement of PIR-B on the $CD4^+$ Th17-dependent colitis.
2. Determine the role of PIR-B in $CD4^+$ Th17 differentiation and function.

Gaps in Knowledge (Chapter 3):

4. Can STARD7 alter the development of colitis by regulating the intestinal epithelial compartment?
5. Is STARD7 essential for mitochondrial homeostasis within intestinal epithelial cells and can it modulate barrier function?
6. Where does STARD7 localize within intestinal epithelial cells, and does it influence mitochondrial respiration?

Central Hypothesis: STARD7 is essential for mitochondrial respiration and promotes intestinal epithelial barrier function to maintain mucosal immune responses.

The specific aims of this hypothesis are:

3. Define the role of STARD7 in the development of the colitic phenotype.
4. Determine if STARD7 is required for mitochondrial homeostasis and maintenance of epithelial barrier function.

CHAPTER 2 - PIR-B Regulates $CD4^+$ $IL\text{-}17a^+$ T Cell Survival and Restricts T-cell Dependent Intestinal Inflammatory Responses.

This chapter has been published:

Uddin J, Tomar S, Sharma A, Waggoner L, Ganesan V, Marella S, Yang Y, Noah T, Vanoni S, Patterson A, et al. PIR-B Regulates $CD4^+$ $IL17a^+$ T-Cell Survival and Restricts T-Cell-Dependent Intestinal Inflammatory Responses. Cellular and Molecular Gastroenterology and Hepatology. 2021;12(4):1479-502.

Synopsis

The inhibitory receptor paired immunoglobulin-like receptor B regulates $CD4^+$ Th17-dependent chronic intestinal inflammatory responses by tempering mTORC1 signaling and enhancing $CD4^+$ $IL\text{-}17a^+$ T cell survival and regulates the outgrowth and maintenance of tissue resident memory $CD4^+$ $IL\text{-}17a^+$ T cells.

Abstract

Background & Aims: $CD4^+$ T cells are regulated by activating and inhibitory cues and dysregulation of these proper regulatory inputs predisposes to aberrant inflammation and exacerbation of disease**.** We investigated the role of the inhibitory receptor, paired immunoglobulin-like receptor B (PIR-B) in the regulation of the $CD4^+$ T-cell inflammatory response and exacerbation of the colitic phenotype.

Methods: We employed *Il10*$^{-/-}$ spontaneous and $CD4^+CD45RB^{hi}$ T cell transfer models of colitis with PIR-B (*Pirb*$^{-/-}$) deficient mice. Flow cytometry, western blot, RNA-seq analysis was performed on wild type and *Pirb*$^{-/-}$ $CD4^+$ T cells. In silico analyses were performed on RNA-seq

dataset of ileal biopsy samples from pediatric CD and non-IBD patients and sorted human memory $CD4^+$ T cells.

Results: We identified PIR-B expression on memory $CD4^+$ $IL\text{-}17a^+$ cells. We show that PIR-B regulates $CD4^+$ Th17-dependent chronic intestinal inflammatory responses and development of colitis. Mechanistically, we reveal that the PIR-B-SHP-1/2 axis tempers mTORC1 signaling and mTORC1-dependent Caspase-3/7 apoptosis resulting in $CD4^+$ $IL\text{-}17a^+$ cell survival. *In silico* analyses reveal enrichment of transcriptional signatures for Th17 cells (*RORC, RORA, IL-17A*) and tissue resident memory (TRM) (*HOBIT, IL7R and BLIMP1*) networks in PIR-B^+ murine $CD4^+$ T cells and human $CD4^+$ T cells that express the human homologue, LILRB3. High levels of LILRB3 expression were strongly associated with mucosal injury and a proinflammatory Th17-signature, and this signature was restricted to a treatment-naïve severe pediatric CD population.

Conclusions: Our findings demonstrate an intrinsic role for PIR-B/LILRB3 in the regulation of $CD4^+$ $IL\text{-}17a^+$ T cell pathogenic memory responses.

Keywords: paired immunoglobulin receptor, $CD4^+$ T cells, interleukin-17 and inflammatory bowel disease

Introduction

Inflammatory bowel diseases (IBD), encompassing Crohn's disease (CD) and ulcerative colitis (UC), are progressive chronic relapsing-remitting diseases, which result from an exaggerated inflammatory response to intestinal microbes in a genetically susceptible individual [151]. Activation of innate immune receptors, such as Toll-like receptors (TLRs) and NLRs by pathogenic bacteria and viruses (dysbiosis), injury or xenobiotic elements [152,153] leads to activation of intestinal macrophages and dendritic cells (DC) and in turn drives proinflammatory cytokine (IL-6, IL-12 and IL-23) production. These cytokines stimulate the development of effector $CD4^+$ -Th1 and -Th2 cells, and -Th17 cells [154-156], activation of Innate lymphoid cells (ILC1, ILC2, NCR^+ILC3 and NCR^-ILC3 cells) which leads to a IL-17A/IFNγ/TNFα-dominant proinflammatory response and the histopathological manifestations of disease [47,48,157-166].

Paired immunoglobulin-like receptor B (PIR-B) is a immunoreceptor tyrosine-based inhibitory motif (ITIM)[167,168] containing Type-I transmembrane glycoprotein predominantly expressed on myeloid cells, B cells and granulocytes [169-171]. Activation of PIR-B via MHC Class I molecules in cis and trans fashion [172] and cell wall components of certain gram negative and gram positive bacteria [170,173,174] induces PIR-B ITIM domain engagement and activation of the intracellular phosphatases SHP-1 and SHP-2. Subsequently, SHP-1 dephosphorylates p65 and ERK1/2 resulting in the inhibition of downstream NFκB- and MAPK-signaling pathways [91] and inhibition of B cell receptor, TLR, and chemokine receptor signaling [96]. We have previously reported that PIR-B restrains innate-immune-induced proinflammatory cytokine (IL-1β, IL-6 and TNF-α) production by macrophages and limits acute intestinal -inflammation and -epithelial cell injury [175].

Utilizing PIR-B (*Pirb*$^{-/-}$) deficient mice and employing the *Il10*$^{-/-}$ spontaneous, αCD3-mediated, and CD4^{+}CD45RB^{hi} T cell transfer models of colitis, we demonstrate that loss of PIR-B expression protected mice from development of CD4^{+} T-cell dependent colitis. Notably, disease protection was associated with significantly reduced frequency of tissue resident memory (TRM) CD4^{+}IL-17a^{+} T cells. Adoptive transfer experiments revealed that PIR-B expression on CD4^{+} T cells conferred a competitive advantage for T cell survival and TRM CD4^{+} T cell development. *In vitro* studies demonstrate that *Pirb*$^{-/-}$ naïve CD4^{+} T cells have decreased capacity to differentiate into Th17 cells, impaired cell cycle entry into G1- and S-phases, and enhanced cell death. Mechanistic analysis reveal that PIR-B acts as rheostat, controlling mTORC1 signaling in CD4^{+} T cells and limiting CD4^{+} IL-17A^{+} T cell outgrowth. LILRB3 expression was strongly associated with mucosal injury and a proinflammatory Th17-signature in a treatment-naïve endoscopically severe pediatric CD population. Flow cytometry and RNA-seq analysis revealed enhanced PIR-B and LILRB3 expression on a subset of memory CD4^{+} Th17 cells in mice and humans, respectively. Collectively, these data suggest an intrinsic role for PIR-B in the regulation of the outgrowth and maintenance of TRM CD4^{+} IL-17a^{+} T cells and development of T-cell dependent colitis.

Results

Decreased susceptibility of *Pirb*$^{-/-}$ mice to *Il10*$^{-/-}$ spontaneous colitis

To define the role of PIR-B in T-cell mediated colitis we backcrossed *Pirb*$^{-/-}$ mice (C57BL6) with *Il10*$^{-/-}$ mice (C57BL6), and monitored for the development of the spontaneous colitis phenotype. *Pirb*^{WT}*Il10*$^{-/-}$ (*Il10*$^{-/-}$) mice demonstrated colitic symptoms including rectal prolapse, anal bleeding, diarrhea, and dehydration by 8 weeks of age and disease progressed until 15 weeks of age (Fig. 1a). These symptoms were associated with failure to thrive and a ~20% mortality rate (Fig. 1b, c). Flow cytometry analysis demonstrated increased frequency of CD4$^+$ IFNγ$^+$ T cells and CD4$^+$ IL-17a$^+$ T cells in the mesenteric lymph nodes (mLN) of the colitic *Il10*$^{-/-}$ mice (Fig. 1a-f). Histological analysis of the colon from *Il10*$^{-/-}$ mice showed significant evidence of epithelial erosions, crypt abscesses and transmural inflammation (Fig. 1g, h). By contrast, *Pirb*$^{-/-}$*Il10*$^{-/-}$ mice had significantly reduced symptoms (Fig. 1a), with increased weight gain and survival rates comparable to healthy control *Il10*$^{+/-}$ mice (Fig. 1b, c). Notably, the frequency of CD4$^+$ IFNγ$^+$ T cells and CD4$^+$ IL-17a$^+$ T cells populations in the mLN of *Pirb*$^{-/-}$*Il10*$^{-/-}$ mice was significantly reduced compared to colitic *Il10*$^{-/-}$ mice (Fig. 1d-f). Congruent with the reduced disease phenotype, the colons of *Pirb*$^{-/-}$*Il10*$^{-/-}$ mice demonstrated reduced histopathological disease phenotype possessing normal colonic epithelial architecture with reduced cellular infiltrate (Fig. 1g, h). Utilizing the PIR 6C1 antibody which recognizes both PIR-A and PIR-B [107], we identified PIR-B expression on colonic lamina propria (LP) LP CD4$^+$ T cells from of *Pirb*^{WT}*Il10*$^{-/-}$ mice (Fig. 1i). Additional qRT-PCR analyses revealed PIR-B mRNA expression in naïve splenic CD4$^+$ T cells (Fig. 1j). Collectively, these data demonstrate that PIR-B is expressed on CD4$^+$ T cells and mice deficient in PIR-B are protected from *Il10*$^{-/-}$ spontaneous colitis.

PIR-B is required for CD4$^+$ T-cell dependent enteropathy

To directly assess the consequence of PIR-B deficiency on CD4$^+$ T-cell activation and T-cell dependent intestinal injury; we employed the αCD3-mediated model of intestinal enteropathy (Fig. 2a) [176,177]. Transient activation of T cells in *Il10*$^{-/-}$ mice by peritoneal injection of αCD3 resulted in the development of clinical signs of diarrhea, piloerection, decreased mobility and exaggerated weight loss (Fig. 2b, c) that was associated with a potent mLN CD4$^+$ IFNγ$^+$ T cells and CD4$^+$ IL-17a$^+$ T cell response (Fig. 2d). Examination of colonic sections revealed substantial epithelial injury including epithelial apoptosis, villus atrophy and an inflammatory infiltrate (Fig. 2e, f). In contrast, *Pirb*$^{-/-}$*Il10*$^{-/-}$ mice demonstrated limited evidence of αCD3-mediated disease showing reduced clinical scores, weight loss and this was associated with reduced numbers of mLN CD4$^+$ IFNγ$^+$ T cells and CD4$^+$ IL-17a$^+$ T cells, and colonic injury (Fig. 2b-f). Systemic levels of TNFα and IFNγ were comparable between *Il10*$^{-/-}$ and *Pirb*$^{-/-}$*Il10*$^{-/-}$ mice; however, IL-17a was significantly reduced in *Pirb*$^{-/-}$*Il10*$^{-/-}$ mice compared to *Il10*$^{-/-}$ mice (Fig. 2g). These studies suggest that PIR-B negatively regulates exacerbation of T-cell dependent enteropathy and may have direct regulatory effects on the CD4$^+$ Th17 compartment.

To test whether PIR-B intrinsically regulates CD4$^+$ T cells, we utilized the CD4$^+$CD45RB^{hi} T cell transfer model of colitis [178,179]. *Rag*$^{-/-}$ mice that received naïve *WT* CD4$^+$ T cells (400,000 cells) developed symptoms of colitis two weeks after T-cell transfer and these mice showed substantial weight loss by day 30 (Fig. 3a-c). Development of colitis was associated with the presence of CD4$^+$ IFN-γ$^+$ T cells and CD4$^+$ IL-17a$^+$ T cells in the mLN (Fig. 3d), colonic inflammation with severe crypt destruction (Fig. 3e, f) and systemic TNFα, IFNγ, and IL-17a cytokines (Fig. 3g).

By contrast, *Rag*$^{-/-}$ mice that received naive *Pirb*$^{-/-}$ CD4^{+} T cells developed a reduced colitic phenotype as evident by clinical score, weight loss, and colon histopathology (Fig. 3b, c, e and f). Consistent with this, the frequency of CD4^{+} IFNγ^{+} T cells and CD4^{+} IL-17a^{+} T cells was significantly reduced in *Rag*$^{-/-}$ mice which received *Pirb*$^{-/-}$ CD4^{+} T cells (Fig. 3d). Importantly, *Pirb* deficiency in the CD4^{+} T cell compartment resulted in the downregulation of systemic levels of IL-17a but not TNFα and IFNγ (Fig. 3g). Together, these data confirm that PIR-B intrinsically regulates IL-17a^{+} inflammatory responses *in vivo* and indicate that PIR-B is required for archetypal CD4^{+} IL-17a^{+} T cell response.

PIR-B intrinsically regulates Th17 cell survival in vitro

To gain mechanistic insight into PIR-B regulation of CD4^{+} T cell function, we assessed proliferation and differentiation capacity of *WT* and *Pirb*$^{-/-}$ naïve CD4^{+} T cells. Polyclonal activation of *WT* and *Pirb*$^{-/-}$ CD4^{+} T cells under Th1 polarizing conditions induced equivalent frequencies of CD4^{+} IFNγ^{+} T cells (Fig. 4a). Consistent with this, we observed comparable number and cellular proliferative capacity in *WT* and *Pirb*$^{-/-}$ CD4^{+} Th1 cells (Fig. 4c). Under Th17 polarizing conditions we observed a significant reduction in the frequency and number of CD4^{+} IL-17a^{+} T cells generated from *Pirb*$^{-/-}$ CD4^{+} T cells compared to *WT* CD4^{+} T cells (Fig. 4b). The reduced frequency in *Pirb*$^{-/-}$ CD4^{+} IL-17a^{+} T cells was not a consequence of reduced proliferative capacity as we observed a similar number of cellular divisions (Fig. 4c). However, quantification of the number of cells at each division revealed a reduced frequency of *Pirb*$^{-/-}$ CD4^{+} T cells at each cell division compared to *WT* CD4^{+} T cells (Fig. 4c) suggesting that PIR-B regulates CD4^{+} IL-17a^{+} T cell survival. Consistent with this, we observed increased cell death occurring via apoptosis, as evidenced by significantly increased Caspase 3/7 activation in *Pirb*$^{-/-}$

$CD4^+$ T cells compared to *WT* $CD4^+$ T cells (Fig. 4d-i). Importantly, this was specific to Th17 polarizing conditions as no significant differences in cell death or Caspase 3/7 activation was observed in *Pirb*$^{-/-}$ $CD4^+$ T cells compared to *WT* $CD4^+$ T cells under Th1 polarizing conditions (Fig. 4d, e, g and h). To determine whether the effects of PIRB were in part associated with $CD4^+$ T cell development, we performed RNAseq on unstimulated *WT* and *Pirb*$^{-/-}$ $CD4^+$ naïve T cells. We identified a total of 12,343 genes expressed (RPKM > 5) by *WT* and *Pirb*$^{-/-}$ $CD4^+$ naïve T cells (*Table* 1; Fig. 5a). 11,463 genes (92.9% of totally expressed genes) were equally expressed (RPKM > 5; fold change > 1.0 and < 1.5) between *WT* and *Pirb*$^{-/-}$ $CD4^+$ naïve T cells and 880 differentially expressed genes (DEG) (19 genes upregulated, 861 genes down regulated) (*Table* 1; Fig. 5). Gene network and pathway analyses revealed no significant enrichment of T cell, cytokine and apoptosis, T cell receptor, apoptosis and cell cycle pathways or differences in core Th17 or mTOR signaling genes (*Table* 1; Fig. 5a-f). Consistent with this, we observed no differences in live dead staining, Annexin V expression or Caspase 3/7 activation between *WT* and *Pirb*$^{-/-}$ naïve $CD4^+$ T cells prior to stimulation indicating that the observed induction of cell death and apoptosis was associated with $CD4^+$ T-cell activation (Fig. 6). We next investigated the impact of PIR-B on early $CD4^+$ T cell activation and cell cycle entry under Th1 and Th17 polarizing conditions (Fig. 4j - o). We observed significantly fewer *Pirb*$^{-/-}$ $CD4^+$ T cells entering the G1 and S phase of cell cycle by comparison to *WT* $CD4^+$ T cells under Th17-polarizing conditions (Fig.4j, l, m and o); importantly the cell cycle G1 and S phase impairment of PIR-B deficient cells was restricted to Th17 and not Th1 differentiation (Fig. 4j-o). Cumulatively, these results indicate that PIR-B acts as a T cell intrinsic factor regulating the outgrowth of Th17 cells by modulating cell survival and cell cycle.

PIR-B suppresses mTORC1 signaling in CD4$^+$ T cells and modulates Th17 differentiation

mTORC1 signaling regulates CD4$^+$ T cell fate decisions [180], and in particular CD4$^+$ Th17 cell differentiation [181]. Indeed, stimulation of *WT* and *Pirb*$^{-/-}$ naïve CD4$^+$ T cells under Th17 conditions leads to rapid activation and phosphorylation of the downstream protein of mTORC1 signaling, S6 kinase (Fig. 7a). Notably, we observed hyper phosphorylation of S6 kinase in *Pirb*$^{-/-}$ CD4$^+$ T cells compared with *WT* CD4$^+$ T cells (Fig. 7a, b). Consistent with this, we observed increased levels of the mTOR activator, the GTP-bound form of the small GTPase Ras homologue enriched in brain (Rheb) in *Pirb*$^{-/-}$ CD4$^+$ T cells compared with *WT* CD4$^+$ T cells (Fig. 7c). The TSC1-TSC2 heterodimeric protein complex [182] stimulates TSC2 GAP activity towards Rheb converting Rheb-GTP (active form) to Rheb-GDP [182,183] (inactive form), which in turn limits mTORC1 activity [184]. TSC2-GAP activity on Rheb is regulated by extracellular signals through the phosphorylation of TSC1 and TSC2 by AKT, AMPK, GSK3, ERK, SGK, or RSK [182,184-187]. Notably, stimulation of *Pirb*$^{-/-}$ naïve CD4$^+$ T cells under Th17 polarizing conditions lead to significantly increased phosphorylation of MAPK, ERK compared with *WT* naïve CD4$^+$ T cells (Fig. 7d). Consistent with this, we observed significantly increased p-TSC2 in *Pirb*$^{-/-}$ naïve CD4$^+$ T cells compared with *WT* naïve CD4$^+$ T cells (Fig. 7e). To determine whether hyperactivated mTORC1 signaling may contribute to the heightened apoptosis and cell death in *Pirb*$^{-/-}$ naïve CD4$^+$ T cells, we assessed *Pirb*$^{-/-}$ naïve CD4$^+$ T cell proliferation under Th17 polarizing conditions in the presence of the mTORC1 inhibitor, rapamycin (Fig. 7f, g). Consistent with previous observations [188,189], Th17 differentiation of naïve *WT* CD4$^+$ T cells in the presence of increasing high concentrations of rapamycin that ablates mTOR activity led to a concentration-dependent reduction in the outgrowth of *WT* IL-17a$^+$ CD4$^+$ T cells (Fig. 8). Given the observation that abolition of mTORC1 activity with high concentration of rapamycin

inhibited both *WT* and *Pirb*$^{-/-}$ CD4^{+} T IL-17^{+} cell outgrowth under Th17 polarizing conditions, we next examined whether partial inhibition of mTORC1 signaling could diminish mTOR activity and enhance *Pirb*$^{-/-}$ CD4^{+} T IL-17^{+} cell frequency and reconstitute the *WT* phenotype. To do this we performed Th17 differentiation of naïve *WT* and *Pirb*$^{-/-}$ CD4^{+} T cells in the presence of 50pM rapamycin which promotes partial inhibition mTOR activity. Indeed, Th17 differentiation of naïve *Pirb*$^{-/-}$ CD4^{+} T cells in the presence of 50pM rapamycin significantly increased the frequency of *Pirb*$^{-/-}$ IL-17a^{+} CD4^{+} T cells compared with that observed in the absence of rapamycin (Fig. 7f, g). Notably, the frequency of *Pirb*$^{-/-}$ IL-17a^{+} CD4^{+} T cells in the presence of 50pM rapamycin was comparable to that observed in *WT* CD4^{+} T cells in the presence of vehicle (Fig. 7g). These studies suggest that tempering of mTORC1 activity in *Pirb*$^{-/-}$ naïve CD4^{+} T cells can enhance CD4^{+} Th17 differentiation and outgrowth and reconstitute the *WT* phenotype.

PIR-B's regulatory function is predominantly mediated via SHP-1/2 inhibition of kinase activity [91,175]. Given our demonstration of heightened kinase activity, ERK and p-TSC2 in *Pirb*$^{-/-}$ naïve CD4^{+} T cell under Th17 polarizing conditions we examined the requirement of SHP-1/2 function in *WT* and *Pirb*$^{-/-}$ naïve CD4^{+} T cell proliferation under Th17 polarizing conditions (Fig. 7h, i). Th17 differentiation in the presence of SHP-1/2 inhibitor led to a reduction in the number of *WT* and *Pirb*$^{-/-}$ IL-17a^{+}CD4^{+} T cells (Fig. 7h, i). Notably, at 25 μM SHP-1/2 inhibitor the number of *WT* CD4^{+} IL-17a^{+} cells were comparable to the number *Pirb*$^{-/-}$ CD4^{+} IL-17a^{+} cells generated in the absence of the inhibitor (Fig. 7i). Collectively, these studies suggest a role for SHP-1/2 and mTORC1 signaling in PIR-B-mediated regulation of CD4^{+} IL-17a^{+} cell maintenance.

PIR-B expression is upregulated on memory CD4$^+$ Th17 cells

Flow cytometry analyses identified significant expression of PIR-B on the surface of CD3$^+$ CD4$^+$ CD44^{high} CD62L$^+$ memory splenic CD4$^+$ T cells and limited expression on CD3$^+$ CD4$^+$ CD44^{low} CD62L$^-$ naïve T cells from *WT* C57BL6 mice (Fig. 9a). Notably, PIR-B$^+$ splenic memory CD3$^+$ CD4$^+$ CD44^{high} CD62L$^+$ CD4$^+$ cells were predominantly IL-17a$^+$ (Fig. 9b). Given the recent demonstration that tissue resident memory (TRM) CD4$^+$ T cells are drivers of chronic inflammation in models of colitis [48]; we next examined PIR-B expression on colonic TRM CD4$^+$ T cells from *Il10*$^{-/-}$ and *Pirb*$^{-/-}$*Il10*$^{-/-}$ colitic mice. Indeed, PIR-B was expressed on a subset of CD3$^+$CD4$^+$CD44$^+$CD69$^+$ LP T-cells in the colon of *Il10*$^{-/-}$ and *Pirb*$^{-/-}$*Il10*$^{-/-}$ mice (Fig. 9c). Furthermore, frequencies of TRM CD4$^+$ T cells (CD3$^+$CD4$^+$CD44$^+$ CD103$^+$CD69$^+$) were enriched in *Il10*$^{-/-}$ mice and *Rag*$^{-/-}$ mice which received *WT* CD4$^+$ T cells compared to *Pirb*$^{-/-}$*Il10*$^{-/-}$ mice and *Rag*$^{-/-}$ mice which received *Pirb*$^{-/-}$ CD4$^+$ T cells respectively (Fig. 9c, d). Analyses with *WT* and *Pirb*$^{-/-}$ IL-17a GFP mice revealed PIR-B was expressed on a subset of CD3$^+$CD4$^+$CD44$^+$IL-17a$^+$ lamina propria mononuclear cells (LPMCs) and that the frequency of CD3$^+$CD4$^+$CD44$^+$IL-17a$^+$ LPMCs in *Pirb*$^{-/-}$ IL-17a GFP mice was reduced compared with *WT* IL-17a GFP mice (Fig. 9e). These observations were validated *in silico* (GSE130446)[190] by the demonstration that TRM CD4$^+$ T IL-17a$^+$ cells identified by expression of *HOBIT, FCGR2B, BLIMP1*, *RORC, RORCA, IL23R, IL17A* expressed high levels of PIR-B relative to naïve or memory CD4$^+$ T cells from the draining lymph nodes of mice (Fig. 9f). To determine if PIR-B expression intrinsically impacted CD4$^+$ T cell survival and TRM formation; we performed competitive adoptive transfer experiments where equal numbers of congenically labeled *WT* (CD45.2$^+$) and *Pirb*$^{-/-}$ (CD45.1$^+$CD45.2$^+$) CD4$^+$ T cells were co-transferred into the same *Rag*$^{-/-}$ recipient. Tracking the donor T cell populations in the peripheral blood revealed greater number

of CD45.2$^+$ *WT* CD4$^+$ T cells than CD45.1$^+$CD45.2$^+$ *Pirb*$^{-/-}$ CD4$^+$ T cells (Fig. 9g, h). Furthermore, we observed significantly more CD45.2$^+$ *WT* CD4$^+$ T cells than CD45.1$^+$CD45.2$^+$ *Pirb*$^{-/-}$ CD4$^+$ T cells in the secondary lymphoid organs and intestinal tissue in the same recipient mice (Fig. 9i). Intriguingly, we observed a significant increase in the number of colonic TRM CD4$^+$ T cells (CD3$^+$ CD4$^+$ CD44$^+$ CD103$^+$) derived from the CD45.2$^+$ *WT* CD4$^+$ T cell donor population (Fig. 9j, k). Collectively, our data shows that PIR-B is expressed on a subset of TRM CD4$^+$ Th17 cells and confers a competitive advantage for T cell survival and TRM formation.

LILRB3 expression is associated with pathogenic IBD and memory Th17 responses

To identify if there was expression of the human homologue of PIR-B (LILRB3) in human CD4$^+$ IL-17A$^+$ cells, and a relationship between LILRB3$^+$ CD4$^+$ IL-17A$^+$ function and the IBD phenotype we next examined a RNA-seq dataset of ileal biopsy samples from a cohort of 259 pediatric individuals consisting of treatment naive CD and non-IBD patients (GSE57945)[191]. Principle component analysis of gene expression data between non-IBD (n = 42), pediatric ileal-involvement CD (iCD) (n = 162) and colonic-only involvement CD (cCD) (n = 55) patients revealed a distinct iCD transcriptome signature (Fig. 10a). Pathway enrichment analyses of DEGs revealed groups of related genes within the iCD gene signature associated with chemical carcinogenesis, IL-17 signaling pathway, cytokine-cytokine receptor interaction (*Table 2*). LILRB3 mRNA expression was significantly upregulated in cCD and iCD compared with Non-IBD controls (Fig. 10b). Stratification of the CD cohort based upon endoscopic severity, Ctl (non-IBD), cCD no microscopic / macroscopic inflammation and no deep ulcer (DU); cCD with macroscopic inflammation and no DU, Undetermined cCD, iCD with macroscopic inflammation with no DU and iCD macroscopic inflammation with DU [191,192] and principle component

analysis of gene expression between non-IBD and the CD clinical subgroups with LILRB3 expression (quartiles Q1, 0.59 – 1.44; Q2, 1.48 – 2.72; Q3, 2.73 – 5.47 and Q4, 5.56 – 73.39; RPKM values) revealed a distinct segregation of the LILRB3 signature within the iCD-DU group compared with other CD disease subgroups (Fig. 10c, *Table 3*). 40 / 65 patients in Q4 LILRB3^{hi} group were iCD-DU (Fig. 10d). Evaluation of the differentially expressed genes (ranked by p-value, n = 25 most upregulated and downregulated genes) between Q4 LILRB3^{hi} iCD-DU patients and LILRB3^{low} non-IBD patients identified significant enrichment of genes involved in cytokine-cytokine receptor interaction, IL-17a signaling and TNF signaling pathway (Fig. 10e, f, *Table 4*) suggesting an interaction between LILRB3 and Th17 responses in CD. Consistent with this, LILRB3 mRNA expression within the iCD-DU group positively correlated with IL1B, IL17A, IL21, TNF, IL6 and S100A9 in iCD-DU group; indicating that LILRB3 was related to mucosal inflammation and correlated with disease severity[193,194] (*Table 5*). To determine whether there was a direct association between LILRB3 and memory CD4^{+}Th17 cells in humans, we examined a RNA-seq dataset on sorted human memory CD4^{+} T cells (GSE140244)[190]. Strikingly, we revealed a subset of memory CD4^{+} T cells with high expression of LILRB3, and these LILRB3^{+} memory CD4^{+} T cells expressed heightened levels of genes that encode Th17 (*Rorc, Rora*) and TRM (*Hobit, Blimp1, KLRG1*) transcription factors (Fig. 10g). Assessment of biological function by analyzing the differentially expressed genes (ranked by p-value, n = 200) between LILRB3^{+} memory CD4^{+} T cells and LILRB3^{-} memory CD4^{+} T cells revealed that LILRB3^{+} memory CD4^{+} T cells were involved in Th17 inflammatory responses (Fig. 10h, i). To determine which signaling pathways were impacted in IBD development and the memory CD4^{+} T cell response, we performed gene set enrichment analysis on the most dysregulated genes from the GSE57945 and GSE140244 datasets. Analyses revealed positive

enrichment in hallmark gene sets for IL-6 STAT3 signaling, apoptosis, and mTORC1 signaling in LILRB3^{hi} CD patients and LILRB3^{+} memory CD4^{+} T cells relative to LILRB3^{low} non-IBD patients and LILRB3^{-} memory CD4^{+} T cells, respectively (Fig. 10j). Cumulatively, our *in silico* results reveals that LILRB3 is highly expressed on a subset of memory CD4^{+}Th17 cells in humans and links LILRB3^{+} memory CD4^{+} T cells with pathogenic Th17 inflammatory responses in IBD.

Discussion

Herein, we have demonstrated that PIR-B is a negative regulator of CD4^{+} T cells and loss of function inhibits the differentiation and outgrowth of TRM CD4^{+} Th17 cells, leading to the protection from CD4^{+} T-cell-dependent colitis. Mechanistically, we show that PIR-B is expressed by naïve and TRM CD4^{+} T-cells and that PIR-B intrinsically regulates CD4^{+} IL-17a^{+} T cell survival. PIR-B modulates ERK and TSC 1/2 heterodimeric protein complex activity restraining mTORC1 signaling and mTORC1-mediated CD4^{+} T cell apoptosis. Finally, we revealed PIR-B expression is upregulated in TRM CD4^{+} IL-17a^{+} cells and that the human ortholog, LILRB3, is associated with a severe pediatric CD phenotype (iCD-DU) and memory CD4^{+} IL-17A^{+} T cell responses in humans. Collectively, these studies reveal an intrinsic role for LILRB receptors in the regulation of the adaptive CD4^{+} T-cell inflammatory response and exacerbation of the TRM CD4^{+} IL-17a^{+} T cell driven CD phenotype.

By employing multiple models of T-cell dependent colitis we show that PIR-B deficiency leads to a loss of CD4^{+} IL-17a^{+} cells, reduced systemic IL-17a and protects mice from colitis. Corroborative evidence from clinical and experimental studies support an important role for

$CD4^+$ IL-$17a^+$ cells in the induction and exacerbation of IBD[38 195 162,163]. IL-17a can be produced by multiple T cell populations including $CD4^+$ αβ T-cells, γδ T cells, natural killer T cells, and non-T cell populations including innate lymphoid cells [196-199]. Studies employing the $CD4^+$ $CD45RB^{high}$ T-cell transfer model of colitis, supports a dominant role for IL-17-producing $CD4^+$ T cells in the augmentation of the colitic response [40]. Analyses of draining LN and colonic LP from *Il10*$^{-/-}$ mice with spontaneous colitis revealed that the IL-17a signal is predominantly derived from $CD3^+$ $CD4^+$ T cells. Further, our demonstration that transfer of *WT* and not *Pirb*$^{-/-}$ $CD4^+$ T cells to immunodeficient mice led to the generation of $CD4^+$ IL-$17a^+$ cells and colitis confirms that PIR-B expression in $CD4^+$ T cells is important for the $CD4^+$ T-cell driven colitic response. Previous studies have reported that germ free *Il10*$^{-/-}$ mice do not spontaneously develop colitis [200] indicating that the *Il10*$^{-/-}$ spontaneous of model of colitis is dependent on the intestinal microbiota. We cannot rule out a possible role for the microbiome in the protected colitic phenotype observed in *Pirb*$^{-/-}$*Il10*$^{-/-}$ mice. However, experiments using *WT* and *Pirb*$^{-/-}$ $CD4^+$ T cell transfer model of colitis and competitive transfer experiments in cohoused recipient *Rag*$^{-/-}$ mice revealed that loss of PIR-B expression specifically in the $CD4^+$ T compartment resulted in significant protection from colitis development and suppressed the survival of the donor naive $CD4^+$ T cells. Collectively, these experiments indicate that the phenotypic differences in the colitic phenotype are likely due to PIR-B's intrinsic regulation of the $CD4^+$ T cell compartment and not attributed to the microbiome.

We revealed high PIR-B expression on $CD3^+$ $CD4^+$ $CD44^{high}$ $CD62L^+$ memory $CD4^+$ IL-$17a^+$ cells. Genetic deletion of *Pirb* led to a marked reduction in the frequency of colonic LP $CD3^+CD4^+CD44^+$IL-$17a^+$ TRM T cells and protection from $CD4^+$ IL-$17a^+$ T-cell driven colitis.

Consistent with this, examination of an independent RNA-seq dataset demonstrated PIR-B expression in sorted TRM $CD4^+$ $IL\text{-}17a^+$ cells [190]. Collectively, these studies suggest that PIR-B regulates TRM $CD4^+$ $IL\text{-}17a^+$ T cells. We and others have identified increased frequency of $CD4^+$ TRM T cells with a proinflammatory Th17 phenotype in biopsy samples from active CD and UC patients compared with healthy control patients [47-50]. Furthermore, elevated levels of $CD69^+CD103^+$ $CD4^+$ TRM T cells have been associated with clinical flares [48]. Previous reports identified a link between $CD4^+$ TRM $IL\text{-}17A^+$ T cells and CD by utilizing biopsy specimens from CD patients undergoing surgery for severe, chronically active, or complicated disease [47].

The contribution of IL-17a to the IBD phenotype is complex [201]. IL-17a signaling has been shown to have beneficial effects on the integrity of the intestinal epithelial barrier and protect against the IBD phenotype [202]. Furthermore, biologics targeting the IL-17a cytokine led to worsening of intestinal inflammation in a subset of CD patients [76,203]. In contrast, targeting of the cytokines IL-6 and IL-23 or their receptors which are essential for the differentiation of pathogenic Th17 cells led to positive outcomes in treating IBD patients [81,204,205]. An emerging explanation to reconcile these divergent findings is that IL-17a is produced by multiple cell populations including $CD4^+$ Th17 cells and ILC3s. ILC3-derived IL-17a in combination with IL-22 is thought to promote intestinal epithelial barrier function and protect against colitis, whereas $CD4^+$ T cell derived IL-17a with cytokines such as TNFα and IFNγ are proinflammatory and drive intestinal inflammation and colitis [206]. Our analyses of RNA-seq datasets from pediatric CD patients at diagnosis revealed the highest expression of LILRB3 to be predominantly restricted to the endoscopic severe subgroup (iCD-DU) and that LILRB3 mRNA expression in iCD-DU individuals positively correlated with mucosal inflammation and disease severity.

Analyses of high LILRB3 expression individuals identified significant enrichment of genes involved in the IL-17A signaling pathway in clinical distinct group iCD-DU. These studies support the notion that PIRB^{+} TRM CD4^{+} T cells may play a critical role in Th17 inflammatory response and the onset of severe mucosal injury observed in iCD-DU phenotype. Cumulatively these studies suggest that specific targeting of CD4^{+} Th17 cells would have a greater beneficial clinical outcome for IBD patients than broadly targeting the IL-17a signaling pathway. We provide multiple lines of evidence that PIR-B is expressed on CD4^{+} Th17 cells. Mining of the Immgen dataset (GSE109125) reveal no expression of PIR-B on ILC3 cells suggesting that targeting on the PIR-B/LILRB3 pathway may permit selective targeting of CD4^{+} Th17 versus ILC3 cells [207].

In vitro studies revealed a link between PIR-B deficiency, increased CD4^{+} T cell apoptosis and hyperactivation of mTORC1 signaling. Our demonstration that rapamycin led to reconstitution of the *WT* phenotype in *Pirb*$^{-/-}$ CD4^{+} IL-17a^{+} T cells suggests that PIR-B negatively regulates CD4^{+} IL-17a^{+} T cell apoptosis via suppression of mTORC1 signaling. mTORC1 regulates CD4^{+} T cell exit from quiescence and determination of CD4^{+} T cell fate [208], in particularly CD4^{+} Th17 differentiation [189]. mTORC1 functions as a CD4^{+} T cell-intrinsic rheostat, with continual mTORC1 activity required to sustain CD4^{+} Th17 differentiation, however oscillation of mTORC1 activity to a hypo- or hyper-activation status perturbs that differentiation process and triggers cell apoptosis and death. Consistent with this, diminished mTORC1 activation and signaling, such as that observed by genetic deletion of mTOR or S6 kinase results a failure of naïve CD4^{+} T cells to differentiate into Th17 cells [209,210] [211]. Conversely, exaggerated mTORC1

signaling as observed by deletion of TSC1 and loss of the TSC1-TSC2 heterodimeric protein inhibitory complex also results in impaired $CD4^+$ T cell survival[212].

The formation and stabilization of the TSC1-TSC2 heterodimeric protein inhibitory complex stimulates TSC2 GAP activity and conversion of Rheb-GTP (active form) to Rheb-GDP[183] (inactive form) switching mTOR into a catalytically inactive state and diminishing mTORC1 activity. The establishment and maintenance of the TSC1-TSC2 protein complex is tightly regulated by serine / threonine kinase activity. Phosphorylation of serine and threonine residues in TSC2 by kinases such as Akt and Erk destabilizes the TSC1-TSC2 protein complex leading to TSC1-TSC2 dissociation and loss of TSC2-dependent activity. As a consequence, mTOR switches into a catalytically active state and induction of mTORC1 activity[182,184-187]. We revealed heightened p-ERK and p-TSC2 and increased mTORC1 signaling in *Pirb*$^{-/-}$ naïve $CD4^+$ T cells under Th17 polarizing conditions. Furthermore, restraining of mTORC1 activity using rapamycin lead to increase in *Pirb*$^{-/-}$ $CD4^+$ Th17 cell survival and the *WT* phenotype.

The PIR-B/LILRB ITIM domains are known to bind and activate intracellular phosphatases, including SHP-1 and SHP-2, which inhibit activating-type receptor-mediated signaling [175,213]. We speculate that activation of PIR-B promotes the recruitment and binding of SHP-1/2 phosphatases to the PIR-B ITIM domain. Activation of SHP-1/2 leads to dephosphorylation of p-ERK and loss of ERK-dependent regulation of the mTORC1 inhibitory complex (TSC1-TSC2), triggering hyperactivation of mTORC1 signaling in $CD4^+$ T cells. Herein, we show significantly increased p-ERK and p-TSC2 in *Pirb*$^{-/-}$ naïve $CD4^+$ T cells under Th17 polarizing conditions. Previous studies have reported that SHP-2 suppresses $CD4^+$ T cell activation by mediating

inhibitory receptors signals including those from CTLA-4 and PD-1 [214,215]. Overexpression of catalytically inactive SHP-2 in T cells promoted T cell differentiation [216], and inhibition of SHP-2 signaling in mice- and human- $CD4^+$ T cells decreased IL-17a/IL-17f production [217]. We predict that PIRB may act in a similar fashion to other T cell inhibitory receptors such as CTLA-4 and PD-1 to temper $CD4^+$ T cell activation and Th17 differentiation.

Our work revealed that PIR-B expression on $CD4^+$ T cells is highly modular. Specifically, we observed limited expression of PIR-B on naïve $CD4^+$ T cells and robust expression of PIR-B on a subset of memory $CD4^+$ Th17 cells. Memory T cells can quickly undergo clonal expansion to mediate proinflammatory responses; these cells are marked by unique epigenetic, transcriptional and protein expression levels that allow for these hallmark memory responses. We speculate that PIR-B provides an additional regulatory mechanism that can control the effector responses which are mediated by memory T cells and importantly ensure this immune compartment can only contribute to the proinflammatory response once the proper signaling threshold is reached. This is consistent with recent work that identified inhibitory receptor signaling was required for the generation and sustainment of memory T cell precursors.[218] Intriguingly, our work identified that PIR-B is only expressed on a fraction of naïve $CD4^+$ T cells. Current literature about memory responses suggests that naïve T cells which will give rise to memory T cells are imprinted early on during T cell development, thus these memory T cell precursors can themselves be identified by discrete transcriptional and protein expression profiles[219]. Presumably, the PIR-B expression we observed in the naïve $CD4^+$ T cell pool might be indicative of precursor cells which will give rise to the memory $CD4^+$ Th17 cells which reside in the colon. Furthermore, we speculate that

PIR-B expression on memory precursor and differentiated memory $CD4^+$ T cells is required to modulate activating cues that feed into mTORC1 signaling and ultimately promote cell survival.

In conclusion, we show that PIR-B is expressed on TRM $CD4^+$ Th17 cells and controls $CD4^+$ Th17–inflammatory responses, and that loss of PIR-B activity leads to inhibition of $CD4^+$ Th17 regulated inflammation and colitis. The demonstration of PIR-B expression on memory $CD4^+$ Th17 cells and a requirement for this pathway in $CD4^+$ Th17-mediated colitic development has promising implications for targeted therapy in IBD. Biologics focused on inhibitory receptors have been shown to be efficacious for treatment of T-cell-mediated diseases including cancer and autoimmunity. Our data supports the notion that targeting PIR-B could regulate pathogenic $CD4^+$ Th17 cells and provide a new therapeutic approach for treatment of TRM $CD4^+$ Th17-driven diseases such as IBD.

Methods

Mice. Male and female, 5 to 10 week *Il10*$^{-/-}$ mice (C57BL/6) and IL-17a GFP mice (C57BL/6) were obtained from Jackson Laboratories (USA)**.** Male and female, 5 to 10 week *Pirb*$^{-/-}$ mice (C57BL/6) were kindly provided by Dr. Hiromi Kubagawa [102]**.** Male and female, 5 to 10 week *Rag*$^{-/-}$ mice (C57BL/6) were kindly provided by Dr. Grace Chen. To generate the *Pirb*$^{-/-}$*Il10*$^{-/-}$ mice (C57BL/6), *Pirb*$^{-/-}$ mice (C57BL/6) were intercrossed with *Il10*$^{-/-}$ mice (C57BL/6). C57BL/6 strain purity was confirmed (> 99%) by DartMouse congenic analyses. To generate *Pirb*$^{-/-}$ IL-17a GFP mice (C57BL/6), *Pirb*$^{-/-}$ mice (C57BL/6) were intercrossed with IL-17a GFP mice (C57BL/6). All mice strains were co-housed in the same room.

Experimental colitis models. For the *Il10*$^{-/-}$ spontaneous model of colitis; co-housed *Il10*$^{-/-}$, *Il10*$^{+/-}$ and *Pirb*$^{-/-}$*Il10*$^{-/-}$ mice were monitored for colitis development from 7 weeks of age. Euthanasia and postmortem analyses were performed at 15 weeks of age. For the αCD3-mediated model of intestinal enteropathy, 7 to 10 week old co-housed mice were treated twice intraperitoneally with 15 μg αCD3 (145-2C11, Thermo fisher) 48 hours apart. Euthanasia and postmortem analyses were performed 4 hours after the second injection. For the CD4^{+}CD45RB^{hi} T-cell transfer model colitis, splenic naïve CD4^{+} T cells from *WT* and *Pirb*$^{-/-}$ donors were enriched by red blood cell lysis and magnetic bead depletion (Biolegend). A total of 400,000 naïve CD4^{+} T cells were transferred intraperitoneally into co-housed *Rag*$^{-/-}$ mice. Euthanasia and postmortem analyses were performed 32 days after injection of cells. The colitic mice were weighed twice every week to measure body weight and lymph nodes, spleen, small intestine, and colonic tissue were collected for analysis at the end of the experiment. Weight changes were calculated as a percentage of weight at the start of the experiment (Day 0). Clinical disease was

scored based on prior descriptions [220]. In brief mice were graded on a scale of 0 to 5 by assessment of symptoms including bump on nose, pilar erecti, rectal prolapse, anal bleeding, decreased activity, diarrhea, hunched back, excreted perianal mucus, shrunken eyes, and dehydration. For all animal experiments, mice that lost ≥ 20% of its body weight (relative to weight at the start of the experiment) were euthanized in accordance with IACUC protocols.

Competitive CD4$^+$ T cell Transfer. We crossed *Pirb*$^{-/-}$ (CD45.2$^+$) with *WT* mice that express the congenic CD45.1 allele to generate congenically labeled *Pirb*$^{-/-}$ (CD45.1$^+$CD45.2$^+$) mice. Splenic naïve CD4$^+$ T cells from *WT* (CD45.2$^+$) and *Pirb*$^{-/-}$ (CD45.1$^+$CD45.2$^+$) donors were enriched by red blood cell lysis and magnetic bead depletion (Biolegend). A total of 800,000 naïve CD4$^+$ T cells (400,000 *WT* (CD45.2$^+$) and 400,000 *Pirb*$^{-/-}$ (CD45.1$^+$CD45.2$^+$)) were transferred intraperitoneally into co-housed *Rag*$^{-/-}$ mice. Blood was collected every 7 days after injection of cells and flow cytometry and intracellular cytokine staining was performed as described below. Euthanasia and postmortem analyses were performed 32 days after injection of cells and flow cytometry and intracellular cytokine staining was performed as described below.

Histology. Harvested tissues were washed with PBS, swiss rolled and fixed overnight in 4% paraformaldehyde. Paraffin embedded tissue were stained with hematoxylin and eosin and analyzed by bright field microscopy. Histological scoring was performed on ascending, transverse and descending colon and rectum segments as previously described [221].

***In vivo* cytokine capture assay.** Systemic TNF-α, IFN-γ, and IL-17a levels were quantified in the serum of mice [222]. Briefly, 10 μg of biotinylated detection antibodies against TNFa (clone

TN3), IFNy (clone R4-6A2) and IL-17a (eBio17B7) were injected intravenously into mice and twenty-four hours later serum collected. Luminescent ELISA's were performed using plates coated with a secondary capture antibody as previously described.

***In vitro* CD4$^+$ T cell culture.** Naïve CD4$^+$ T cells were isolated from spleens using the naïve CD4$^+$ T cell isolation kit (Biolegend) and were stimulated with plate bound αCD3 (1 μg/mL) and soluble αCD28 (2 μg/mL) alone or in the presence of polarizing cytokines and antibodies. For Th1 polarizing conditions cell were cultured in the presence of IL-12 (10 ng/mL) cytokine and neutralizing antibody αIL-4 (1 μg/mL). For Th17 polarizing conditions cell were cultured in the presence of IL-6 (20 ng/mL), IL-23 (20 ng/mL), and TGFβ1 (2 ng/mL) cytokines and neutralizing antibodies αIFN-γ (10 μg/mL) and αIL-4 (1 μg/mL). Cells were cultured in supplemented RPMI media containing 10% FBS, 2% penicillin/streptomycin, and 50 μM 2-mercaptethanol. To assess proliferation, naïve CD4$^+$ T cells were labeled with 5 μM CTV in 0.2% FBS for 20 minutes. For chemical inhibitor experiments, either rapamycin (Sigma Aldrich) (50 pM) or SHP-1/2 inhibitor (NSC-87877, Millipore Sigma) (25 μM) were added at the beginning of the experiment.

Flow cytometry and intracellular cytokine staining. Single cell suspensions of spleen, mesenteric lymph nodes, and colon lamina propria cells were surface stained *ex vivo* with fluorescent antibodies to T cell markers (CD3, CD4, CD62L, CD44, CD69, CD103, CD45.1, CD45.2) and for PIRA/B (6C1). For cytokine staining, cells were *ex vivo* stimulated at 37°C for 4 hours with PMA (50 ng/mL), Ionomycin (1 mg/mL), and Brefeldin A. Cells were then processed and stained using an intracellular cytokine staining kit (BD Biosciences) according to

manufacturer's instructions with IFN-γ and IL-17a. For apoptosis staining, the dead cell apoptosis kit and live/dead viability assay (Thermo fisher) was followed according to manufacturer's instructions. For activated Caspase 3/7 staining, the Caspase 3/7 kit (Thermo fisher) was followed according to manufacturer's instructions. To assess cell cycling and entry into G1, Pyronin Y (Sigma Aldrich) staining was performed as previously described[223]. To assess cell cycling and entry into S phase, the Edu flow cytometry kit (Sigma) was followed according to manufacturer's instructions. All flow cytometry samples were acquired on an Novocyte (ACEA Biosciences) and data were analyzed using FlowJo (Tree Star, San Carlos, CA) and Prism (GraphPad Software). Absolute cell numbers were calculated using Precision Count Beads (Biolegend) according to the manufacturer's instructions.

Lamina propria mononuclear cell isolation. Colons were cut longitudinally and incubated in HBSS with 5 mM EDTA at 37°C for 30 minutes before vortexing to remove epithelial cells. The remaining tissues were minced and digested with 2.4 mg/ml collagenase A (Roche), and 0.2 mg/mL DNase I (Roche) at 37°C for 45 minutes. After removal of tissue debris, cells suspended in 44% Percoll were loaded above 67% Percoll before centrifugation. Colonic lamina propria cells were collected from the interface between 44% and 67% Percoll.

Western Blot and Immunoprecipitation. $CD4^+$ T cells were lysed in protein lysis buffer (10% glycerol, 20 mM Tris HCl [pH 7], 137 mM NaCl, 2 mM EDTA, and 1% NP-40) supplemented with proteinase inhibitor cocktail (Thermo fisher) and PhoSTOP phosphatase inhibitors (Roche). Protein lysates were cleared of insoluble material through centrifugation, and the resulting protein lysates were subjected to SDS-PAGE. Proteins were wet transferred to 0.2 mm

nitrocellulose membranes (Thermo fisher), which were blocked using 3% BSA in 1% TBST buffer for 1 hour at room temperature. Membranes were incubated overnight using the following primary antibodies: α-β-actin, α-S6 kinase, α-pS6 kinase, α-TSC2, α-pTSC2, α-ERK1/2, and α-pERK1/2. Primary antibodies were used at a 1:1,000 dilutions in blocking buffer. Membranes were washed in TBST and incubated with the secondary antibody, goat α-rabbit-HRP, at a 1:2,000 dilution in blocking buffer. Rheb-GTP was immunoprecipitated using the Rheb activation assay kit (NewEast Biosciences). Immunoprecipitation was performed according to manufacturer's description. Protein bands were visualized following exposure of the membranes to ECL substrate solution (Thermo fisher) and quantified by densitometry analysis using Image Studio (Licor) software.

Quantitative Real-time PCR. RNA was isolated from sorted naïve $CD4^+$ T cells using the Quick RNA microprep kit (Zymo Research). cDNA was generating by reverse transcription using SuperScript II (Invitrogen) ad Oligo-dT (Invitrogen) according to manufactures instructions. qPCR was performed for *Pirb* and murine *Gapdh* using specific primers designed in Snapgene (Insightful Science) software. Samples were normalized to housekeeping expression of *Gapdh* using the $2^{-\Delta Ct}$ method.

RNA-seq Analysis

RNA was isolated from sorted naïve $CD4^+$ T cells using the Quick RNA microprep kit (Zymo Research). RNA was submitted to the University of Michigan Advanced Genomics Core for library preparation and sequencing (Illumina). Raw reads were aligned to the reference mm9 mouse genome (GRCm38) using Hisat-build pipeline. Relative gene expression was quantified

using featureCounts function from the subread-2.0.0 package. Pseudogenes, RIKEN cDNA sequences, and immunoglobulin variable genes were removed from downstream analysis of expressed genes. Downstream analysis was performed in R (R Core Team, Vienna, Austria) where the read counts were analyzed in IDEP 9.1 and DESeq was used to identify the differentially expressed genes (DEGs)[224]**.** DEGs were identified with an adjusted p value <= 0.05 and at least ≥ ± 1.5-fold reads per kb of transcript, per million mapped reads (RPKM) and heat map was generated using Python (Python Software Foundation, Wilmington, Del) on the normalized scale. KEGG pathway analysis was used to identify important pathways altered by differentially regulated genes. Statistical analysis was performed using SPSS 17.0. The Frequencies procedure was used for the LILRB3 quartile analysis. χ^2 test was used to assess the association of CD categories with 4 LILRB3 quartiles. The association of LILRB3 with Th17 pathways associated genes IL1B, IL17A, IL21, TNF, IL6 and S100A9 was evaluated by Pearson's correlation as quantitative variables.

Additional RNA-seq data analyses were obtained from the NCBI GEO database, with accession numbers GSE130446, GSE57945, and GSE140244**.** With the RISK Study (GSE57945); we examined a RNA-seq dataset of ileal biopsy samples from a cohort of 259 pediatric individuals consisting of treatment naive CD and non-IBD patients. Principle component analysis of differentially expressed genes between non-IBD (n = 42), pediatric ileal-involvement CD (iCD, n = 162) and colonic-only involvement CD (cCD, n = 55) patients revealed a distinct CD transcriptome signature (results not shown). We next stratified the CD cohort based upon endoscopic severity, NL, cCD no microscopic / macroscopic inflammation and no deep ulcer (DU); cCD with macroscopic inflammation and no DU; iCD with macroscopic inflammation with no DU and iCD macroscopic inflammation with DU[191,192]. LILRB3 quartiles were

established based on RPKM values; quartiles Q1 (0-25%), 0.59 – 1.44; Q2 (26-50%), 1.48 – 2.72; Q3 (51-75%), 2.73 – 5.47 and Q4 (76-100%), 5.56 – 73.39). Differential expression was defined with a significant change in expression by limma[225]. Heatmaps of gene expression were generated using Morpheus (https://software.broadinstitute.org/morpheus/) and Phantasus[226]. Gene ontology analysis was performed using Enrichr and Gene Set Enrichment Analysis (GSEA).

Statistics

Statistical parameters are defined in the figure legends. Data are presented as mean ± SEM. Data was considered significant at $p < 0.05$. Comparisons between 2 groups were made using a t test. Comparisons between more than 2 group were made using 2-way ANOVA and where appropriate were followed with a Dunnett's Multiple Comparison Test or Sidak's Multiple Comparison Test. Statistical analysis was performed in Prism (GraphPad Software).

Study Approval

All animal studies were approved by the IACUC of the University of Michigan, Ann Arbor, MI and performed in accordance with University guidelines.

Acknowledgements

We would like to acknowledge members of the Divisions of Allergy and Immunology and Immunobiology at Cincinnati Children's Hospital Medical Center, Mary H. Weiser Food Allergy Center and Division of Experimental Pathology at the University of Michigan Medicine for thoughtful discussions. This work was supported by National Institutes of Health grants

DK073553, DK090119, DK125007, DK099222, AI138177, AI112626, and AI007413; Food Allergy Research & Education (FARE); Department of Defense grant W81XWH-15-1-051730; M-FARA; and the Mary H. Weiser Food Allergy Center supported (to S.P.H.).

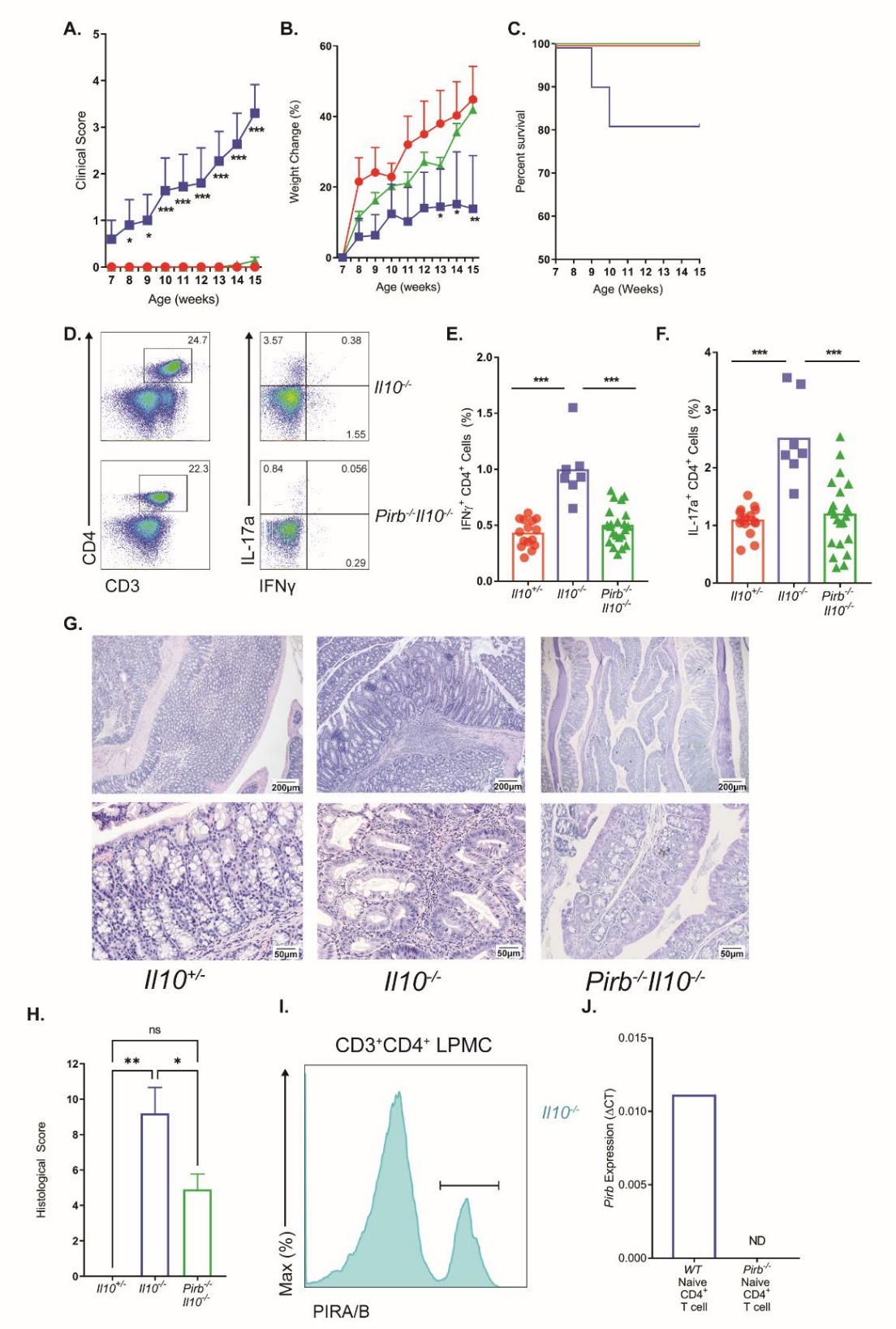

Figure 2-1 Loss of *Pirb* Suppresses the Development of Spontaneous Colitis in *Il10*$^{-/-}$ Mice.

(A) Clinical score, (B) % Body weight change (relative to weight at start of experiment), and (C) Percent survival rate of *Il10*$^{+/-}$(red), *Il10*$^{-/-}$(blue), *Pirb*$^{-/-}$*Il10*$^{-/-}$(green) mice corresponding to age (*Il10*$^{+/-}$ *n*= 18, *Il10*$^{-/-}$ *n*= 11, *Pirb*$^{-/-}$*Il10*$^{-/-}$ *n*= 22). (D) Flow cytometry analysis of CD4^{+}IFN-γ^{+} and CD4^{+}IL-17a^{+} T cells in the mLN of mice at 15 weeks of age. Percentage (%) of (E) CD4^{+}IFN-γ^{+} or (F) CD4^{+}IL-17a^{+} T cells in the mLN of mice at 15 weeks of age (*Il10*$^{+/-}$ *n*= 15, *Il10*$^{-/-}$ *n*= 7, *Pirb*$^{-/-}$*Il10*$^{-/-}$ *n*= 22). (G) Representative image of colon histology (H&E staining) from *Il10*$^{-/-}$ and *Pirb*$^{-/-}$*Il10*$^{-/-}$ mice. Top row 4x magnification (Scale bar represents 200 µm), bottom row 20x magnification (Scale bar represents 50 µm). (H) Colon histological scoring from *Il10*$^{+/-}$, *Il10*$^{-/-}$, *Pirb*$^{-/-}$*Il10*$^{-/-}$ mice at 15 weeks of age (*Il10*$^{+/-}$ *n*= 4, *Il10*$^{-/-}$ *n*= 10, *Pirb*$^{-/-}$*Il10*$^{-/-}$ *n*= 22). (I) Representative flow cytometry histogram of the expression of PIRA/B on CD3^{+}CD4^{+} T cells isolated from colonic lamina propria of *Il10*$^{-/-}$ mice. (J) *Pirb* mRNA expression in splenic naïve CD4^{+} T cells from *WT* and *Pirb*$^{-/-}$ mice (*WT* *n*= 3, *Pirb*$^{-/-}$ *n*= 3). Data are presented as mean ± SEM. Statistical analysis was performed using two-way analysis of variance ($p < 0.05$) followed by Dunnett's Multiple Comparison Test (A, B) or unpaired t test (E, F, H). *p <0.05, **p <0.01, ***p <0.001. Data shown in (A), (B), (C), (E), (F), (H) encompasses three independent experiments.

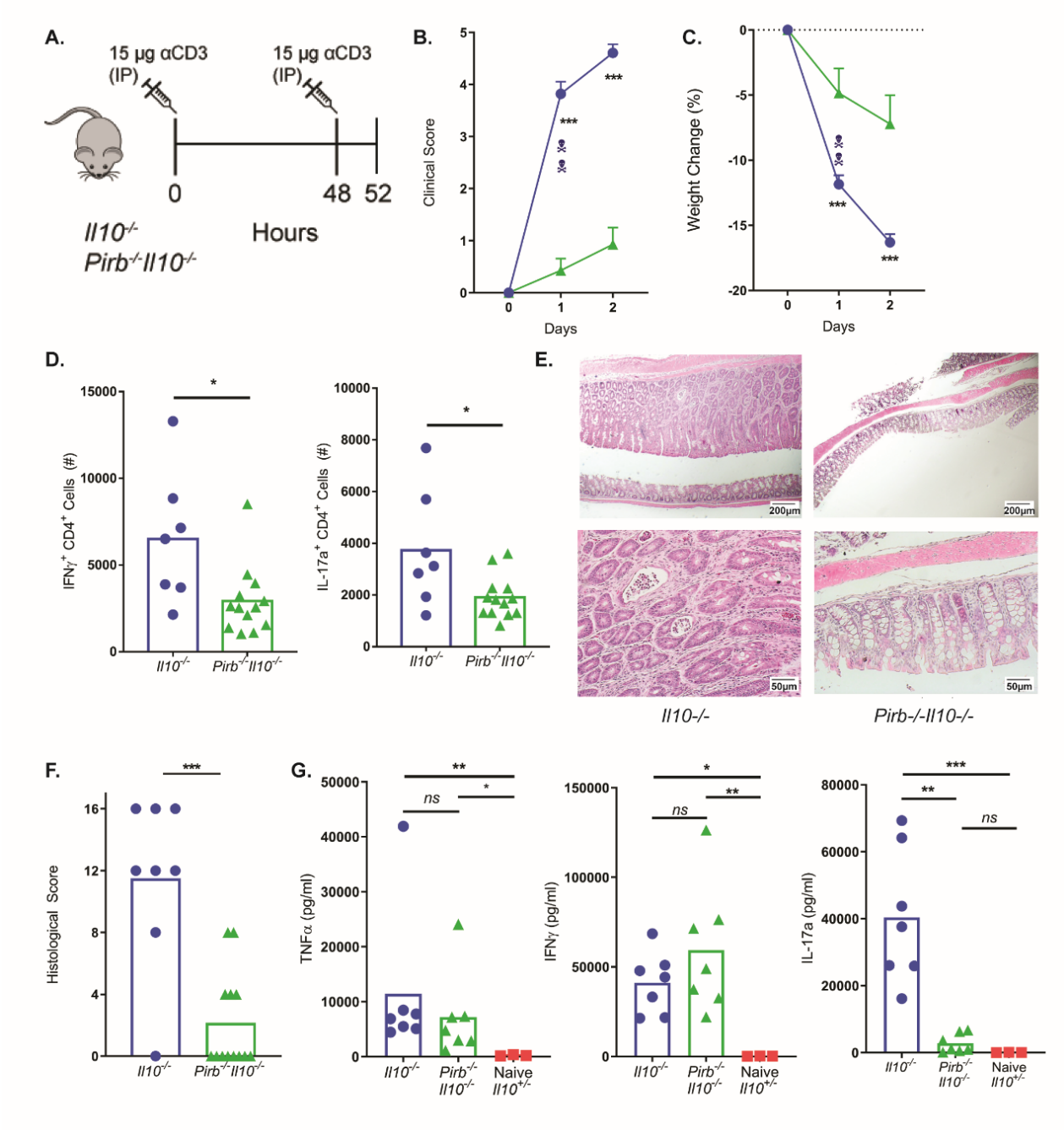

Figure 2-2 *Pirb* Deficient CD4^{+} T cells Fail to Induce Acute Intestinal Enteropathy.

(A) Schematic representation of αCD3 treatment protocol. (B) Clinical score, (C) % Body weight change (relative to weight before initial αCD3 injection) of *Il10*$^{-/-}$ and *Pirb*$^{-/-}$*Il10*$^{-/-}$ mice following αCD3 injection (*Il10*$^{-/-}$*n*= 14, *Pirb*$^{-/-}$*Il10*$^{-/-}$*n*= 14). (D) Cell counts (#) of CD4^{+}IFN-γ^{+} and CD4^{+}IL-17a^{+} T cells in the mLN of mice (*Il10*$^{-/-}$*n*= 7, *Pirb*$^{-/-}$*Il10*$^{-/-}$*n*= 13). (E) Representative image of colon histology (H&E staining) from *Il10*$^{-/-}$ and *Pirb*$^{-/-}$*Il10*$^{-/-}$ mice. Top row 4x magnification (Scale bar represents 200 μm), bottom row 20x magnification (Scale bar represents 200 μm). (F) Colon histological scoring from *Il10*$^{-/-}$and *Pirb*$^{-/-}$*Il10*$^{-/-}$ mice (*Il10*$^{-/-}$*n*= 8, *Pirb*$^{-/-}$*Il10*$^{-/-}$*n*= 13). (G) Systemic levels of TNF-α IFN-γ, and IL-17a in serum of *Il10*$^{-/-}$ and *Pirb*$^{-/-}$ *Il10*$^{-/-}$ mice at 52 hours following aCD3 injection, Cytokine levels were detected by IVCCA (*Il10*$^{-/-}$*n*= 7, *Pirb*$^{-/-}$*Il10*$^{-/-}$*n*= 7, *Il10*$^{+/-}$ *n*= 3). Cytokine levels were detected by IVCCA. Data are presented as mean ± SEM. Statistical analysis was performed using two-way analysis of variance ($p < 0.05$) followed by Sidak's Multiple Comparison Test (B), (C) or unpaired t test (D), (F), (G). *p <0.05, **p <0.01, ***p <0.001. Data shown encompasses three independent experiments.

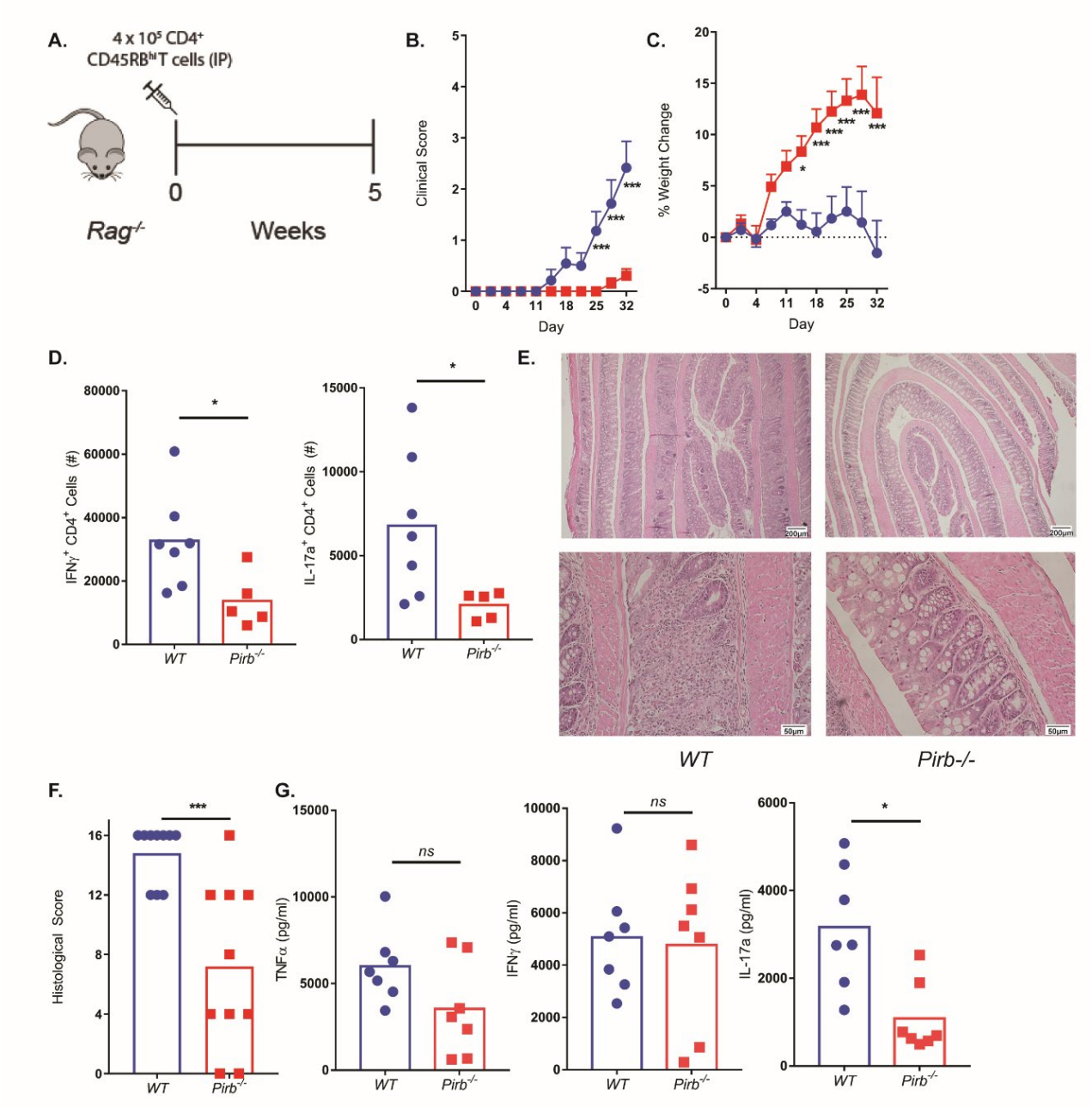

Figure 2-3 *Pirb* Deficient CD4$^+$ T cells Fail to Induce Chronic Colitis.

(A) Schematic representation of T cell transfer protocol. *Rag*$^{-/-}$ mice received either 400,000 CD4^{+} CD45RB^{hi} *WT* (blue) or *Pirb*$^{-/-}$ (red) T cells. (B) Clinical score, (C) % Body weight change (relative to weight at start of experiment) of *Rag*$^{-/-}$ mice following T cell injection (*WT n*= 13, *Pirb*$^{-/-}$ *n*= 14). (D) Cell counts (#) of CD4^{+}IFN-γ^{+} and CD4^{+}IL-17a^{+} T cells in the mLN of mice (*WT n*= 7, *Pirb*$^{-/-}$ *n*= 5). (E) Representative image of colon histology (H&E staining) from *Rag*$^{-/-}$ mice. Top row 4x magnification (Scale bar represents 200 μm), bottom row 20x magnification (Scale bar represents 50 μm). (F) Colon histological scoring from *Rag*$^{-/-}$ mice (*WT n*= 10, *Pirb*$^{-/-}$ *n*= 10). (G) Systemic levels of TNF-α, IFN-γ, and IL-17a in serum of *Rag*$^{-/-}$ mice at 5 weeks after T cell transfer (*WT n*= 7, *Pirb*$^{-/-}$ *n*= 7). Cytokine levels were detected by IVCCA. Data are presented as mean ± SEM. Statistical analysis was performed using two-way analysis of variance ($p < 0.05$) followed by Sidak's Multiple Comparison Test (B), (C) or unpaired t test (D), (F), (G). *p <0.05, **p <0.01, ***p <0.001. Data shown encompasses three independent experiments.

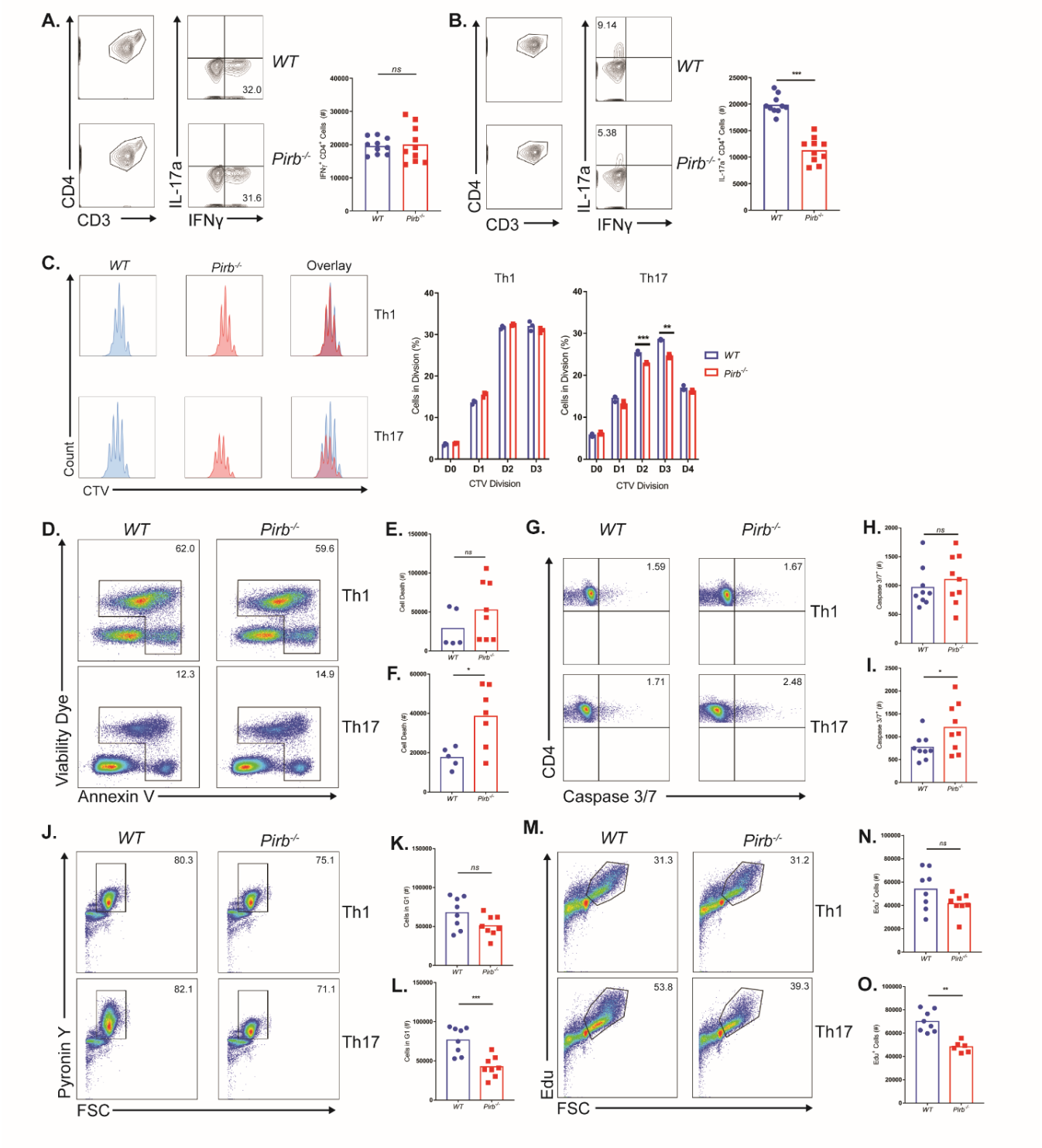

Figure 2-4 *Pirb*$^{-/-}$ CD4^{+} T cells have impaired survival and differentiation under Th17 polarizing conditions.

Gating strategy and cell counts (#) of *WT* and *Pirb*$^{-/-}$ CD4^{+} T cells cultured under (A) Th1 polarizing and (B) Th17 polarizing conditions for 72 hours (*WT n*= 10, *Pirb*$^{-/-}$ *n*= 10). (C) Representative plots of Cell Trace Violet staining on Th1 polarized (top) and Th17 polarized (bottom) CD4^{+} T cells (left). Percentages of cells within each division (right) (*WT n*= 3, *Pirb*$^{-/-}$ *n*= 3). (D) Representative plots of the Annexin V expression and Viability in CD4^{+} T cells activated under Th1 (top) and Th17 (bottom) conditions. Counts of dead (Annexin^{+} or Viability Dye^{+}) CD4^{+} T cells cultured under (E) Th1 conditions or (F) Th17 conditions (*WT n*= 5, *Pirb*$^{-/-}$ *n*= 8). (G) Representative plots of the expression of active Caspase 3/7 in CD4^{+} T cells activated under Th1 (top) and Th17 (bottom) conditions for 4 hours. Frequency of activated Caspase 3/7^{+} CD4^{+} T cells cultured under (H) Th1 polarizing conditions or (I) Th17 polarizing conditions for 4 hours (*WT n*= 9, *Pirb*$^{-/-}$ *n*= 9). (J) Representative plots showing G1 cell cycle entry via the expression of Pyronin Y in CD4^{+} T cells under Th1 (top) and Th17 (bottom) polarizing conditions for 12 hours. Frequency of CD4^{+} T cells which have entered G1 (Pyronin Y^{+}) under (K) Th1 conditions or (L) Th17 conditions for 12 hours (*WT n*= 8, *Pirb*$^{-/-}$ *n*= 8). (M) Representative plots showing the incorporation of Edu in CD4^{+} T cells under Th1 (top) and Th17 (bottom) conditions for 28 hours. Frequency of CD4^{+} T cells which have entered S phase (Edu^{+}) under (N) Th1 conditions or (O) Th17 conditions for 28 hours (*WT n*= 8, *Pirb*$^{-/-}$ *n*= 6). Data are presented as mean ± SEM. Statistical analysis was performed using unpaired t test. *p <0.05, **p <0.01, ***p <0.001. Data shown in (A), (B), (E), (F), (H), (I), (K), (L), (N), and (O) encompasses three independent experiments. Data shown in (C) are from one experiment representative of three independent experiments.

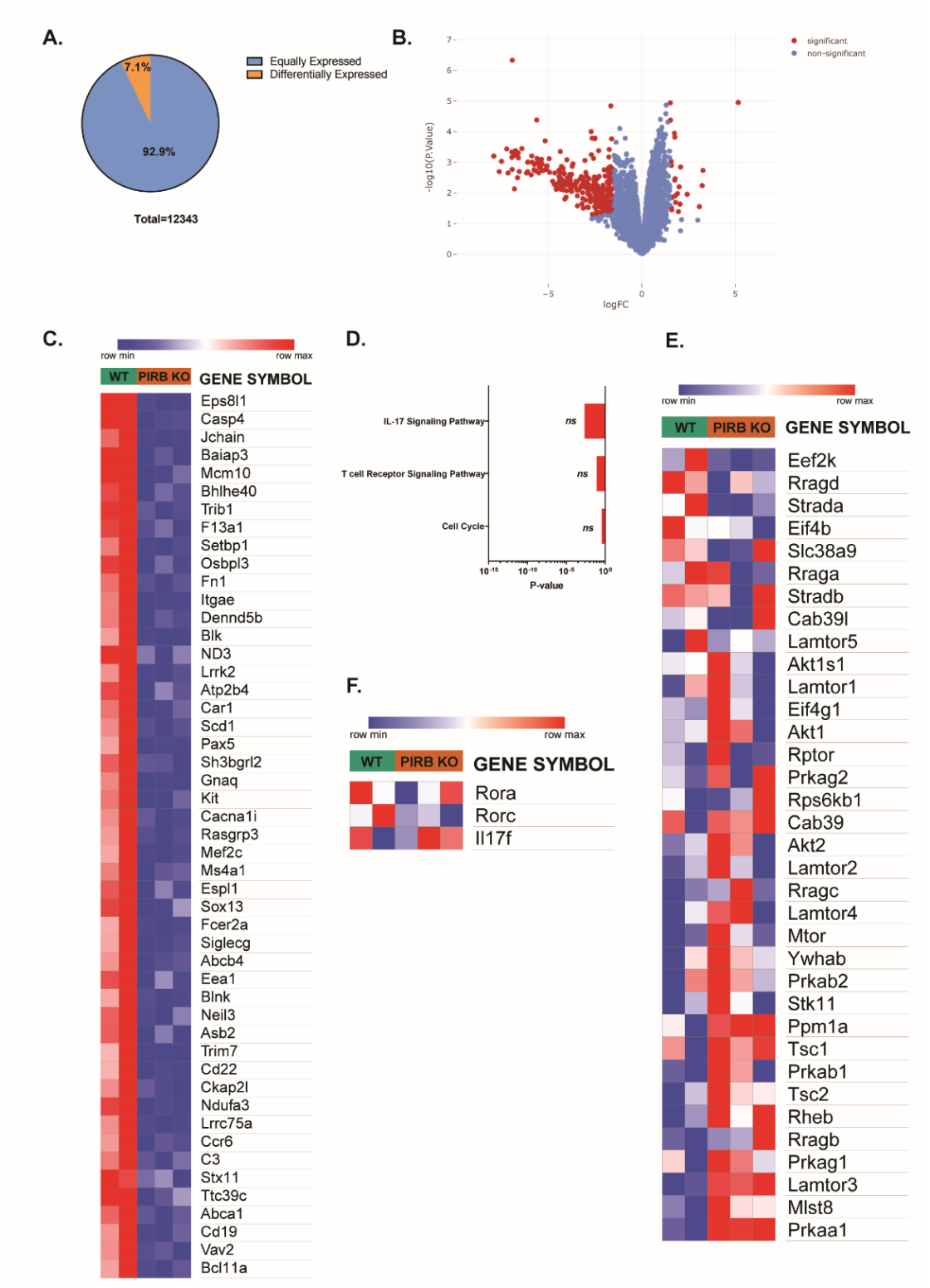

Figure 2-5 RNA-seq analysis of unstimulated WT and *Pirb*$^{-/-}$ Naïve CD4^{+} T cells.

(A) Venn diagram indicating equal (blue, RPKM ≥ 5, Fold Change ≥ 1 and ≤ 1.5, n=11463) and differential (orange, RPKM ≥ 5, padj ≤ 0.05 & abs_FC≥ 1.5, n = 880) gene expression between *WT* naïve $CD4^+$ T cells and *Pirb*$^{-/-}$ $CD4^+$ naive T cells. (B) Volcano plot of RNA-seq data analysis. Red indicates significantly enriched genes (| logFC | > 1; p < 0.05) (C) Heat map of differentially expressed genes comparing *WT* naïve $CD4^+$ T cells and *Pirb*$^{-/-}$ $CD4^+$ naive T cells. (D) Bar graphs of pathway analysis of differentially expressed genes in *WT* naïve $CD4^+$ T cells relative to *Pirb*$^{-/-}$ $CD4^+$ naive T cells; assessed via KEGG 2019, ranked by p-value. Heat map demonstrating relative expression of (E) mTORC1 core signaling and (F) Th17 transcriptome signature genes between *WT* naïve $CD4^+$ T cells and *Pirb*$^{-/-}$ $CD4^+$ naive T cells. Raw reads from *WT* (n = 2) and Pirb$^{-/-}$ $CD4^+$ T cells (n = 3) were aligned to the reference mm9 mouse genome (GRCm38) using Hisat-build pipeline. Relative gene expression was quantified using featureCounts function from the subread-2.0.0 package. Gene list was filtered for pseudogenes, RIKEN cDNA sequences, and immunoglobulin variable genes and downstream analysis of expressed genes was performed IDEP 9.1. Raw data and description of common expressed genes and DEGs are described in *Table* 1.

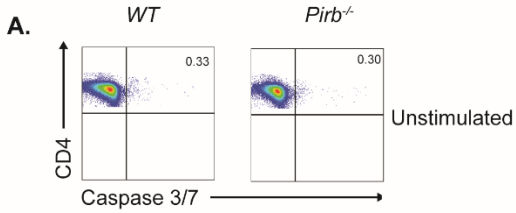

Figure 2-6 WT and *Pirb*$^{-/-}$ Naïve CD4^{+} T cells have limited Caspase 3/7 activation prior to stimulation.

Representative flow cytometry plots of the expression of active Caspase 3/7 in unstimulated *WT* (left) and *Pirb*$^{-/-}$ (right) naive CD4^{+} T cells. Representative data of 3 independent experiments.

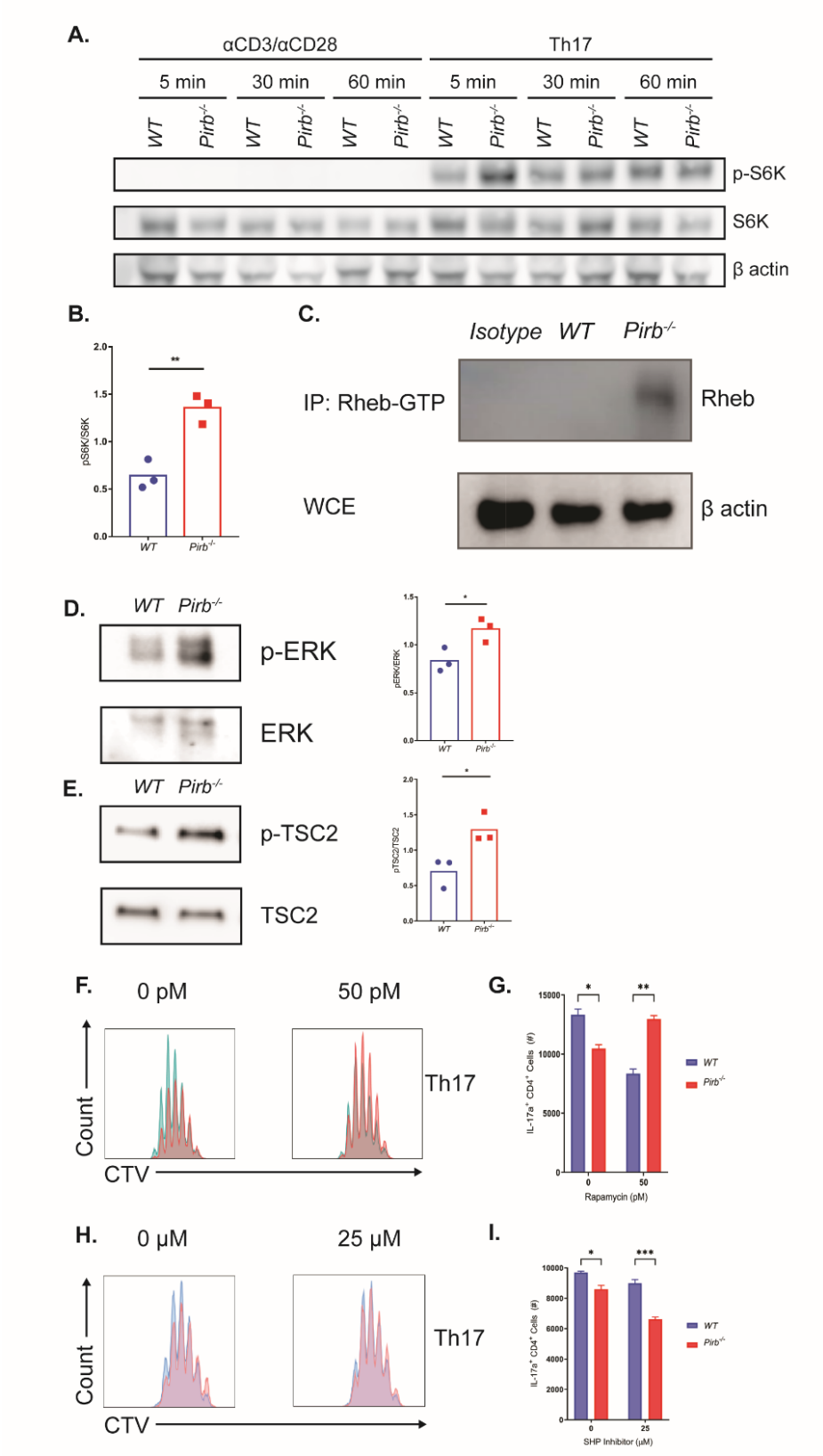

Figure 2-7 *Pirb* regulates CD4$^+$ IL-17a$^+$ cells via negative regulation of mTORC1 signaling.

(A) Western blot analyses of phosphorylation of S6 kinase in purified $CD4^+$ T cells cultured under Th17 polarizing conditions for 5 minutes. (B) Densitometry analyses of phosphorylation of S6 kinase in purified $CD4^+$ T cells cultured under Th17 polarizing conditions for 5 min (*WT* n= 3, *Pirb*$^{-/-}$ n= 3). (C) *WT* and *Pirb*$^{-/-}$ $CD4^+$ T cell lysates were immunoprecipitated with Rheb-GTP antibody. Western blot was performed for Rheb. (D) Western blot analyses of phosphorylation of ERK in purified $CD4^+$ T cells cultured under Th17 polarizing conditions for 5 minutes (Left). Densitometry analyses of phosphorylation of ERK in purified $CD4^+$ T cells cultured under Th17 polarizing conditions for 5 min (Right) (*WT* n= 3, *Pirb*$^{-/-}$ n= 3). (E) Western blot analyses of phosphorylation of TSC2 in purified $CD4^+$ T cells cultured under Th17 polarizing conditions for 5 minutes (Left). Densitometry analyses of phosphorylation of TSC2 in purified $CD4^+$ T cells cultured under Th17 polarizing conditions for 5 min (Right) (*WT* n= 3, *Pirb*$^{-/-}$ n= 3). *WT* and *Pirb*$^{-/-}$ $CD4^+$ T cells were cultured in the presence of rapamycin (50 pM). (F) Representative flow cytometry plots of Cell Trace Violet staining on Th17 polarized cells and quantification of (G) IL-$17a^+CD4^+$ T cells (*WT* n= 3, *Pirb*$^{-/-}$ n= 3). *WT* and *Pirb*$^{-/-}$ $CD4^+$ T cells were cultured in the presence of SHP-1/2 inhibitor (25 μM). (H) Representative flow cytometry plots of Cell Trace Violet staining on Th17 polarized cells and quantification of (I) IL-$17a^+CD4^+$ T cells (*WT* n= 3, *Pirb*$^{-/-}$ n= 3). Data are presented as mean ± SEM. Statistical analysis was performed using two-way analysis of variance ($p < 0.05$) followed by Sidak's Multiple Comparison Test (G), (I) or unpaired t test (B), (D), (E). *$p < 0.05$, **$p < 0.01$, ***$p < 0.001$. Data shown in (B), (D), (E) encompasses three independent experiments. Data shown in (A), (C), (F-I) are from one experiment representative of three independent experiments.

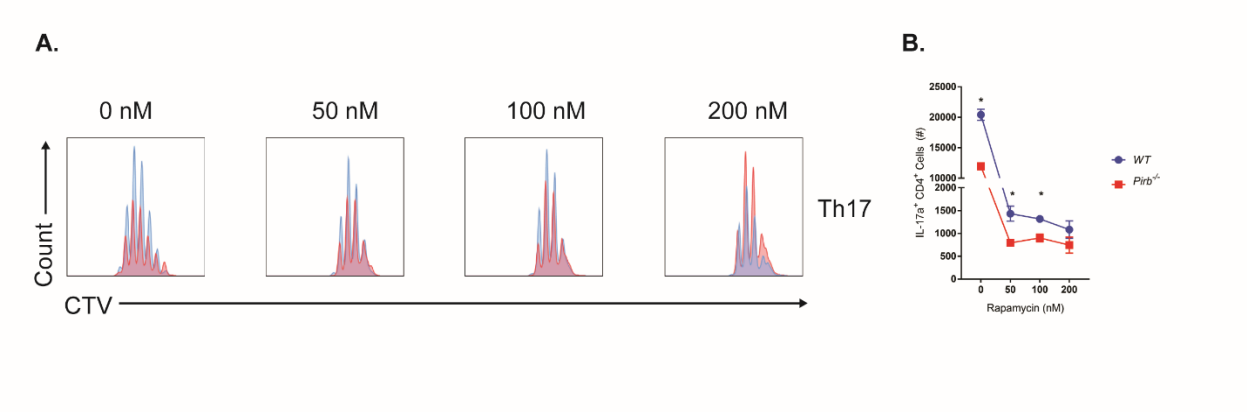

Figure 2-8 Th17 Polarization is Impaired at High Doses of Rapamycin in WT and *Pirb*$^{-/-}$ Naïve CD4^{+} T cells.

WT and *Pirb*$^{-/-}$ CD4^{+} T cells were cultured in the presence of different concentrations of rapamycin (0 nM, 50 nM,100 nM, 200 nM). (A) Representative flow cytometry plots of Cell Trace Violet staining on Th17 polarized cells and quantification of (B) IL-17a^{+}CD4^{+} T cells (*n*= 3). Data are presented as mean ± SEM. Statistical analysis was performed using unpaired t test. *p <0.05. Data shown in (A), (B) are from one experiment representative of three independent experiments.

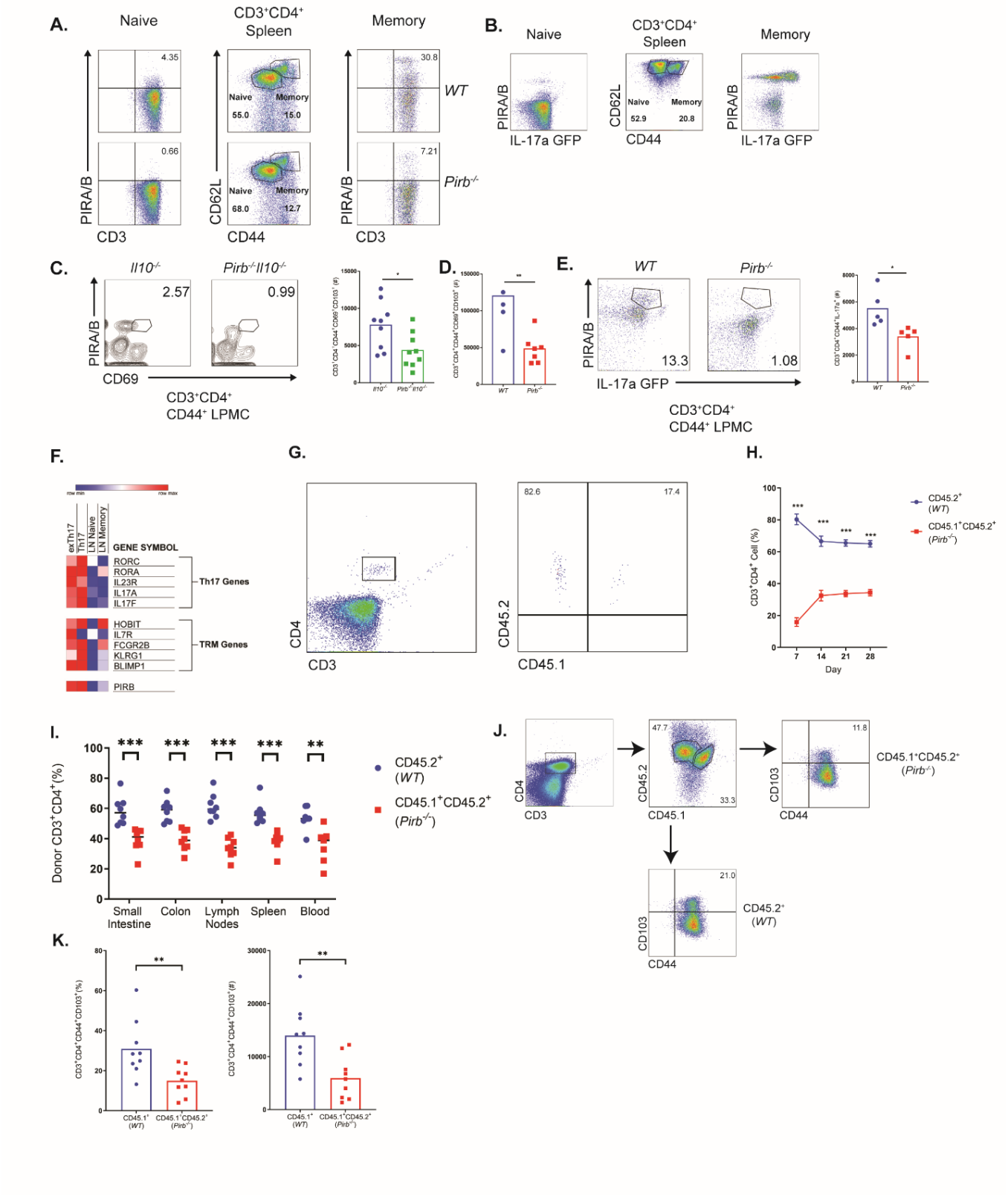

Figure 2-9 *Pirb* is expressed on a subset of memory $CD4^+$ $IL\text{-}17a^+$ cells.

Flow cytometry strategy for gating on $CD3^+CD4^+$ naive and memory T cells. Splenocytes from (A) *WT* (top row), *Pirb*$^{-/-}$ (bottom row), and (B) IL-17a GFP reporter mice were analyzed for PIRA/B expression on T cell subsets. Plots were pregated on $CD3^+CD4^+$ T cells. (C) Flow cytometry of the expression of PIRA/B and CD69 on $CD3^+CD4^+CD44^+$ T cells isolated from colonic lamina propria of *Il10*$^{-/-}$ and *Pirb*$^{-/-}$*Il10*$^{-/-}$ at 10 weeks of age (left). Quantification of colonic lamina propria $CD3^+CD4^+CD44^+CD69^+CD103^+$ T cells (right) (*Il10*$^{-/-}$ *n*= 9, *Pirb*$^{-/-}$*Il10*$^{-/-}$ *n*= 9). (D) Quantification of colonic lamina propria $CD3^+CD4^+CD44^+CD69^+CD103^+$ T cells from *Rag*$^{-/-}$ mice which received either 400,000 $CD4^+$ $CD45RB^{hi}$ *WT* or *Pirb*$^{-/-}$ T cells (*WT n*= 4, *Pirb*$^{-/-}$ *n*= 7). (E) Flow cytometry of the expression of PIRA/B and IL-17a on $CD3^+CD4^+CD44^+$ T cells isolated from colonic lamina propria of *WT* IL-17a GFP and *Pirb*$^{-/-}$ IL-17a GFP reporter mice at 10 weeks of age (left). Quantification of $CD3^+CD4^+CD44^+$IL-17a$^+$ T cells (right) (*WT n*= 5, *Pirb*$^{-/-}$ *n*= 5). (F) Heat map of differentially expressed genes based on RNA-seq data (GSE130446) of selected subset of genes known to be involved in resident memory T cells and Th17 cells comparing between exTh17 resident memory T cells, Th17 resident memory T cells, lymph node naïve $CD4^+$ T cells, and lymph node memory $CD4^+$ T cells. (G) Representative plots of donor *WT* ($CD45.2^+$) and *Pirb*$^{-/-}$ ($CD45.1^+CD45.2^+$) $CD4^+$ T cells circulating in the peripheral blood of a *Rag*$^{-/-}$ recipient mouse. (H) Percentage of donor *WT* ($CD45.2^+$) and *Pirb*$^{-/-}$ ($CD45.1^+CD45.2^+$) $CD4^+$ T cells circulating in the peripheral blood in *Rag*$^{-/-}$ recipient mice at different time points (*WT n* = 10, *Pirb*$^{-/-}$ *n* = 10). (I) Percentage of donor *WT* ($CD45.2^+$) and *Pirb*$^{-/-}$ ($CD45.1^+CD45.2^+$) $CD4^+$ T cells which accumulated in different tissues in *Rag*$^{-/-}$ recipient mice (*WT n* = 9, *Pirb*$^{-/-}$ *n* = 9). (J) Representative plots of colonic $CD3^+CD4^+CD44^+$ $CD103^+$ T cells which have been derived from donor *WT* ($CD45.2^+$) and *Pirb*$^{-/-}$ ($CD45.1^+CD45.2^+$) $CD4^+$ T cells injected in a *Rag*$^{-/-}$ recipient mouse. (K) Percentage (%, left) and cell counts (#, right) of colonic $CD3^+CD4^+CD44^+$ $CD103^+$ T cells which have been derived from donor *WT* ($CD45.2^+$) and *Pirb*$^{-/-}$ ($CD45.1^+CD45.2^+$) $CD4^+$ T cells injected in a *Rag*$^{-/-}$ recipient mouse (*WT n*= 9, *Pirb*$^{-/-}$ *n*= 9). Data are presented as mean ± SEM. Statistical analysis was performed using two-way analysis of variance ($p < 0.05$) followed by Sidak's Multiple Comparison Test (H), (I), (K) or unpaired t test (C), (D), (E). *p <0.05, **p <0.01, ***p <0.001. Data shown encompasses three independent experiments.

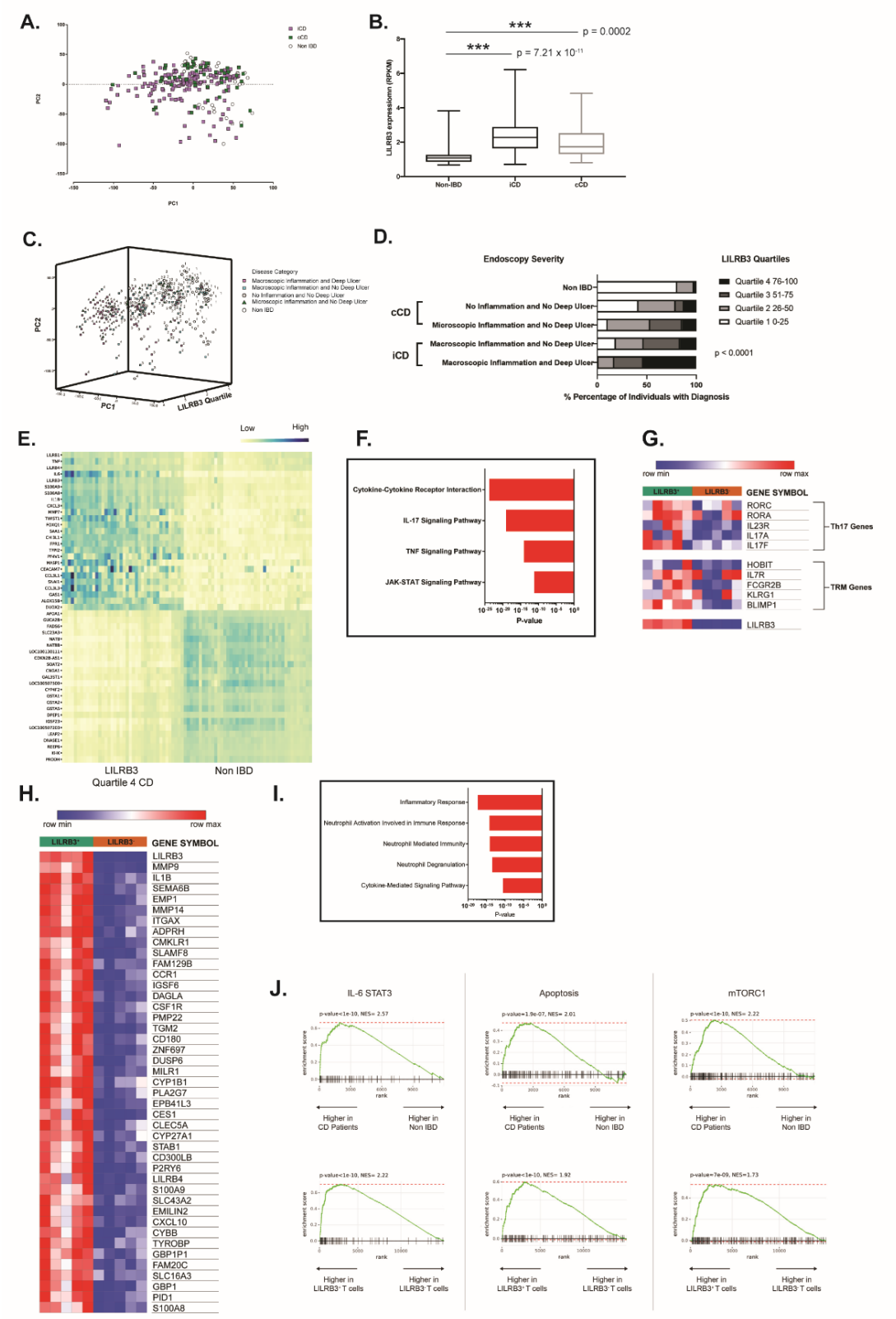

Figure 2-10 LILRB3 expression is upregulated in IBD patients and Memory CD4$^+$ T cells characterized by a Th17 signature.

(A) Principal component analysis (PCA) of differentially expressed genes between non-IBD (NL, n = 42), pediatric ileal-involvement CD (iCD, n = 162) and colonic-only involvement CD (cCD, n = 55) patients (GSE57945) (B) Box plots showing LILRB3 expression (RPKM) CD or non-IBD tissue biopsies. (C) 3D PCA plot of CD cohort stratified by endoscopic severity. (D) Stratification of the CD cohort based upon endoscopic severity and LILRB3 expression (quartiles, RPKM). (E) Heat map of differentially expressed genes based on RNA-seq data (GSE57945) comparing Crohn's Disease patients and healthy control individuals. (F) Pathway analysis of differentially expressed genes in Crohn's Disease patients relative to healthy individuals; assessed via KEGG 2019, ranked by p-value. (G) Heat map of differentially expressed genes based on RNA-seq data (GSE140244) of selected subset of genes known to be involved in resident memory T cells and Th17 cells comparing between LILRB3^{+} CD4^{+} memory T cells and LILRB3^{-}CD4^{+} memory T cells. (H) Heat map of differentially expressed genes based on RNA-seq data (GSE140244) comparing LILRB3^{+} CD4^{+} memory T cells and LILRB3^{-}CD4^{+} memory T cells collected from 10 donors. (I) Bar graphs of pathway analysis of differentially expressed genes in LILRB3^{+} CD4^{+} memory T cells relative to LILRB3^{-}CD4^{+} memory T cells; assessed via Gene Ontology Biological Pathways, ranked by p-value. (J) GSEA for the indicated Hallmark genes comparing a ranked list of differentially expressed genes between Crohn's Disease patients and healthy control individuals (GSE57945) (top row) and comparing between LILRB3^{+} CD4^{+} memory T cells and LILRB3^{-}CD4^{+} memory T cells (GSE140244) (bottom row). Statistical analysis was performed using student's t test. ***p <0.001.

Table 2.1 RNAseq analyses and identification of gene expression of naïve unstimulated WT and *Pirb*$^{-/-}$ CD4^{+} T cells.

Large dataset Excel file available here:

https://www.dropbox.com/s/3pmoqpzt41sk45w/Supplementary_Table_1.xlsx?dl=0

A) Total expressed genes (n = 12 343) in naïve unstimulated WT and *Pirb*$^{-/-}$ CD4^{+} T cells. (B) Common expressed genes (n = 11463; RPKM ≥ 5, Fold Change ≥ 1 and ≤ 1.5) and (C) differentially expressed genes (n = 880; (RPKM ≥ 5, padj ≤ 0.05 and abs_FC ≥ 1.5) between naïve unstimulated WT and *Pirb*$^{-/-}$ CD4^{+} T cells. Raw reads from WT (n = 2) and *Pirb*$^{-/-}$ CD4^{+} T cells (n = 3) were aligned to the reference mm9 mouse genome (GRCm38) using Hisat-build pipeline. Relative gene expression was quantified using featureCounts function from the subread-2.0.0 package. Gene list was filtered for pseudogenes, RIKEN cDNA sequences, and immunoglobulin variable genes and downstream analysis of expressed genes was performed IDEP 9.1.

Table 2.2 Pathway Enrichment Analysis in iCD Patients Relative to Non-IBD Patients.

Pathway enrichment analyses of iCD gene signature.		
Direction	**adj.Pval**	**Pathways**
Down Regulated	2.00E-04	Drug metabolism
Down Regulated	2.00E-04	Chemical carcinogenesis
Down Regulated	2.00E-04	Metabolism of xenobiotics by cytochrome P450
Down Regulated	2.00E-04	Retinol metabolism
Down Regulated	2.00E-04	Fat digestion and absorption
Down Regulated	2.00E-04	Steroid hormone biosynthesis
Down Regulated	2.00E-04	Pentose and glucuronate interconversions
Down Regulated	2.00E-04	Mineral absorption
Down Regulated	2.00E-04	Drug metabolism
Up Regulated	2.00E-04	IL-17 signaling pathway
Up Regulated	2.00E-04	Rheumatoid arthritis
Up Regulated	2.00E-04	Cytokine-cytokine receptor interaction
Up Regulated	2.00E-04	Leishmaniasis
Up Regulated	2.00E-04	Pertussis
Up Regulated	2.00E-04	TNF signaling pathway
Up Regulated	2.00E-04	Staphylococcus aureus infection
Up Regulated	2.00E-04	Osteoclast differentiation

Pathway enrichment analyses of iCD gene signature.		
Direction	**adj.Pval**	**Pathways**
Up Regulated	2.00E-04	Toll-like receptor signaling pathway
Up Regulated	2.00E-04	NOD-like receptor signaling pathway
Up Regulated	2.00E-04	Tuberculosis
Up Regulated	2.00E-04	Malaria
Up Regulated	2.00E-04	Legionellosis
Up Regulated	2.00E-04	Influenza A
Up Regulated	2.00E-04	Autoimmune thyroid disease
Up Regulated	2.00E-04	Phagosome
Up Regulated	2.00E-04	Salmonella infection
Up Regulated	2.00E-04	AGE-RAGE signaling pathway in diabetic complications
Up Regulated	2.00E-04	Chemokine signaling pathway
Up Regulated	2.00E-04	Amoebiasis
Up Regulated	2.00E-04	Measles

KEGG pathway analysis was used to identify important pathways altered by differentially regulated genes.

Table 2.3 Colonic-Only Involvement CD Patients (cCD) and Ileal Involvement CD Patients (iCD) Stratified by Endoscopic Severity and LILRB3 Expression.

LILRB3 expression signature in pediatric CD cohort based upon endoscopic severity					
Disease Category	**LILRB3_Q1**	**LILRB3_Q2**	**LILRB3_Q2**	**LILRB3_Q4**	**P-value**
Macroscopic Inflammation and Deep Ulcer (iCD)	1 (1.3%)	12 (16%)	22 (29.3%)	40 (53.3%)	2.09×10^{-22}
Mcroscopic Inflammation and No Deep Ulcer (iCD)	16 (18.8%)	24 (28.2%)	31 (36.5%)	14 (16.4%)	
No Inflammation and No Deep Ulcer (cCD)	10 (41.7%)	9 (37.5%)	2 (8.3%)	3 (12.5%)	
Undetermined and No Deep Ulcer (cCD)	0 (0%)	0	1 (33.3%)	2 (66.7%)	
Microscopic Inflammation and Deep Ulcer (iCD)	0	1 (100%)	0	0	
Non-IBD	34 (81%)	7 (16.7%)	0	1 (2.4%)	
LILRB3 expression (quartiles defined Q1, 0.59 – 1.44; Q2, 1.48 – 2.72; Q3, 2.73 – 5.47 and Q4, 5.56 – 73.39; RPKM values) value (%) represents the number of patients (% of total of disease category)					

LILRB3 quartiles were established based on RPKM values; quartiles Q1 (0-25%), 0.59 – 1.44; Q2 (26-50%), 1.48 – 2.72; Q3 (51-75%), 2.73 – 5.47 and Q4 (76-100%), 5.56 – 73.39). Statistical analysis was performed using SPSS 17.0. The Frequencies procedure was used for the LILRB3 quartile analysis. χ^2 test was used to assess the association of CD categories with 4 LILRB3 quartiles.

Table 2.4 Pathway Enrichment Analysis in Q4 LILRB3^{hi} iCD Patients with Macroscopic Inflammation with Deep Ulcer Relative to LILRB3^{low} Non-IBD Patients.

Pathway enrichment analyses of DEGs in Q4 LILRB3hi iCD-DU patients.		
Direction	**adj.Pval**	**Pathways**
Down regulated	5.00E-21	Metabolic pathways
Down regulated	4.73E-16	Drug metabolism
Down regulated	1.02E-15	Chemical carcinogenesis
Down regulated	1.45E-14	Metabolism of xenobiotics by cytochrome P450
Down regulated	1.92E-14	Retinol metabolism
Down regulated	4.32E-11	Fat digestion and absorption
Down regulated	1.37E-09	Steroid hormone biosynthesis
Down regulated	1.37E-09	Mineral absorption
Down regulated	2.64E-09	PPAR signaling pathway
Down regulated	5.98E-09	Protein digestion and absorption
Down regulated	1.27E-07	Vitamin digestion and absorption
Down regulated	1.08E-06	Bile secretion
Down regulated	1.43E-06	Arachidonic acid metabolism
Down regulated	3.14E-06	Pentose and glucuronate interconversions
Down regulated	1.67E-05	Drug metabolism
Up regulated	2.88E-24	Cytokine-cytokine receptor interaction
Up regulated	1.51E-19	IL-17 signaling pathway
Up regulated	8.99E-18	Rheumatoid arthritis
Up regulated	8.28E-17	Staphylococcus aureus infection
Up regulated	6.72E-15	Complement and coagulation cascades
Up regulated	6.72E-15	Amoebiasis
Up regulated	1.39E-14	TNF signaling pathway
Up regulated	3.45E-14	Osteoclast differentiation
Up regulated	3.45E-14	Pertussis
Up regulated	1.32E-13	Leishmaniasis
Up regulated	1.37E-13	Malaria
Up regulated	3.54E-13	Tuberculosis
Up regulated	8.96E-13	AGE-RAGE signaling pathway in diabetic complications
Up regulated	1.05E-11	Chemokine signaling pathway
Up regulated	1.05E-11	JAK-STAT signaling pathway

Pathway enrichment analyses of DEGs in Q4 LILRB3hi iCD-DU patients.		
Direction	**adj.Pval**	**Pathways**
KEGG pathway analysis was used to identify important pathways altered by DEG signature between Q4 LILRB3^{hi} iCD-DU patients and LILRB3^{low} non-IBD patients.		

LILRB3 quartiles were established based on RPKM values; quartiles Q1 (0-25%), 0.59 – 1.44; Q2 (26-50%), 1.48 – 2.72; Q3 (51-75%), 2.73 – 5.47 and Q4 (76-100%), 5.56 – 73.39). KEGG pathway analysis was used to identify important pathways altered by differentially regulated genes.

Table 2.5 Correlation Analyses Between LILRB3 and LILRB5 mRNA Expression and Proinflammatory and Mucosal Injury Markers in iCD Patients Stratified by Endoscopic Severity and LILRB3 Expression.

		Table 5. Pearson correlation analyses of LILRB3, LILRB5, IL1B, IL17A, IL21, TNF, IL6 and S100A9mRNA expression in the iCD-DU group.								
		LILRB3	S100A9	IL1B	IL17A	IL17B	IL21	TNF	IL6	LILRB5
LILRB3	Pearson Correlation	1	.929**	.863**	.730**	0.112	.454**	.843**	.842**	-0.195
	Sig. (2-tailed)		p < 0.005	p < 0.005	p < 0.005	0.339	p < 0.005	p < 0.005	p < 0.005	0.093
	N	75	75	75	75	75	75	75	75	75
LILRB5	Pearson Correlation	-0.195	-0.177	-0.163	-0.191	-0.181	-.234*	-0.157	-0.11	1
	Sig. (2-tailed)	0.093	0.129	0.163	0.101	0.12	0.044	0.179	0.346	
	N	75	75	75	75	75	75	75	75	75

LILRB3 quartiles were established based on RPKM values; quartiles Q1 (0-25%), 0.59 – 1.44; Q2 (26-50%), 1.48 – 2.72; Q3 (51-75%), 2.73 – 5.47 and Q4 (76-100%), 5.56 – 73.39). Statistical analysis was performed using SPSS 17.0. The Frequencies procedure was used for the LILRB3 quartile analysis. χ^2 test was used to assess the association of CD categories with 4 LILRB3 quartiles. The association of LILRB3 with Th17 pathways associated genes IL1B, IL17A, IL21, TNF, IL6 and S100A9 was evaluated by Pearson's correlation as quantitative variables.

CHAPTER 3 - STARD7 is Required for Maintenance of Intestinal Epithelial Mitochondria Architecture, Barrier Function and Protection from Colitis

Abstract

Background & Aims: Susceptibility to the inflammatory bowel diseases (IBD), Crohn's Disease (CD) and Ulcerative Colitis (UC) have been linked with loss of intestinal epithelial barrier integrity and mitochondria dysfunction. Steroidogenic acute regulatory (StAR) protein-related lipid transfer (START) domain-containing protein 7, STARD7 is a lipid transfer protein that transports phosphatidylcholine to the mitochondria and facilitates mitochondria membrane stabilization and function. The aim of this study is to define the involvement of STARD7 in the regulation of the intestinal epithelial mitochondrial function and susceptibility to colitis.

Methods: We employed the DSS-induced and *Il10*$^{-/-}$ spontaneous models of colitis with STARD7 heterozygous mice (*Stard7*^{Tg}). Intestinal epithelial barrier, electron and fluorescence microscopy, mitochondria function and western blot analyses were performed on wild type and *Stard7* knockdown epithelial cells. In silico analyses were performed on RNA-seq datasets of ileal biopsy samples from pediatric UC, CD and non-IBD patients.

Results: In silico analyses identified significantly reduced expression of *Stard7* in UC patients which was associated with downregulation of metabolic function and a more severe disease phenotype. STARD7 was expressed in intestinal epithelial cells and STARD7 knockdown resulted

in deformed mitochondria and diminished aerobic respiration. Loss of mitochondria function was associated with diminished expression of tight junction proteins and loss of intestinal epithelial barrier integrity that could be recovered by AMPK activation. *Stard7*^{Tg} mice were more susceptible to the development of DSS-induced and *Il10*$^{-/-}$ spontaneous models of colitis.

Conclusions: STARD7 is central to intestinal epithelial mitochondrial function and barrier integrity and loss of STARD7 function increases susceptibility to IBD.

Keywords: steroidogenic acute regulatory proteins, mitochondria, epithelial barrier, and inflammatory bowel disease

Introduction

Inflammatory bowel diseases (IBD), Crohn's Disease (CD) and Ulcerative Colitis (UC) are chronic inflammatory diseases associated with debilitating symptoms, poor quality of life and high risk of surgical intervention at 5 years[11,227].Clinical and experimental evidence suggests that the manifestations of IBD result from loss of intestinal epithelial barrier integrity and activation of an unrestrained intestinal inflammatory response to intestinal microbes in a genetically susceptible host[228 229]. Genome-wide association studies (GWAS) have identified over 200 single nucleotide polymorphisms (SNPs) associated with IBD, and > 15 of these SNPs are linked to loci associated with epithelial junctional proteins and maintenance of epithelial barrier function[230,231], indicating an important role of intestinal barrier regulation in the pathogenesis of IBD.

Maintenance of intestinal epithelial barrier integrity is an energy-demanding process involving intestinal epithelial cell proliferation, differentiation and formation and maintenance of complex interactions between epithelial adherence junctional proteins, tight junction proteins and cytoskeletal elements[232 233]. Disruption of ATP-generating processes in intestinal epithelial cells alters intestinal epithelial homeostasis including stemness, survival and microbial sensing and barrier integrity. Colonic biopsy samples from IBD patients are characterized by diminished ATP levels and cellular stress[234,235]. Diminished levels of ATP within the inflamed regions of the colonic mucosa from UC and CD patients were associated with downregulation of critical tight junction proteins and reduced intestinal epithelial barrier function[236]. Furthermore, enterocytes from UC patients possess impaired mitochondria with disrupted cristae which was associated

with loss of epithelial barrier integrity[237]. Collectively, these studies link mitochondrial dynamics with intestinal epithelial barrier function and IBD.

The mitochondria consist of an outer and inner membrane phospholipid bilayer which is comprised of lipids including phosphatidylcholine (PC), phosphatidylethanolamine (PE), cardiolipin (CL), phosphatidylinositol (PI), phosphatidylserine (PS) and phosphatidylglycerol (PG). These phospholipids are essential for mitochondrial membrane structure, function, and energy production[238]. While mitochondria possess enzymes to generate CL, PG, and PE; they are incapable of directly synthesizing PC. PC is synthesized in the endoplasmic reticulum (ER) from the substrates, choline and diacylglycerol via the de novo CDP-choline Kennedy pathway[239]. PC is transported from the ER to the mitochondria via lipid binding proteins such as the steroidogenic acute regulatory (StAR) protein-related lipid transfer (START) domain-containing protein 7, STARD7[240]. STARD7, a member of the steroidogenic acute regulatory (StAR) protein family, possesses a START domain that specifically binds to PC[241,242] and transports the phospholipid from the ER to the outer and inner mitochondrial membrane[243,148]. While previous studies have established that STARD7 expression can modulate mitochondrial homeostasis; the role of this protein in intestinal epithelial mitochondrial function, barrier integrity and exacerbation of the IBD phenotype remain unknown.

Herein, we show that STARD7 is differentially expressed in both UC and CD patients compared with healthy controls. Notably, STARD7^{low} UC patients were characterized with a more severe disease phenotype and *Stard7* expression was strongly associated with a metabolic dysfunction transcriptome. STARD7 knockdown in colonic epithelial cells disrupted intestinal epithelial

mitochondria architecture and respiration and this was associated with diminished intestinal epithelial barrier integrity. Notably, reconstitution of mitochondria function by AMPK activation in human intestinal cells led to improved intestinal epithelial barrier integrity. Utilizing STARD7 deficient (*Stard7*^{Tg}) mice and employing the DSS-induced and *Il10*$^{-/-}$ spontaneous model of colitis, we found that STARD7 deficiency exacerbated the development of acute and chronic colitis. Collectively we identify STARD7 as a critical component in ATP-generating processes and maintenance of intestinal epithelial barrier integrity and susceptibility to IBD.

Results

UC patients are characterized by downregulated *Stard7* expression

We examined an RNA-seq dataset of rectal biopsy samples from a cohort of 322 pediatric individuals consisting of treatment naive CD, UC and non-IBD subjects (GSE57945)[191]. We identified 133 differentially expressed genes (DEGs) between UC and non-IBD patients and 6748 DEGs between CD and non-IBD individuals (p adjusted value < 0.05, Table 1a, b). Of the 133 DEGs in UC, 74 of these genes were also differentially expressed in CD (Table 1c). Gene Ontology (GO) pathway analyses of the common IBD transcriptome revealed significant enrichment for genes involved in mitochondrial homeostasis including TRMT5, BAK1 and STARD7 (Fig. 1a). Notably, *Stard7* mRNA expression was significantly more diminished in UC patients relative to CD patients compared with non-IBD (Fig. 1b). To validate differential expression of STARD7 in UC, we evaluated a dataset of rectal biopsy samples from a cohort of 226 pediatric individuals which included treatment naïve UC and non-IBD patients (GSE109142)[244]. STARD7 mRNA expression was significantly downregulated in UC patients compared to non-IBD healthy individuals (Fig. 1c). Stratification of UC patients into quartiles based on STARD7 mRNA RPKM values [Q1 (0-25%), 16.78 – 39.31; Q2 (26-50%), 39.37 – 43.81; Q3 (51-75%), 43.90 – 48.55 and Q4 (76-100%), 48.68 – 64.84] revealed that UC patients with the lowest STARD7 mRNA expression [STARD7^{low} (STARD7 Q1)] had a more severe disease phenotype (Pediatric ulcerative colitis activity index (PUCAI) and Mayo score) relative to STARD7^{high} UC patients with the highest STARD7 mRNA expression [STARD7^{high} (STARD7 Q4)] (Fig. 1d-f, Table 2). Additionally, > 80% of STARD7^{low} UC patients were shown to have more severe intestinal inflammation as indicated by exaggerated levels of fecal

calprotectin 4 weeks after their initial diagnosis relative to 53.6% of STARD7^{high} UC patients (Fig. 1g). Notably, downregulation of STARD7 mRNA expression within UC patients was associated with an increase in mRNA expression of GATA3, IFNG, IL13, IL1B, IL23A, and IL6 expression; indicating that STARD7 was inversely related to mucosal inflammation (Table 3). Collectively, these studies suggest that IBD is associated with decreased STARD7 mRNA expression and levels of STARD7 expression are associated with disease severity.

To begin to define the role STARD7 in the IBD phenotype, we performed pathway enrichment analyses on the DEGs (up and down; 3238 total number genes; p adjusted value < 0.05) between STARD7^{low} UC patients (n = 56) from non-IBD patients (n = 16) (Fig. 1h). We identified that the downregulated DEGs in the STARD7^{low} UC transcriptome were enriched for genes associated with mitochondrial transmembrane transport, regulation of lipid metabolic process, glucose homeostasis, and transmembrane transport (Fig. 1j, k). In contrast, analysis of upregulated DEGs identified significant enrichment of genes involved in cytokine-mediated signaling, acute inflammatory responses, and regulation of immune effector responses (Fig. 1j, k). Collectively, our in-silico studies revealed that STARD7 expression is highly diminished in UC patients and suggests a critical role for this lipid binding protein in regulating metabolic processes which can alter inflammatory disease outcomes.

Loss of STARD7 perturbs mitochondrial function

To determine the cellular expression of STARD7 we examined the human protein atlas database which revealed that STARD7 expression was predominant in cardiomyocytes, hepatocytes, myeloid cells and intestinal epithelial cells[245]. Indeed, immunofluorescence staining for STARD7

in colonic tissue from WT (C57BL6) mice and *Stard7*^{Tg} (*Stard7*$^{+/-}$, C57BL6) mice revealed that STARD7 was ubiquitously expressed in intestinal epithelial cells and co staining for mitochondrial tracker (MitoTracker) localized STARD7 to the mitochondria of colonic epithelial cells (Fig. 2a). To determine what epithelial populations express STARD7 we utilized a scRNA-seq dataset consisting of different colonic epithelial subsets isolated from UC patients (SCP259)[246]. We show STARD7 expression was enriched in transit amplifying cells and enterocytes (Supplementary Fig. 1a, b). Remarkably, these *Stard7* high intestinal epithelial cell populations were also enriched for the mitochondrial genes, *Tomm20* and *Cox14* (Supplementary Fig. 1a, b). To define the impact of STARD7 deficiency on intestinal epithelial mitochondria function we utilized lentiviral technology to knockdown STARD7 in the colonic epithelial adenocarcinoma cell line Caco-2 BBe cells. Western blot and immunofluorescence confirmed that STARD7 shRNA transduction led to knockdown of STARD7 protein and STARD7 localization to mitochondria in human intestinal epithelial cells (Fig. 2b, c). Electron microscopy analyses of Caco-2 BBe cells transduced with control shRNA revealed mitochondria with large matrix volume within double membranes and cristae membrane projections into the matrix compartment (Fig. 2d). In contrast, Caco-2 BBe cells transduced with STARD7 shRNA lentiviral particles revealed altered mitochondria architecture including loss of the distinct double membrane structure, collapse of mitochondria matrix volume and clustered cristae membrane projections (Fig. 2d). Analyses of mitochondrial proteins in Caco-2 BBe cells revealed that loss of STARD7 was associated with significant reduction in mitochondrial respiratory proteins, such as Complex I, Complex II, and Complex IV, but did not impact the expression of the mitochondrial outer membrane protein, TOMM20 (Fig. 2e). To gain a better understanding of the relationship between STARD7 and mitochondrial network dynamics, we stained for STARD7 and the mitochondrial inner membrane protein Complex I (Fig. 2f) and

the mitochondrial outer membrane protein TOMM20 (Fig. 2g). Caco-2 BBe cells transduced with empty vector, pLKO.1 shRNA, displayed a robust mitochondrial network consisting of inter-connected fused mitochondria with large domains that were in close proximity to STARD7 (Fig. 2f, g). In contrast, STARD7 shRNA transduced Caco-2 BBe cells displayed disrupted mitochondrial network with fragmented mitochondria (Fig. 2f, g). Quantification of mitochondrial network and STARD7 expression revealed significantly reduced expression of STARD7 and Complex I in STARD7 shRNA transduced Caco-2 BBe cells compared with empty vector transduced cells (Fig. 2h, i). Notably, we observed no change in expression of the outer mitochondrial membrane TOMM20, suggesting that reduced STARD7 expression did not impact the number of mitochondria per cell (Fig. 2j). Immunofluorescence analyses revealed that STARD7 predominantly localized with TOMM20, suggesting that STARD7 was primarily localized to the outer mitochondrial membrane (Fig. 2k). To a lesser extent STARD7 also colocalized with the inner mitochondrial membrane Complex I, suggesting that STARD7 can also traffic to the inner mitochondrial membrane (Fig. 2k). To determine whether loss of STARD7 and altered mitochondrial structure compromised mitochondrial function we examined glycolytic and oxidative phosphorylation metabolic pathways in the Caco-2 BBe transduced with pLKO.1 shRNA and Caco-2 BBe cells transduced with STARD7 shRNA. We show that STARD7 knockdown was associated with severely impaired mitochondrial respiration (Fig. 2l) including basal (Fig. 2m) and maximal respiration (Fig. 2n), spare respiratory capacity (Fig. 2o) and ATP production (Fig. 2p). This was specific to oxidative phosphorylation pathway as we did not observe significant impact on glycolytic function in STARD7 deficient cells (Supplementary Fig. 2a, b). In line with this, evaluation of oxidative phosphorylation with isolated mitochondria revealed that loss of STARD7 compromised mitochondrial function and significantly impacted ATP production

(Supplementary Fig. 3a-d). Collectively, our data demonstrates that STARD7 knockdown in intestinal epithelial cells alters mitochondria structure and cellular respiration.

Intestinal epithelial barrier integrity is dependent on STARD7 expression

Mitochondrial function plays an important role in intestinal epithelial function including barrier integrity[247-249]. To determine if STARD7-mediated mitochondrial dysfunction impacted intestinal epithelial barrier integrity we examined intestinal permeability in WT and *Stard7*^{Tg} mice. Analyses of tight junction protein expression in purified colonic intestinal epithelial cells revealed that haplotypic STARD7 expression was associated with significantly altered IEC tight junction proteins. Notably, IECs from *Stard7*^{Tg} mice had decreased Claudin-1, Claudin-3, and Claudin-4 and increased Claudin-2 expression compared to WT IECs (Fig. 3a, b).

Analyses of the colonic mucosa of *Shh*^{cre}*Stard7*^{WT} (WT) and *Shh*^{cre}*Stard7*$^{fl/fl}$ mice revealed that STARD7 deletion in epithelial cells resulted in a significant decrease in transepithelial resistance (TER) and increased macromolecular (FITC-dextran) apical to basolateral flux relative to WT (*Shh*^{cre}) epithelial cells (Fig. 3c, d). The diminished colonic epithelial barrier function was associated with dysregulated expression of the adherence junctional and tight junction proteins E-cadherin and Claudin-4 (Fig. 3e). Consistent with these analyses backcrossing *Stard7*$^{fl/fl}$ mice onto the *Villin*^{cre} mouse background revealed that deletion of STARD7 in the intestinal epithelial compartment led to decreased TER and increased FITC-dextran flux across the mucosa of *Vilin*^{cre}*Stard7*$^{fl/fl}$ mice compared with WT mice (Fig. 3f, g). Consistent with our ex vivo findings, STARD7 knockdown in Caco-2BBe cells exhibited a significant reduction in TER and FITC-dextran flux (Fig. 3h, i). Notably, diminished barrier was associated with downregulated

expression of adherence junctional protein E-cadherin and tight junction proteins Claudin-3 and Claudin-4 (Fig. 3j). Collectively our data reveal that loss of STARD7 increases the permeability of the intestinal barrier due to loss of epithelial junctional protein expression.

AMPK agonists can recover STARD7 deficiency in epithelial barrier function

Dysregulation of mitochondria respiration leads to activation of protection mechanisms such as adenosine monophosphate-activated protein kinase (AMPK) signaling which upregulates mitochondrial biogenesis and respiration[250,251]. Activation of AMPK pathway has been shown to improve epithelial barrier integrity [252,253]. To test the relationship between mitochondrial stress and barrier dysfunction; STARD7 knockdown Caco-2BBe cell monolayers were stimulated with the AMPK activator, metformin and were assessed for mitochondrial structure and barrier function. Remarkably, we demonstrate that metformin exposure could recover mitochondria architecture including large mitochondria matrix volume and long cristae membrane projection networks in the STARD7 shRNA transduced Caco-2 BBe cells (Fig. 4a). Metformin also increased intestinal epithelial barrier integrity in STARD7 knockdown Caco-2 BBe cells; notably barrier integrity in metformin-treated STARD7 deficient Caco-2 BBe cells was comparable to WT epithelial cells (Fig. 4b, c). Increased barrier integrity was associated with increased expression of tight junction proteins including ZO-1 and Claudin-3 (Fig. 4d). Cumulatively, our results demonstrate that activation of AMPK-pathway can overcome STARD7-mediated of intestinal epithelial barrier function.

STARD7 deficiency enhances susceptibility to colitis

To test the requirement of STARD7 in the colitic phenotype we treated WT (C57BL6) and *Stard7*$^{+/-}$ (*Stard7*^{Tg}, C57BL6) mice with water containing 2.5% dextran sulfate sodium (DSS) and monitored for disease development over the course of 6 days. *Stard7*$^{-/-}$ mice die embryonically at day 11 while *Stard7*$^{+/-}$ mice survive and are fertile[150]. DSS exposure of WT mice induced colitic symptoms by day 4 including dehydration, bloody stool and rectal prolapse which got progressively worse throughout the duration of the experiment (Fig. 5a). These symptoms were associated with a loss in body weight from day 5 of DSS exposure (Fig. 5b). Histological analysis of the colonic tissue from WT mice showed substantial epithelial injury including epithelial apoptosis, villus atrophy, and inflammatory infiltrates (Fig. 5c, d). DSS treatment of *Stard7*^{Tg} mice led to significantly exaggerated colitic phenotype including increased loss of body weight, colon shortening and histopathological changes to the colon including severe transmural infiltration and exaggerated epithelial destruction (Fig. 5a-e).

To further interrogate the role of STARD7 in the colitic phenotype we backcrossed the *Stard7*^{Tg} mice (C57BL6) onto the *Il10*$^{-/-}$ background (C57BL6) and monitored for the development of the spontaneous colitis phenotype[254]. *Il10*$^{-/-}$ mice demonstrated colitic symptoms and diminished weight gain ~ 7 weeks of age (Fig. 5f, g). Histological analysis of the colon from *Il10*$^{-/-}$ mice showed evidence of epithelial erosion and inflammation (Fig. 5h, i). *Stard7*^{Tg}*Il10*$^{-/-}$ mice exhibited more severe symptoms of colitis and demonstrated exaggerated weight loss before they reached 5-6 weeks of age, indicating that the STARD7 deficiency was associated with early-onset colitic development (Fig. 5f, g). Congruently, histological analyses revealed that the colon of *Stard7*^{Tg}*Il10*$^{-/-}$ mice were characterized by increased transmural inflammation and crypt

destruction relative to *Il10*$^{-/-}$ mice (Fig. 5h, i). Consistent with increased inflammation, we observed increased cell number of CD3^{+}CD4^{+} T cells and CD11b^{+}F4/80^{+} myeloid populations in the mesenteric lymph nodes (mLN) of *Stard7*^{Tg}*Il10*$^{-/-}$ mice compared with *Il10*$^{-/-}$ mice (Fig. 5j, k). Together, these data show that mice deficient in STARD7 have increased susceptibility to development of acute and chronic colitis.

Discussion

Our study demonstrates that STARD7 is a critical regulator of intestinal epithelial cell mitochondria fitness and deficiency of this lipid transfer protein compromises the integrity of the intestinal barrier and leads to enhanced susceptibility for colitis. Importantly, we revealed that STARD7 expression is downregulated in the colon of UC patients and inversely associated with severity of inflammation. Mechanistically, we found that STARD7 directly regulates mitochondrial dynamics and that loss of STARD7 results in mitochondrial stress, and loss of intestinal epithelial barrier integrity. Notably, STARD7 deficiency could be overcome by treatment of epithelial cells through pharmacological activation of AMPK which could recover mitochondrial defects and barrier function. Finally, loss of STARD7 in vivo enhanced susceptibility to acute and chronic colitis.

STARD7 is an essential lipid transport protein that plays an important role in maintaining the distribution of PC between different biological membranes. PC is the most abundant phospholipid in the outer and inner mitochondrial membranes and depletion of PC dysregulates inner mitochondrial membrane protein function and negatively impacts mitochondrial respiration[255]. Our studies revealed that STARD7 predominately localizes to the outer mitochondrial membrane, but we also observed STARD7 in association with the inner mitochondrial membrane. Intriguingly, knockdown of STARD7 did not impact the expression of the outer mitochondrial membrane protein TOMM20 but did result in significant loss of Complex I expression in the inner mitochondrial membrane. Respiratory Complex I is a multi-subunit protein complex that serves as the major entry point of electrons to the respiratory chain

and is suggested as the rate-limiting step in overall respiration[256]. Complex I acts as a redox-driven proton pump transferring four protons from the mitochondrial matrix across the inner mitochondrial membrane to the periplasmic space[257]. The concentration of protons in the periplasmic space generates the proton-motive force across the inner mitochondrial membrane at Complex I, III, and IV to produce ATP from ADP and inorganic phosphate.

To increase the surface area of the inner mitochondrial membrane and the total amount of respiratory complexes that a single mitochondrion can hold mitochondria consist of cristae. The structural integrity of the cristae are critical for maximal mitochondrial energy production and disruption of the cristae structure has been linked to dysfunctional oxidative phosphorylation and compromised cell metabolism[258]. We show that STARD7 is critical for correct cristae structure formation and maintenance. Diminished STARD7 in intestinal epithelial cells disrupts cristae formation and this was associated with significant loss of inner mitochondrial membrane folds and disruption of Complex I networks which compromised energy production. We suggest that STARD7 may not directly regulate mitochondrial energy production, but rather plays a role in the formation and integrity of the mitochondrial inner membrane through trafficking PC which is required for the necessary architecture for oxidative phosphorylation.

STARD7 binds PC at the ER and transports the lipid across the cytosol to the mitochondrial outer membrane. Importantly, STARD7 possesses an N terminal mitochondrial targeting signal (MTS) (STARD7-I) that is required for non-vesicular transport of PC to the outer membrane of the mitochondria[149]. STARD7-I is recruited across the mitochondrial outer membrane through translocase of the outer membrane (TOM) complexes and is further transported into the inner

mitochondrial membrane through translocase of the inner membrane (TIM) complexes where the MTS is cleaved by mitochondrial processing peptidase and anchors STARD7 to the inner membrane[148]. Inner membrane embedded STARD7 is further processed by presenilin-associated rhomboid-like (PARL) protease to generate the mature form of STARD7 (STARD7-II) which is released into the mitochondrial intermembrane space[148]. The mature form of STARD7 possesses a negatively charged N-terminus which promotes the relocation of the protein back to the cytosol[148]. The role of STARD7-II has not yet been identified. Our own microscopy studies confirmed that STARD7 localization was not restricted to the mitochondria with significant STARD7 expression observed in the cytosol. Given that STARD7-II still possesses an intact START domain, we predict that the mature form could still uptake PC from the ER and perhaps facilitate PC transfer to non-mitochondrial organelle membranes. Lipid metabolism is regulated by nuclear receptors such as peroxisome proliferator–activated receptors (PPAR) and liver X receptors (LXR) which can form heterodimers with retinoid x receptors (RXR) and bind to DNA response elements[259]. These nuclear heterodimers interact with fatty acid ligands and have been shown to transcriptionally regulate gene expression of proteins involved in lipid and cholesterol transport and we speculate that STARD7 expression may be similarly regulated based on PC levels in different cellular compartments[260]. There is also little understanding regarding lipid transport between the outer and inner mitochondrial membranes. However, studies have established that lipid trafficking occurs through the ER via membrane contact sites and not though vesicles[261]. Critically ER-mitochondria membrane contact sites still feature a distance of 10-30 nm between the two compartments; highlighting the necessity of transfer proteins to move lipid molecules across the final stage of their transport[262].

We found that STARD7 is essential for the maintenance of mitochondrial homeostasis and furthermore STARD7 deficiency was highly detrimental to the integrity of the intestinal epithelial barrier. Importantly we found the compromised barrier was due to a disrupted tight junction protein expression pattern which is consistent with what is observed in IBD patients[263]. IECs from the colons of *Stard7*^{Tg} mice featured downregulated expression of seal forming Claudin-3; consistent with CD and UC patients who are marked with diminished expression of Claudin-3[264]. STARD7 haploinsufficiency also resulted in significant increase in the expression of the pore forming Claudin-2 which has been observed in CD and UC patients as well[265]. The regulation of these different classes of claudin tight junction proteins can heavily modulate the barrier capacity of IECs and STARD7 mediated changes in the claudin expression profile can severely alter intestinal mucosal homeostasis. Clinical studies have also established a role for mitochondrial dysfunction in IBD[266,267]. Specifically changes in the mitochondrial electron transport chain complex activity, Complex II and Complex IV, were observed in UC[267]. Intestinal epithelial cells are particularly susceptible to mitochondrial defects; these cells require high levels of energy for homeostasis. The intestinal epithelial monolayer is renewed every 3 days due to environmental damage which compromises cell integrity and impacts permeability[233]. UC specifically is a disease characterized by energy defects in epithelial cells that results in compromised cell turnover and barrier defects within the colon[235]. A recent study directly implicated mitochondrial dysfunction in UC; ATP production is directly regulated by 13 genes which are encoded by the mitochondrial genome and all of them have been shown to be downregulated in UC patients. The most significant change was observed in MT-ND3 which is a critical subunit of the respiratory chain Complex I. Notably, only colonic epithelial cells from

UC patients but not CD patients were marked by suppressed mitochondrial DNA encoded gene expression[244].

Murine-based studies have identified that compromised mitochondrial health can alter development of experimental colitis; PPARγ co-activator 1α (PGC1α) is a regulator of mitochondrial biogenesis and loss of this gene exacerbated the development of DSS-induced colitis[268]. Under inflammatory conditions, mitochondria can undergo dynamic changes in their shape and number, and these changed are regulated by genes such as Drp1 and Fis1 which control mitochondria fission[269]. Modulation of these essential mitochondrial dynamics has been linked to colitis, moreover selective inhibition of Drp1-Fis1 mediated mitochondrial fission provided protection from severe experimental colitis[270]. Healthy mitochondria are required for energy production and efficient renewal and turnover of intestinal epithelial cells [271]. Our work revealed compromised mitochondrial integrity in STARD7 deficient colonic epithelial cells with loss of Complex I within the inner mitochondrial membrane that heavily disrupted ATP production. Thus, loss of STARD7 results in detrimental changes to essential mitochondrial structure and reduces the total amount of ATP that is available to intestinal epithelial cells for maintenance of barrier function.

Our work highlights the importance of STARD7 trafficking of PC within the intestinal epithelium. Notably, PC is consistently found to be decreased in large intestine mucosa isolated from UC patients relative to CD patients[272]. Previous studies have demonstrated that UC patients treated with PC oral supplementation were marked with lower disease activity and endoscopy conformed improved histology in the rectal mucosa[273,274]. STARD7 maintenance of

PC composition in the mitochondrial membranes impacts the intestinal barrier; genetic deletion or knockdown of STARD7 enhanced barrier permeability. Previous studies reported that inhibition of mitochondrial respiratory chain and reduction in ATP production downregulates expression of tight junction proteins in intestinal epithelial cells[247]. In epithelial cells, the ATP-dependent Na^+K^+ ATPase regulates the formation of tight junctions through RhoA GTPase[275]. Inhibition of Na^+K^+ ATPase impairs the formation of tight junctions and intestinal epithelial cell polarization which was associated with reduction of RhoA GTPase activity[276]. The Rho GTPase family members are critical to the maintenance and remodeling of epithelial tight junction proteins via regulation of cytoskeletal filaments. Therefore, we speculate that loss of STARD7 mediated changes in energy production can alter the activity of these enzymes which is necessary to sustain expression of critical tight junction proteins[277,278].

STARD7 haploinsufficiency in mice leads to increased IBD susceptibility as a consequence of altered tight junction protein expression which results in loss of barrier integrity. Consistently, $STARD7^{low}$ UC patients were characterized by mitochondrial dysfunction which predisposed these individuals to compromised intestinal barrier function that promoted detrimental mucosal inflammation. Remarkably, we show that AMPK activation could compensate for loss of STARD7 by recovering mitochondrial architecture which reduced barrier permeability and promoted expression of junctional proteins. AMPK regulates mitochondrial fission through phosphorylation of mitochondrial fission factor (MFF) which directly binds to DRP1 in the mitochondrial outer membrane[279]. Importantly, mitochondrial fission is essential for mitophagy and required for removal of damaged mitochondria[280]. Furthermore, AMPK induces binding of PPARγ to PGC1α to ultimately initiate mitochondrial biogenesis under stress conditions[250,251]. It

is intriguing to speculate the impact of modulating the AMPK-STARD7 axis to enhance the integrity of the epithelial barrier and alter detrimental outcomes in IBD. AMPK signaling has been shown to have beneficial impact on the formation of tight junction proteins and enhancing barrier function[281-283]. In vivo studies found that AMPK deficient mice are more susceptible to DSS-induced colitis[284]. In WT mice AMPK activation was impaired during the onset and maintenance of the colitic phenotype; however, treatment of WT mice with metformin attenuated DSS-induced colitis in a dose dependent manner[281]. In line with the reduced colitic phenotype, metformin prevented the loss of tight junction proteins in colonic epithelial cells[281]. We identified that mitochondrial stress due to STARD7 deficiency impacts the formation of essential tight junction proteins but treatment from AMPK agonists could recover the expression of Claudin-3 and ZO-1 and ultimately recover barrier function. Thus, we speculate that stimulation of AMPK could provide a viable therapeutic approach in UC patients for enhancing the integrity of the intestinal epithelium.

In conclusion, we show that STARD7 expression in colonic epithelial cells regulates intestinal inflammatory responses, and that loss of STARD7 leads to a defect in intestinal barrier function and enhances susceptibility to colitis. The demonstration of STARD7 modulating barrier health and a requirement for this lipid transporter in mitochondrial homeostasis and energy production emphasizes the importance of mitochondrial associated networks to treat the detrimental inflammation associated with IBD. Our data suggests that loss of STARD7 mediated lipid trafficking results in metabolic dysfunction within the intestinal epithelium and supports the notion that treatment with AMPK agonists can recover mitochondrial health and provide a viable therapeutic approach for treatment of UC patients marked by STARD7-mitochondriial defects.

Methods

Mice. Male and female, 5 - 10 week *Il10*$^{-/-}$ mice (C57BL/6), *Vilin*^{cre} mice (C57BL/6) and *Shh*^{cre} mice (C57BL/6) were obtained from Jackson Laboratories (USA)**.** Male and female, 5 - 10 week *Stard7*^{Tg} mice (C57BL/6) and *Stard7*$^{fl/fl}$ (C57BL/6) were kindly provided by Dr. Timothy Weaver[150,285]. To generate the mice *Stard7*^{Tg}*Il10*$^{-/-}$ (C57BL/6), *Stard7*^{Tg} mice (C57BL/6) were intercrossed with *Il10*$^{-/-}$ mice (C57BL/6). All mice strains were co-housed in the same room.

Experimental colitis models. DSS (ICN Biomedical Inc.) was supplied in the drinking water as a 2.5% (w/v) solution. Euthanasia and postmortem analyses were performed at 6 days after treatment with DSS. Clinical disease was scored based on prior descriptions[141]. For the *Il10*$^{-/-}$ spontaneous model of colitis; co-housed *Il10*$^{-/-}$ and *Stard7*^{Tg}*Il10*$^{-/-}$ mice were monitored for colitis development from 5 weeks of age. Euthanasia and postmortem analyses were performed at 10 weeks of age. The colitic mice were weighed twice every week to measure body weight and lymph nodes, small intestine, and colonic tissue were collected for analysis at the end of the experiment. Weight changes were calculated as a percentage of weight at the start of the experiment (Day 0). Clinical disease was scored based on prior descriptions [220]. In brief mice were graded on a scale of 0 to 5 by assessment of symptoms including bump on nose, pilar erecti, rectal prolapse, anal bleeding, decreased activity, diarrhea, hunched back, excreted perianal mucus, shrunken eyes, and dehydration. For all animal experiments, mice that lost ≥ 20% of its body weight (relative to weight at the start of the experiment) were euthanized in accordance with IACUC protocols.

Histology. Harvested tissues were washed with PBS, fixed flat or swiss rolled overnight in 4% paraformaldehyde. Paraffin embedded tissue were stained with hematoxylin and eosin and analyzed by bright field microscopy. Histological scoring was performed on ascending, transverse and descending colon and rectum segments as previously described[141].

Western Blot. Intestinal epithelial cells were lysed in protein lysis buffer (10% glycerol, 20 mM Tris HCl [pH 7], 137 mM NaCl, 2 mM EDTA, and 1% NP-40) supplemented with proteinase inhibitor cocktail (Thermo fisher) and PhoSTOP phosphatase inhibitors (Roche). Protein lysates were cleared of insoluble material through centrifugation, and the resulting protein lysates were subjected to SDS-PAGE. Proteins were wet transferred to 0.2 mm nitrocellulose membranes (Thermo fisher), which were blocked using 3% BSA in 1% TBST buffer for 1 hour at room temperature. Membranes were incubated overnight using the following primary antibodies: α-β-actin (13E5, CST), α-STARD7 (PA5-30772, Thermo), α-Claudin-1 (MH25, Thermo), α-Claudin-2 (12H12, Thermo), α-Claudin-3 (OTIIE7, Novus), α-Claudin-4 (ZMD.306, Thermo), α-E-Cadherin (R&D), α-CK8 (EP1628Y, Thermo), α-TOM20 (Abcam) and Oxphos WB cocktail (Abcam). Primary antibodies were used at either 1:500, 1:1000, or 1:2000 dilutions in blocking buffer. Membranes were washed in TBST and incubated with the secondary antibody, (goat α-rabbit-HRP, goat α-mouse-HRP), at a 1:10,000 dilution in blocking buffer. Protein bands were visualized following exposure of the membranes to ECL substrate solution (Thermo fisher) and quantified by densitometry analysis using Image Studio (Licor) software.

Lentiviral Transduction. Caco-2 BBe cells at 70–90% confluence were transduced with lentiviral particles containing shRNAs targeting STARD7 or a nontarget control shRNA

(Mission® nontarget shRNA control; Sigma). STARD7 shRNA and nontarget control shRNA lentivirus was generated by the Cincinnati Children's Hospital Medical Center Viral Core using a 4-plasmid packaging system. Lentiviral particles were incubated with Caco-2 BBe cells (multiplicity of infection ~10) in the presence of Polybrene (4 μg/ml; Sigma) for 24 h followed by selection in puromycin at a concentration (2 μg/ml) that killed uninfected cells within 3 days. The lentiviral-transduced Caco-2 BBe cells (passage 1–5) were grown to confluency under puromycin selection pressure. STARD7 knockdown was assessed by Western blot and immunofluorescence analysis.

Transmission Electron Microscopy. Caco-2 BBe cells were fixed for transmission electron microscopy as described[285]. Electron micrographs were collected using a Hitachi H-7650 TEM (Hitachi High Technologies America, Inc., Dallas, TX) equipped with an AMT transmission electron microscope charge-coupled device camera (Advanced Microscopy Techniques, Woburn, MA).

Immunofluorescence Microscopy. Caco-2 BBe cells were seeded onto #1.5 glass coverslips in 6 well plates at a density of 600,000 cells per well. The cells were fixed with 4% paraformaldehyde at room temperature for 15 minutes, followed by permeabilization for 5 minutes with the wash buffer (PBS containing 0.1% Triton X-100), and blocked with 10% Normal Goat Serum control (Invitrogen) in the wash buffer for 30 minutes. Coverslips were incubated with in staining buffer with primary antibody (1:1000) for 45 minutes at room. The following primary antibodies were used: α-TOM20, α-Complex I, and α-STARD7. Coverslips were washed then incubated in staining buffer with secondary antibody (1:500) for 45 min at

room Alexa Fluor-488 α-mouse antibody and Alexa Fluor-594 α-rabbit antibody. Cells were counterstained with Phalloidin (Thermo Fisher, C34552) and DAPI (Thermo Fisher, D1306) according to manufacturing protocol. Coverglasses were washed and mounted onto microscope slides using Prolong Diamond Antifade Mountant (Thermo Fisher, P36970). Cells were imaged at 100× magnification using a Yokogawa CSU-X1 Spinning Disk confocal microscope (Nikon). Images were analyzed using the open source software CellProfiler[286] and ImageJ[287].

Ussing Chamber. For ex vivo barrier function experiments, one centimeter, freshly isolated, of jejunum and colonic tissue was mounted between the hemi-chambers of an Ussing apparatus For in vitro barrier function experiments, 500,000 Caco-2 BBe cells were plated on Snapwell or Transwell filters (12-mm diameter, 0.4-μm pore; Corning, Lowell, MA) and cultured for 10–14 days. Transepithelial resistance (TER) was measured with an EVOM/Endohm or STX2 electrode (Costar), with correction for filter resistance. Only Snapwell filters with TER >250 Ω·cm2 were used. For stimulation studies, cells were stimulated with AICAR or metformin basolaterally and TER was monitored for 24 h. For permeability studies, Snapwell filters were placed in Ussing chambers and baseline TER measurements were performed. After addition of 2.2 mg/ml FITC-dextran (4.4 kDa; Sigma Aldrich) and 1 mg/ml horseradish peroxidase (40 kDa; Sigma Aldrich) to the apical bath, 0.25-ml aliquots were removed from the basolateral bath and replaced with fresh Krebs solution every 30 min for 3 h. Horseradish peroxidase concentrations were determined by tetramethylbenzidine detection (BD Pharmingen, San Diego, CA) and spectrophotometry at 550–450 nm. Dextran-FITC levels were measured by spectrophotofluorometry (490 nm excitation, 530 nm emission).

Seahorse Assay. To measure glycolytic and mitochondrial metabolic function in intestinal epithelial cells we use the Seahorse XFe96 Analyzer (Agilent Technologies, Santa Clara, CA, USA). We used isolated mitochondria or transduced Caco-2 BBe and plated them in a 96 well Seahorse plate. Wells were washed twice with the appropriate Seahorse assay media (Agilent Technologies, Santa Clara, CA, USA) and incubated for 30 minutes in a CO_2 free incubator at 37°C. Oxygen consumption rate (OCR) was determined using a cell Mito Stress Test kit (Agilent Technologies, Santa Clara, CA, USA) according to manufacturer's instructions. Oligomycin (2μM); FCCP (Carbonyl cyanide 4-(trifluoromethoxy) phenylhydrazone) (1.5μM); Rotenone (0.5μM), and Antimycin (0.5μM) were used in the assay. Glycolytic function was determined using Glyco stress test kit (Agilent Technologies, Santa Clara, CA, USA). Glucose free media was used in the determination of glycolytic function. Glucose (10mM); Oligomycin (2μM); and 2-deoxy D-glucose (2-DG) (50mM) were used in the glycolysis assay. Cell lysate was collected from 96 well plates after assay and equal protein content was confirmed using BCA protein assay kit (Pierce Thermo scientific). Data was analyzed using Wave 2.6 software.

RNA-seq Analysis. RNA-seq data analyses were obtained from the NCBI GEO database, with accession numbers GSE109142 and GSE57945. Downstream analysis was performed in R (R Core Team, Vienna, Austria) where the read counts were analyzed in IDEP 9.1 and DESeq was used to identify the differentially expressed genes (DEGs)[224]. DEGs were identified with an adjusted p value <= 0.05 and at least ≥ ± 1.5-fold reads per kb of transcript, per million mapped reads (RPKM) and heat map was generated using Python (Python Software Foundation, Wilmington, Del) on the normalized scale. KEGG pathway analysis was used to identify important pathways altered by differentially regulated genes. Statistical analysis was performed

using SPSS 17.0. Differential expression was defined with a significant change in expression by limma[288]. Heatmaps of gene expression were generated using Morpheus (https://software.broadinstitute.org/morpheus/) and Phantasus[226]. Gene ontology analysis was performed using Enrichr and Gene Set Enrichment Analysis (GSEA).

Statistics

Statistical parameters are defined in the figure legends. Data are presented as mean ± SEM. Data was considered significant at $p < 0.05$. Comparisons between 2 groups were made using a t test. Comparisons between more than 2 group were made using 2-way ANOVA and where appropriate were followed with a Dunnett's Multiple Comparison Test or Sidak's Multiple Comparison Test. Statistical analysis was performed in Prism (GraphPad Software).

Study Approval

All animal studies were approved by the IACUC of the University of Michigan, Ann Arbor, MI and performed in accordance with university guidelines.

Acknowledgements

We would like to acknowledge members of the Divisions of Allergy and Immunology and Immunobiology at Cincinnati Children's Hospital Medical Center, Mary H. Weiser Food Allergy Center and Division of Experimental Pathology at the University of Michigan Medicine for thoughtful discussions. This work was supported by National Institutes of Health grants DK073553, DK090119, DK125007, DK099222, AI138177, AI112626, and AI007413; Food

Allergy Research & Education (FARE); Department of Defense grant W81XWH-15-1-051730; M-FARA; and the Mary H. Weiser Food Allergy Center supported (to S.P.H.).

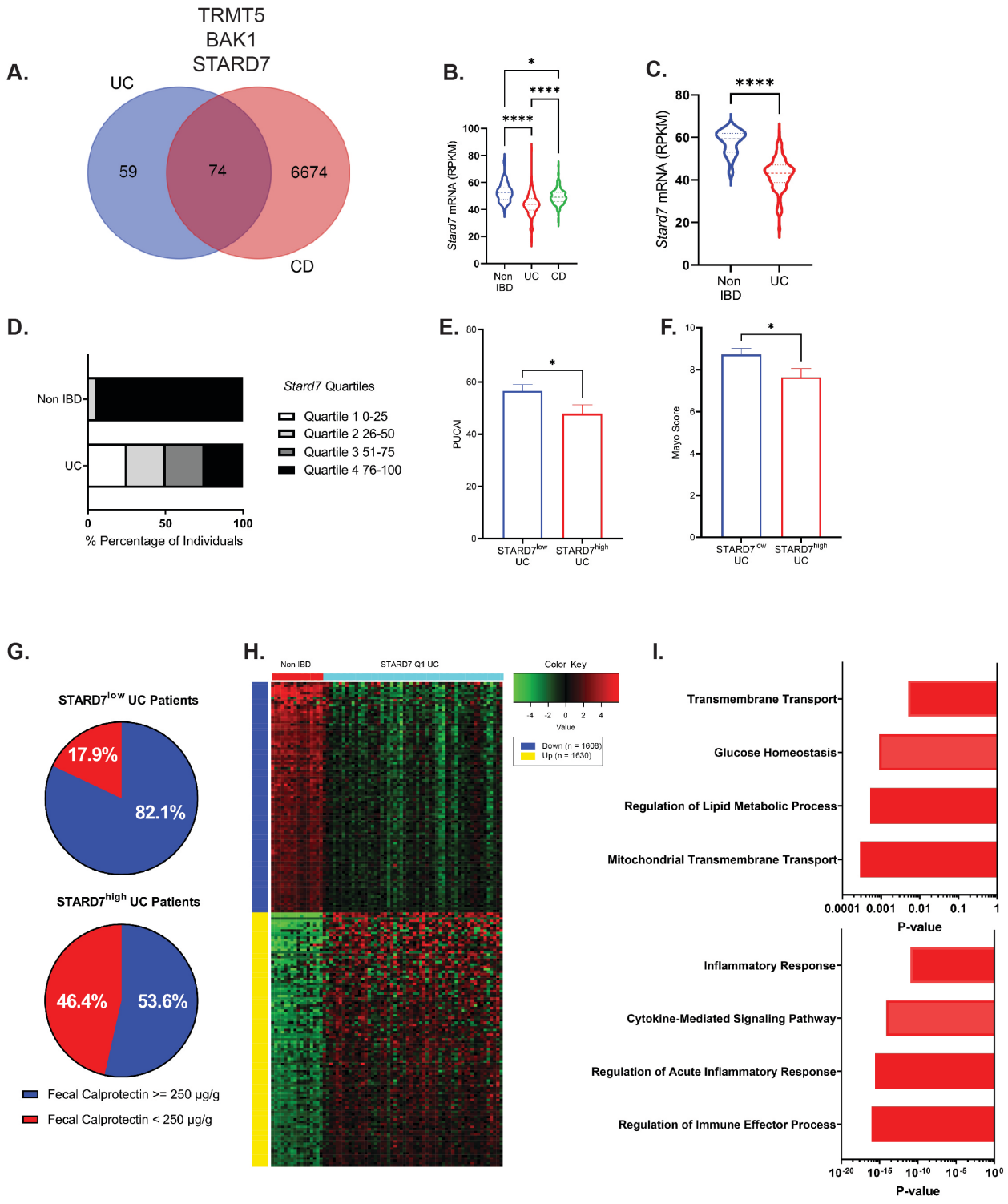
A.
TRMT5
BAK1
STARD7
UC
59
74
6674
CD
B.
Stard7 mRNA (RPKM)
Non IBD
UC
CD
C.
Stard7 mRNA (RPKM)
Non IBD
UC
D.
Non IBD
UC
Stard7 Quartiles
Quartile 1 0-25
Quartile 2 26-50
Quartile 3 51-75
Quartile 4 76-100
% Percentage of Individuals
E.
PUCAI
STARD7low UC
STARD7high UC
F.
Mayo Score
STARD7low UC
STARD7high UC
G.
STARD7low UC Patients
17.9%
82.1%
STARD7high UC Patients
46.4%
53.6%
Fecal Calprotectin >= 250 µg/g
Fecal Calprotectin < 250 µg/g
H.
Non IBD
STARD7 Q1 UC
Color Key
Value
Down (n = 1608)
Up (n = 1630)
I.
Transmembrane Transport
Glucose Homeostasis
Regulation of Lipid Metabolic Process
Mitochondrial Transmembrane Transport
P-value
Inflammatory Response
Cytokine-Mediated Signaling Pathway
Regulation of Acute Inflammatory Response
Regulation of Immune Effector Process
P-value

J.

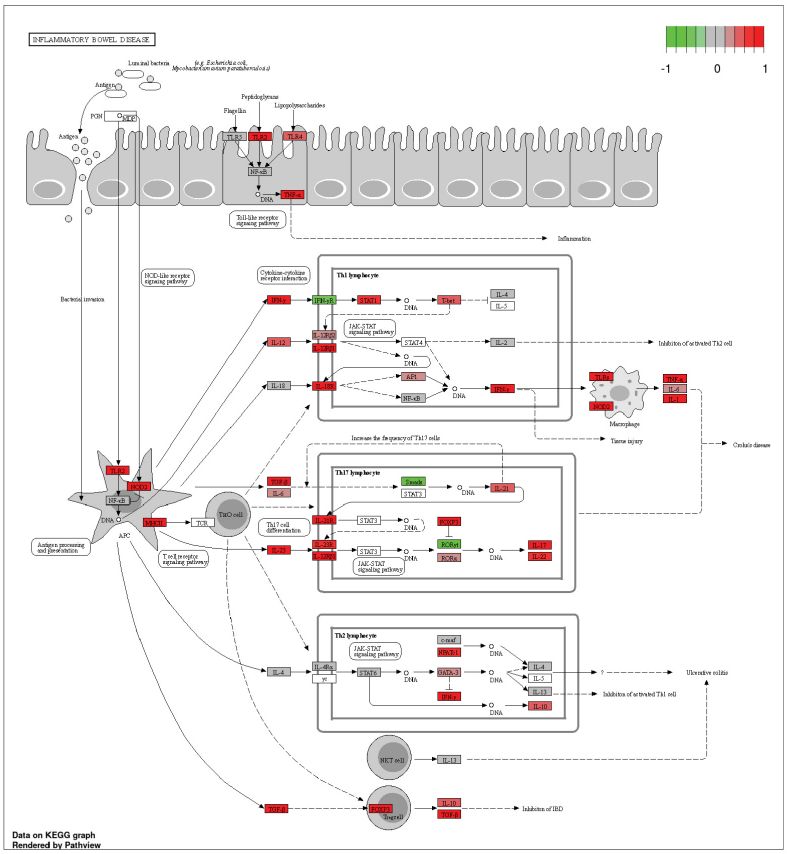

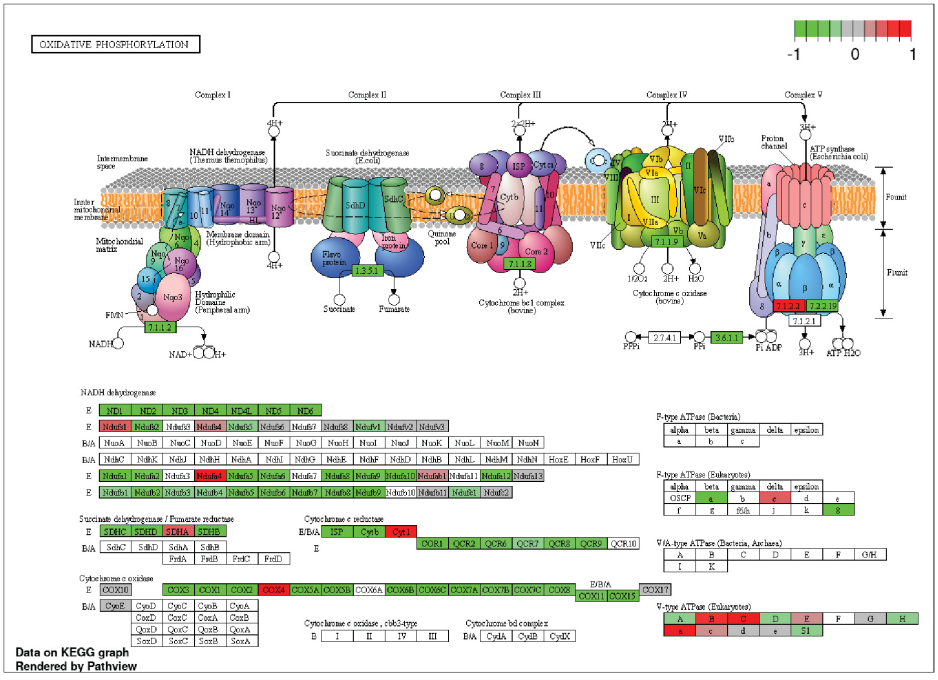

Figure 3-1 *Stard7* mRNA Expression is Downregulated in IBD and Levels are Associated with Disease Severity.

(A) Venn diagram of overlapping DEGs between UC vs non-IBD and CD vs non-IBD patients. Select common DEGs are indicated (GSE57945). (B) Violin plot showing *Stard7* expression (RPKM) in UC, CD or non-IBD tissue biopsies (non-IBD *n*= 42; UC *n*= 206, CD *n* = 175). (C) Violin plot showing *Stard7* expression (RPKM) in UC or non-IBD tissue biopsies (non-IBD *n*= 17; UC *n*= 206) (GSE109142). (D) Stratification of non-IBD and UC cohort based upon *Stard7* expression (quartiles, RPKM). (E) PUCAI and (F) Mayo scores in $STARD7^{low}$ and $STARD7^{high}$ UC patients. (G) Pie chart indicating the % of $STARD7^{low}$ and $STARD7^{high}$ UC patients which had high levels of fecal calprotectin (>= 250 μg/g) 4 weeks after their initial diagnosis. (H) Heat map of differentially expressed genes based on RNA-seq data between non-IBD (*n*= 16) and Quartile 1 *Stard7* UC (*n*= 56) patients. (I) Bar graphs of pathway analysis of upregulated genes (bottom) and downregulated genes (top) in Quartile 1 *Stard7* UC patients relative to non-IBD patients; assessed via Gene Ontology Biological Process Pathways, ranked by p-value. (J) Pathway analysis of differentially expressed genes in Quartile 1 *Stard7* UC patients relative to non-IBD patients involved in inflammatory bowel disease (top) and oxidative phosphorylation (bottom). Data are presented as mean ± SEM. Statistical analysis was performed using one-way analysis of variance followed by Tukey's multiple comparison test or performed using an unpaired t test. *p <0.05, **p <0.01, ****p <0.0001.

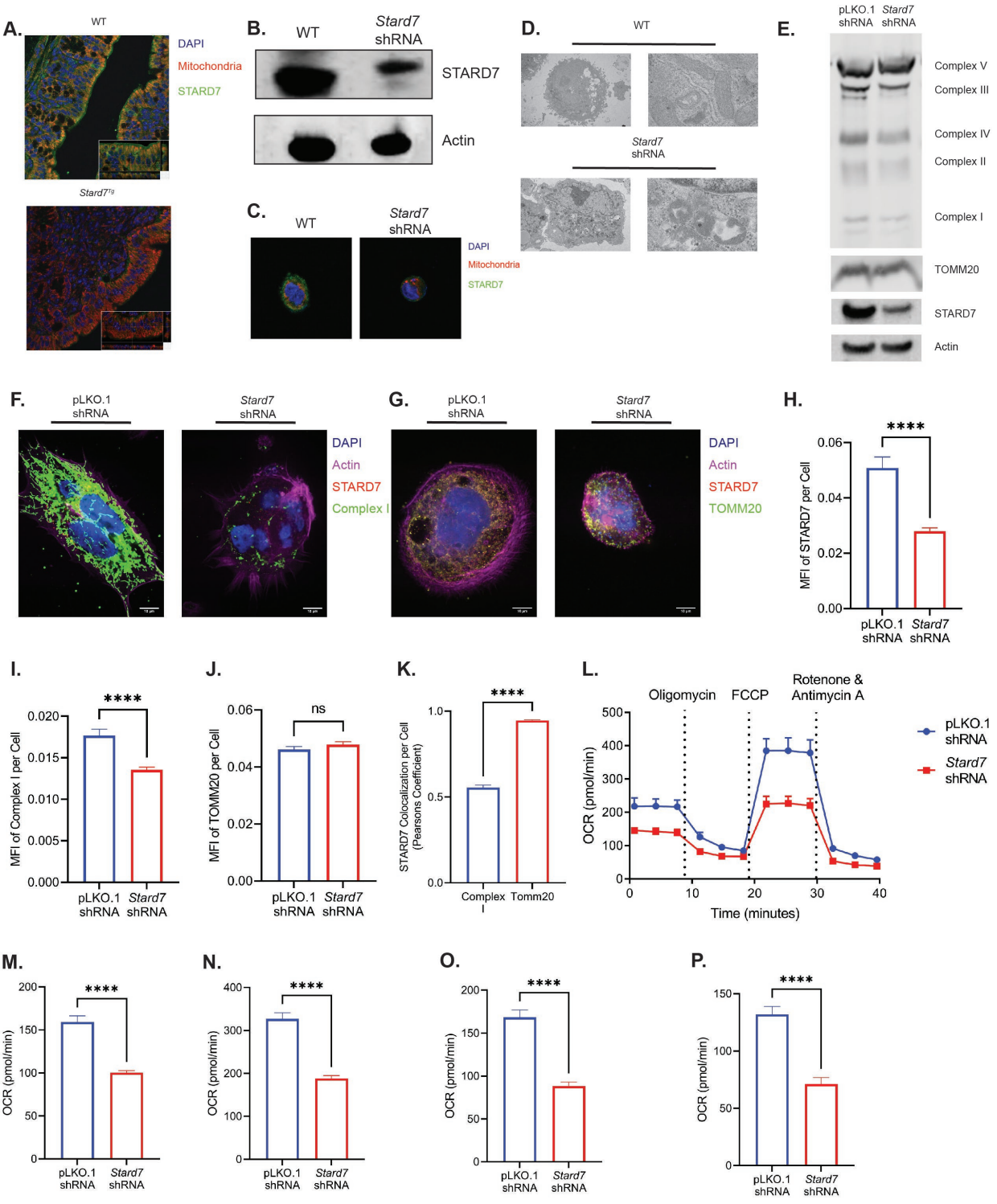

Figure 3-2 Mitochondrial Function is Negatively Altered in STARD7 Deficient Colonic Epithelial Cells.

(A) Immunofluorescence analysis of STARD7 localization in colonic tissue from WT and *Stard7*^{Tg} mice. (B) Western blot analyses of STARD7 expression in WT and *Stard7* shRNA transduced Caco-2 BBe cells. (C) Immunofluorescence analysis of STARD7 expression in WT and *Stard7* shRNA transduced Caco-2 BBe cells. (D) Transmission electron microscopy analysis of mitochondrial structure in WT and *Stard7* shRNA transduced Caco-2 BBe cells. (E) Western blot analyses of oxidative phosphorylation proteins in pLKO.1 shRNA and *Stard7* shRNA transduced Caco-2 BBe cells. Immunofluorescence analysis of STARD7 expression and either (F) Complex I or (G) TOMM20 expression in pLKO.1 shRNA and *Stard7* shRNA transduced Caco-2 BBe cells. Quantification (mean fluorescence intensity) of (H) STARD7, (I) Complex I, and (J) TOMM20 expression using CellProfiler image analysis software. (K) Colocalization analysis between STARD7 and Complex I and TOMM20 in pLKO.1 shRNA transduced Caco-2 BBe cells. (L) Seahorse Mito Stress Test was performed on pLKO.1 shRNA and *Stard7* shRNA transduced Caco-2 BBe cells where oxygen consumption rate (OCR) was measured over time as cells were exposed at the indicated time points to oligomycin, carbonyl cyanide p-trifluoromethoxyphenylhydrazone (FCCP), and rotenone/antimycin A. Measurement of (M) basal respiration, (N) maximal respiration, (O) spare respiratory capacity and (P) ATP production in pLKO.1 shRNA and *Stard7* shRNA transduced Caco-2 BBe cells. Data are representative of at least 2 independent experiments with at least five replicates per group. Data are presented as mean ± SEM. Statistical analysis was performed using unpaired t test. ****p <0.0001.

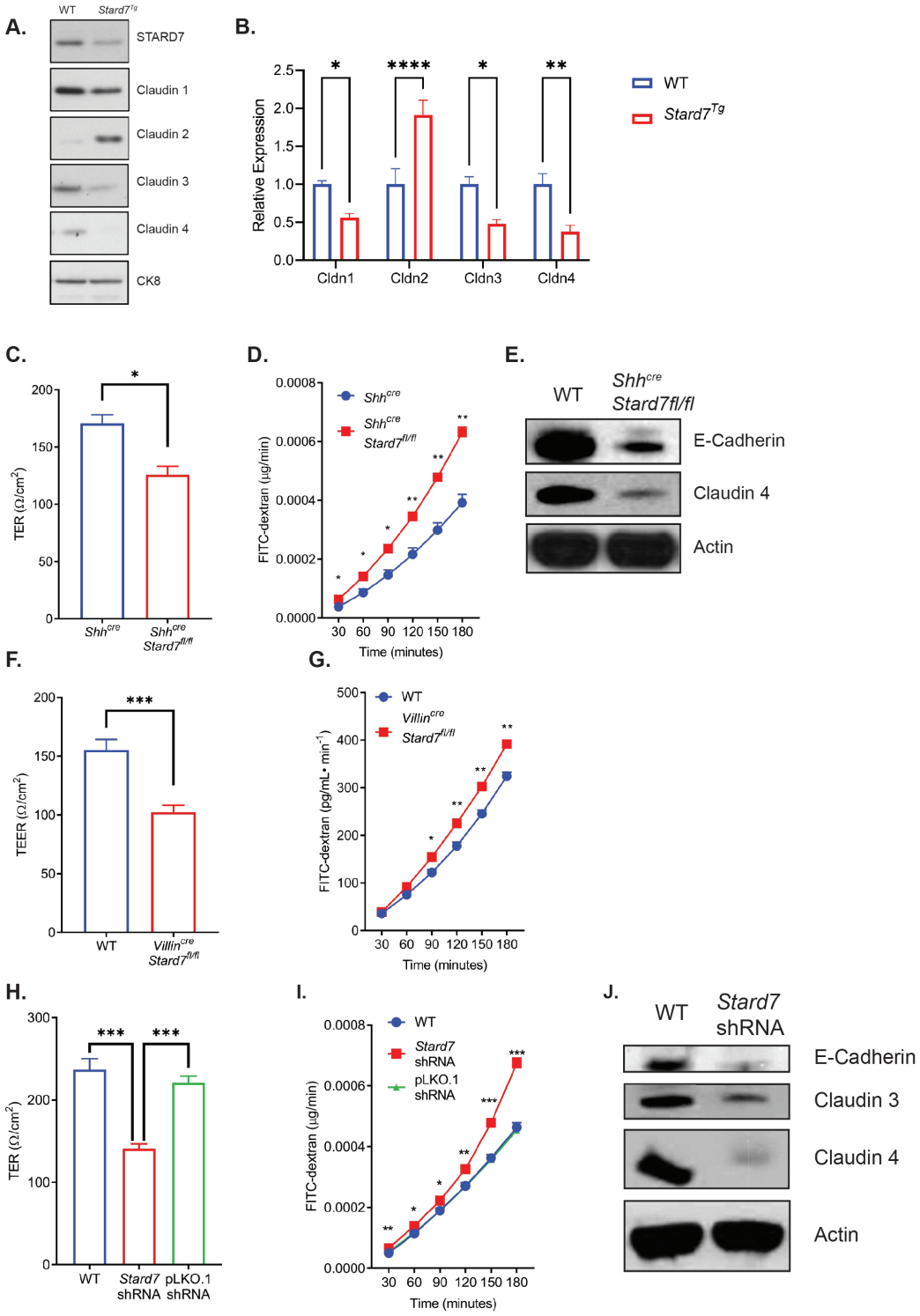

Figure 3-3 STARD7 Deficiency Alters Homeostatic Intestinal Epithelial Barrier Function.

(A) Western blot analyses of tight junction proteins in WT and *Stard7*^{Tg} colonic epithelial cells. (B) Densitometry analyses of tight junction proteins in WT and *Stard7*^{Tg} colonic epithelial cells (WT *n*= 6; *Stard7*^{Tg} *n*= 6). (C) Transepithelial electric resistance in *Shh*^{cre}*Stard7*$^{fl/fl}$ colonic epithelial cells (*Shh*^{cre} *n*= 3; *Shh*^{cre}*Stard7*$^{fl/fl}$ *n*= 3). (D) Time course of FITC-dextran flux in *Shh*^{cre}*Stard7*$^{fl/fl}$ colonic epithelial cells (*Shh*^{cre} *n*= 3; *Shh*^{cre}*Stard7*$^{fl/fl}$ *n*= 3). (E) Western blot analyses of tight junction proteins in WT and *Shh*^{cre}*Stard7*$^{fl/fl}$ colonic epithelial cells. (F) Transepithelial electric resistance in *Vilin*^{cre}*Stard7*$^{fl/fl}$ colonic epithelial cells (WT *n*= 3; *Vilin*^{cre}*Stard7*$^{fl/fl}$ *n*= 8). (G) Time course of FITC-dextran flux in *Vilin*^{cre}*Stard7*$^{fl/fl}$ colonic epithelial cells (WT *n*= 3; *Vilin*^{cre}*Stard7*$^{fl/fl}$ *n*= 3). (H) Transepithelial electric resistance in WT, pLKO.1 shRNA transduced and *Stard7* shRNA transduced Caco-2 BBe cell monolayers (WT *n*= 4; pLKO.1 *n*= 8; *Stard7 n*= 8). (I) Time course of FITC-dextran flux in WT and *Stard7* shRNA transduced Caco-2 BBe cell monolayers (WT *n*= 4; pLKO.1 *n*= 4; *Stard7 n*= 4). (J) Western blot analyses of tight junction proteins in WT and *Stard7* shRNA transduced Caco-2 BBe cells. Data are representative of at least 2 independent experiments with at least three replicates per group. Data are presented as mean ± SEM. Statistical analysis was performed using one-way analysis of variance followed by Tukey's multiple comparison test or performed using an unpaired t test. *p <0.05, **p <0.01, ***p <0.001, ****p <0.0001.

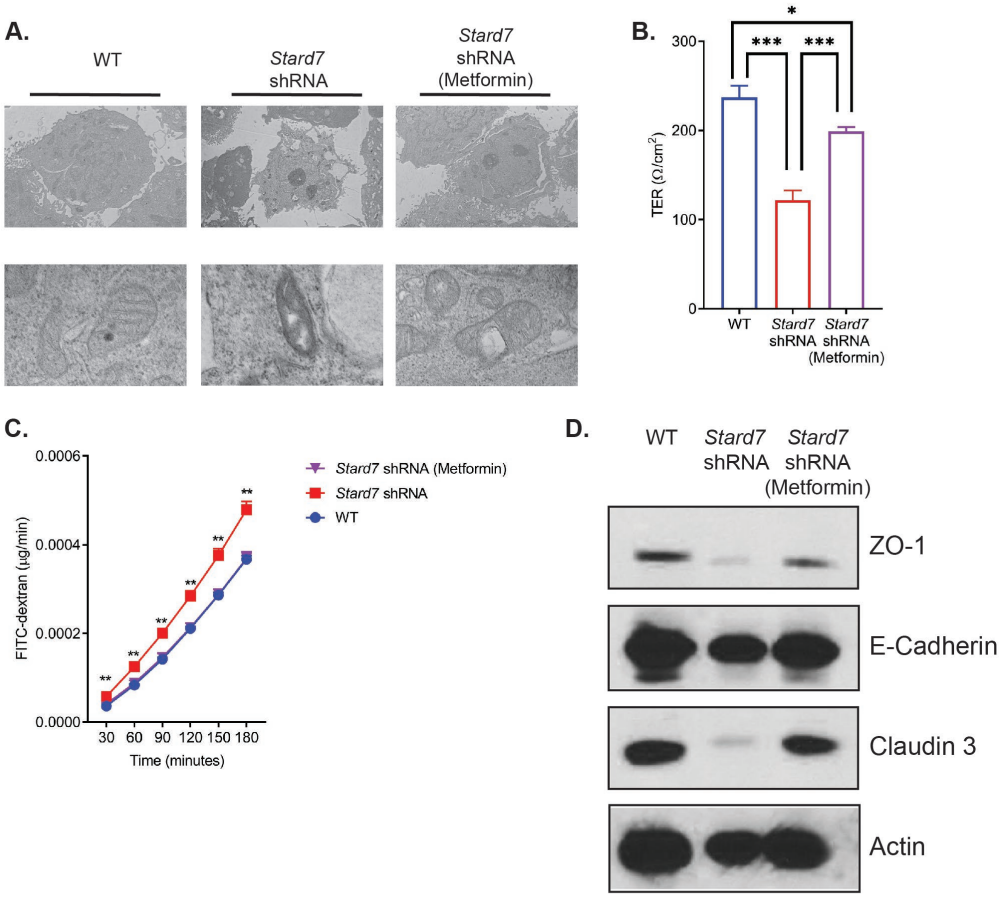

Figure 3-4 STARD7 Knockdown in Human Colonic Epithelial Cells Enhances Barrier Permeability and can be Overcome with AMPK Activation.

(A) Transmission electron microscopy analysis of mitochondrial structure in WT, *Stard7* shRNA transduced and metformin stimulated *Stard7* shRNA transduced Caco-2 BBe cells. (B) Transepithelial electric resistance in WT, *Stard7* shRNA transduced and metformin stimulated *Stard7* shRNA transduced Caco-2 BBe cell monolayers (WT *n*= 4; *Stard7 n*= 4; metformin stimulated *Stard7 n*= 4). (C) Time course of FITC-dextran flux in WT, *Stard7* shRNA transduced and metformin stimulated *Stard7* shRNA transduced Caco-2 BBe cell monolayers (WT *n*= 4; *Stard7 n*= 4; metformin stimulated *Stard7 n*= 4). (D) Western blot analyses of tight junction proteins in WT, *Stard7* shRNA transduced and metformin stimulated *Stard7* shRNA transduced Caco-2 BBe cells. Data are representative of at least 3 independent experiments with at least three replicates per group. Data are presented as mean ± SEM. Statistical analysis was performed using one-way analysis of variance followed by Tukey's multiple comparison test or performed using an unpaired t test. *p <0.05, **p <0.01, ***p <0.001.

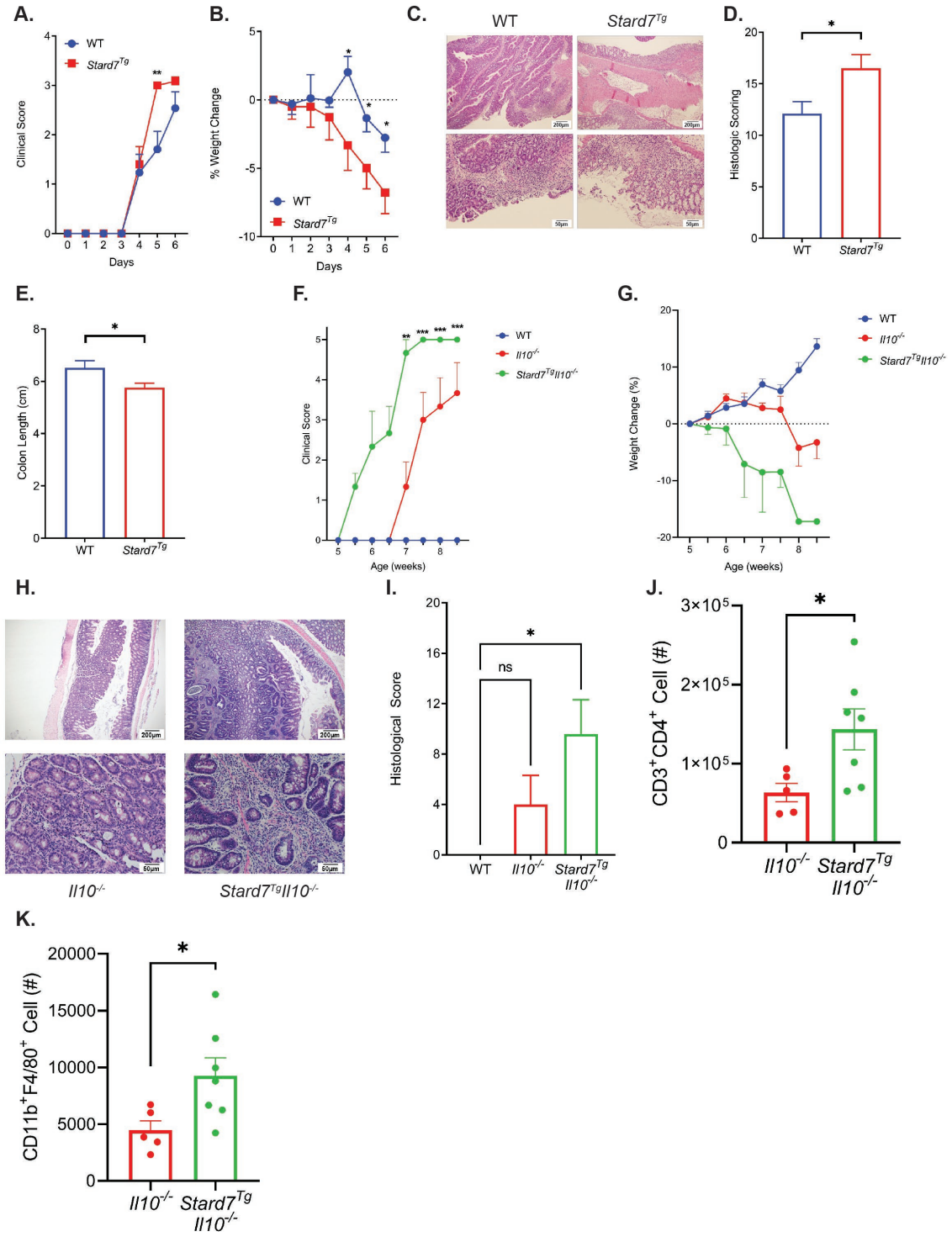

Figure 3-5 Loss of *Stard7* Exaggerates the Development of Colitis.

(A) Clinical score (WT *n*= 17; *Stard7*^{Tg} *n*= 15). (B) % Body weight change (relative to weight at start of experiment) (WT *n*= 17; *Stard7*^{Tg} *n*= 15). (C) Representative image of colon histology (H&E staining) from WT and *Stard7*^{Tg} mice. Top row 4x magnification (Scale bar represents 200 µm), bottom row 20x magnification (Scale bar represents 50 µm). (D) Colon histological scoring from WT and *Stard7*^{Tg} mice (WT *n*= 10; *Stard7*^{Tg} *n*= 9). (E) Colon lengths from WT and *Stard7*^{Tg} mice (WT *n*= 10; *Stard7*^{Tg} *n*= 10). (F) Clinical score (*Il10*$^{-/-}$ *n*= 5; *Stard7*^{Tg}*Il10*$^{-/-}$ *n*= 6). (G) % Body weight change (relative to weight at start of experiment) (*Il10*$^{-/-}$ *n*= 5; *Stard7*^{Tg}*Il10*$^{-/-}$ *n*= 6). (H) Representative image of colon histology (H&E staining) from *Il10*$^{-/-}$ and *Stard7*^{Tg}*Il10*$^{-/-}$ mice. Top row 4x magnification (Scale bar represents 200 µm), bottom row 20x magnification (Scale bar represents 50 µm). (I) Colon histological scoring from *Il10*$^{-/-}$ and *Stard7*^{Tg}*Il10*$^{-/-}$ mice (*Il10*$^{-/-}$ *n*= 5; *Stard7*^{Tg}*Il10*$^{-/-}$ *n*= 6). (J) Cell counts (#) of $CD3^{+}CD4^{+}$ T cells in the mLN of mice (*Il10*$^{-/-}$ *n*= 5; *Stard7*^{Tg}*Il10*$^{-/-}$ *n*= 6). (K) Cell counts (#) of $CD11b^{+}F4/80^{+}$ macrophages in the mLN of mice (*Il10*$^{-/-}$ *n*= 5; *Stard7*^{Tg}*Il10*$^{-/-}$ *n*= 6). Data encompasses 3 independent experiments. Data are presented as mean ± SEM. Statistical analysis was performed using an unpaired t test. *p <0.05, **p <0.01, ***p <0.001.

Table 3.1 RNAseq analyses and Identification of DEGs in UC and CD.

Large dataset excel file available here:

https://www.dropbox.com/s/npye5evnwe0k91w/Supplementary_Table_1.xlsx?dl=0

(A) Expression values for DEGs between UC and Non IBD individuals. (B) Expression values for DEGs between CD and Non IBD individuals. (C) List of common 74 DEGs between UC and Non IBD individuals and between CD and Non IBD individuals. Downstream analysis of expressed genes was performed IDEP 9.1.

Table 3.2 UC Patients Stratification by STARD7 Expression.

Supplementary Table 2: STARD7 expression signature in pediatric UC cohort based upon endoscopic Severity					
Disease Category	**STARD7_ Q1**	**STARD7_ Q2**	**STARD7_ Q2**	**STARD7_ Q4**	**P-value**
Controls (Non IBD), N= 17	0 (0%)	1 (5.9%)	0 (0%)	16 (94.1%)	2.18×10^{-10}
Ulcerative Colitis, N=206	56 (27.2%)	55 (26.7%)	56 (27.2%)	39 (18.9)	
STARD7 quartiles were established based on RPKM values: Q1 (0-25%), 16.78 – 39.31; Q2 (26-50%), 39.37 – 43.81; Q3 (51-75%), 43.90 – 48.5					
value (%) represents the number of patients (% of total of disease category)					

STARD7 quartiles were established based on RPKM values; quartiles Q1 (0-25%), 16.78 – 39.31; Q2 (26-50%), 39.37 – 43.81; Q3 (51-75%), 43.90 – 48.55 and Q4 (76-100%), 48.68 – 64.84. Statistical analysis was performed using SPSS 17.0. The Frequencies procedure was used for the STARD7 quartile analysis.

Table 3.3 Proinflammatory Gene Expression in STARD7^{low} and STARD7^{high} UC Patients.

Supplementary Table 3: Proinflammatory Gene Expression in STARD7^{low} and STARD7^{high} UC Patients			
Proinflammatory Genes	STARD7_ Q1 (N = 56)	STARD7_ Q4 (N = 55)	p-Value
GATA3	1.68 ± 0.054	1.21 ± 0.09	0.035
IFNG	1.018 ± 0.12	0.69 ± 0.11	0.15
IFNGR1	72.83 ± 2.81	87.90 ± 2.81	<0.0001
IL13	0.18 ± 0.02	0.07 ± 0.02	0.121
IL17A	1.59 ± 0.16	0.86 ± 0.13	0.001
IL18	50.20 ± 2.06	59.69 ± 2.77	0.018
IL1A	2.43 ± 0.22	1.44 ± 2.69	0.079
IL1B	51.72 ± 5.78	30.04 ± 7.52	0.123
IL23A	3.85 ± 0.37	2.00 ± 0.26	0.003
IL23R	0.35 ± 0.02	0.65 ± 0.21	<0.0001
IL4R	38.89 ± 2.03	46.90 ± 2.19	<0.0001
IL6	5.39 ± 0.76	2.54 ± 0.53	0.133
JUN	25.53 ± 2.47	43.86 ± 3.33	<0.0001
NFKB1	16.18 ± 0.71	24.57 ± 0.60	<0.0001
RELA	25.38 ± 0.85	30.94 ± 0.79	<0.0001
RORA	2.41 ± 0.14	3.00 ± 0.18	<0.0001
RORC	5.50 ± 0.31	10.65 ± 0.48	<0.0001

SMAD2	25.66 ± 0.89	34.70 ± 0.52	<0.0001
SMAD3	11.64 ± 0.65	14.66 ± 0.51	<0.0001
STAT1	66.18 ± 4.50	88.11 ± 7.63	0.009
STAT6	58.85 ± 2.39	83.95 ± 2.71	<0.0001
TLR5	1.46 ± 0.08	2.13 ± 0.10	<0.0001

Expression values for innate and adaptive proinflammatory genes in UC patients stratified by STARD7 expression.

Appendix

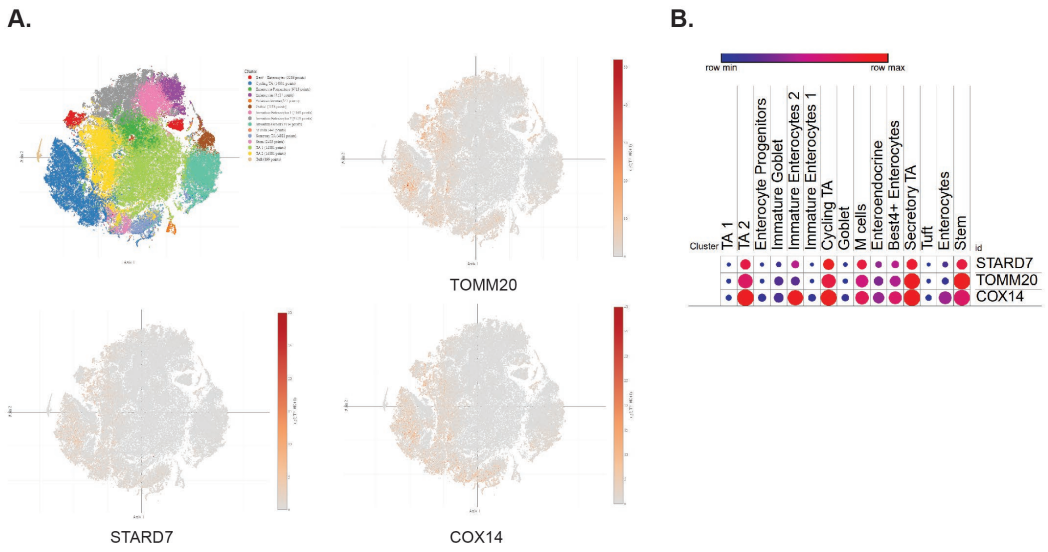

Supplementary Figure 3-1 Single Cell RNAseq Analysis of IECs Reveals Enrichment for STARD7 in Cell Subsets.

(A) tSNE plots of epithelial cells isolated from UC patients (Single Cell Portal accession SCP259). Cell clusters are colored based on cell subsets. Additional heatmaps for expression of STARD7 and mitochondrial genes TOMM20 and COX14 are shown. (B) Dot plots for STARD7, TOMM20, and COX14 across different colonic epithelial subsets. Fractions of expressing cells (dot size) and mean expression level in expressing cells (dot color) are shown.

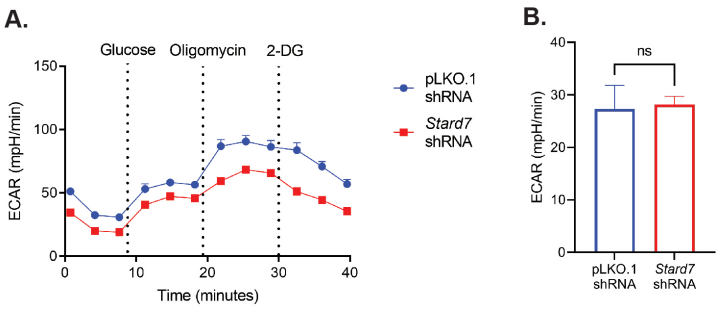

Supplementary Figure 3-2 STARD7 Deficiency Does Not Impact Glycolysis in Human Colonic Epithelial Cells.

(A) Seahorse Glycolysis Stress Test was performed on pLKO.1 shRNA and *Stard7* shRNA transduced Caco-2 BBe cells where extracellular acidification rate (ECAR) was measured over time as cells were exposed at the indicated time points to glucose, oligomycin, and 2-deoxy-D-glucose. (B) Measurement of glycolysis in pLKO.1 shRNA and *Stard7* shRNA transduced Caco-2 BBe cells. Data are representative of at least 2 independent experiments with at least five replicates per group. Data are presented as mean ± SEM. Statistical analysis was performed using unpaired t test.

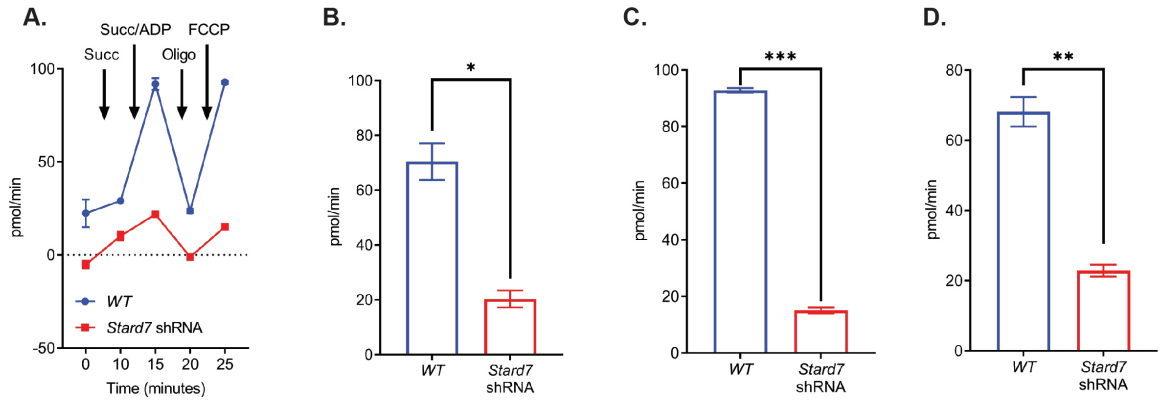

Supplementary Figure 3-3 Isolated Mitochondria from STARD7 Deficient Human Colonic Epithelial Cells Display Compromised Respiration.

(A) Mitochondria from WT and *Stard7* shRNA transduced Caco-2 BBe cells were isolated measured over time and exposed at the indicated time points to succinate, succinate/adenosine dipshosphate (ADP), oligomycin and carbonyl cyanide p-trifluoromethoxyphenylhydrazone (FCCP) for OCR assessment. Measurement of (B) spare respiratory capacity, (C) maximal respiration, and (D) ATP production in isolated mitochondria from WT and *Stard7* shRNA transduced Caco-2 BBe cells. Data are representative of at least 2 independent experiments with at least two replicates per group. Data are presented as mean ± SEM. Statistical analysis was performed using unpaired t test. *p <0.05, **p <0.01, ***p <0.001.

CHAPTER 4 - Discussion and Future Directions

Summary of major findings:

PIR-B

- Loss of PIR-B provides protection from the development of experimental colitis.
    - *Pirb*$^{-/-}$*Il10*$^{-/-}$ mice have decreased susceptibility to spontaneous colitis.
    - *Pirb*$^{-/-}$ mice have decreased susceptibility to αCD3-mediated intestinal enteropathy.
    - *Rag*$^{-/-}$ mice that received naïve *Pirb*$^{-/-}$ CD4^{+} T cells were significantly protected from disease in CD4^{+}CD45RB^{hi} T cell transfer model of colitis.
- PIR-B intrinsically regulates the development of CD4^{+} Th17 cells.
    - Reduced Th17 cell frequency in *Pirb*$^{-/-}$ mice.
    - In vitro polarization of naïve *Pirb*$^{-/-}$ CD4^{+} T cells led to impaired Th17 differentiation.
    - *Pirb*$^{-/-}$ CD4^{+} Th17 cells were characterized by increased apoptosis and Caspase 3/7 activation.
    - Significantly fewer *Pirb*$^{-/-}$ CD4^{+} Th17 cells progressed through G1 and S phase of cell cycle.
- PIR-B suppresses mTORC1 signaling in CD4^{+} Th17 cells.
    - *Pirb*$^{-/-}$ CD4^{+} Th17 cells featured hyper phosphorylation of S6 kinase and increased levels of the mTOR activator Rheb-GTP.

- Treatment of *Pirb*$^{-/-}$ naïve CD4^{+} T cells with a low dose of rapamycin enhanced CD4^{+} Th17 differentiation.

- PIR-B expression is upregulated on memory CD4^{+} Th17 cells.
- PIR-B expression confers a competitive advantage for TRM CD4^{+} T cell survival in intestinal tissue.
- LILRB3 expression is associated with severe CD and pathogenic memory CD4^{+} Th17 cell responses.

STARD7

- CD and UC patients are characterized by downregulation of STARD7 mRNA expression.
    - STARD7 expression directly correlated with the expression of genes associated with lipid metabolic processes and mitochondrial transmembrane transport.
    - STARD7 expression inversely correlated with expression of proinflammatory genes implicated in mucosal inflammation and severe UC.
- STARD7 regulates mitochondrial dynamics.
    - STARD7 knockdown in IECs compromised mitochondrial architecture and decreased expression of respiratory Complex I.
    - STARD7 knockdown significantly impaired maximal respiration and ATP production from oxidative phosphorylation in IECs.
- STARD7 regulates intestinal epithelial cell barrier function.
    - *Stard7*$^{+/-}$ IECs were characterized by significantly altered adherence and tight junction protein expression profile.
    - STARD7 knockdown in IECs decreased epithelial barrier integrity

- Activation of AMPK signaling can reconstitute STARD7 deficiency defects in intestinal epithelial cell adherence, tight junction protein expression profile, and epithelial barrier function.
    - AMPK activator metformin reconstitutes mitochondria architecture in STARD7 knockdown IECs.
    - Treatment with metformin resulted in increased barrier integrity that was associated with increased expression of tight junction proteins in STARD7 knockdown IECs.
- STARD7 deficiency enhances susceptibility to experimental colitis.
    - *Stard7*^{Tg} mice have increased susceptibility to DSS-induced colitis.
    - *Stard7*^{Tg} mice have increased susceptibility to *Il10*$^{-/-}$ spontaneous colitis.

Chapter 2

In this portion of the dissertation, we aimed to build on our understanding of the mechanisms by which the immune system is regulated in the intestinal mucosa and how changes in this compartment can skew the balance between intestinal homeostasis and inflammatory bowel disease (IBD). Our previous work established a role for paired immunoglobulin-like receptor type B (PIR-B) in restricting macrophage-driven proinflammatory responses in an innate immune driven model of colitis[141]. While intestinal macrophages sample luminal contents and are essential for the initiation of inflammation for IBD, $CD4^+$ T cells are the key effector immune cell that maintain and exacerbate the development of chronic colitis. Intriguingly, the majority of successful therapeutics for IBD in the past decade have focused on the $CD4^+$ T cell compartment, which highlights the need to continue exploring how these cells are activated, differentiated, and recruited to the gastrointestinal (GI) tract and drive the uncontrolled inflammatory response. With this in mind, we hypothesized PIR-B is required for the development of $CD4^+$ T cell pathogenic immune responses and induction of T-cell dependent colitis.

In **Chapter 2**, we demonstrated that PIR-B regulates a subset of pathogenic $CD4^+$ T cells, Th17 cells. We show PIR-B expression on $CD4^+$ T cells is essential for the optimal generation of IL-$17a^+$ $CD4^+$ T cells as PIR-B tempers mTORC1 signaling to limit apoptosis and promote cell cycle progression and survival (Fig. 1). Importantly, we could recover the generation of Th17 cells from PIR-B deficient $CD4^+$ T cells with treatment of the mTORC1 inhibitor, rapamycin. The identification of PIR-B's regulatory role being restricted to a specific $CD4^+$ T cell helper subset is consistent with the concept that different $CD4^+$ T cells are activated by discrete stimuli that allow for targeted responses against specific pathogens. Th17 cells recognize and can be

induced by a wide variety of epithelial binding microbes, including segmented filamentous bacteria or *Citrobacter rodentium*, and produce a wide range of mediators which can have divergent effects on mucosal immunity[289]. For example, IL-17a recruits neutrophils to the lamina propria which will produce the proinflammatory cytokines TNF-α and IL-6; yet IL-17a is also known to promote secretion of antimicrobial peptides from the epithelium[290]. Th17 cells also produce IL-22, a beneficial cytokine in the intestine which enhances the integrity of the epithelial barrier, mucus production, and the release of antimicrobial peptides[291]. The dichotomy of Th17 responses has resulted in significant challenges in specifically targeting the pathogenic proinflammatory responses without interfering with the protective effector response that maintains intestinal homeostasis. We believe PIR-B is a unique inhibitory receptor that is expressed on a subset of pathogenic Th17 cells within the colonic lamina propria, and therapeutically targeting this compartment could alleviate detrimental inflammatory responses in IBD. Pathogenic Th17 cells that are dual producers for IFN-γ and IL-17a are increased in mucosal samples from IBD patients and are believed to be a major driver of mucosal inflammation and the IBD phenotype[292].We speculate that PIR-B acts as a survival factor in pathogenic Th17 cells and thus blocking PIR-B survival signaling would result in the loss of these proinflammatory Th17 cells and lead to less intestinal inflammation.

An intriguing component of PIR-B's regulatory mechanism on $CD4^+$ Th17 cells is the ligands it can interact with. As discussed earlier in this dissertation, PIR-B can recognize microbial components which are readily present in the GI tract. We speculate that PIR-B^+ mucosal pathogenic Th17 cells likely express TCR clonotypes that can recognize microbial antigens. Given the high antigenic load present in the large intestine, it's probable that these pathogenic Th17 cells require additional regulatory mechanisms to control aberrant

overactivation which can result in activation of apoptotic pathways. Thus, it stands to reason that PIR-B can modulate TCR activation and maintain a proper threshold of signaling needed to maintain cell survival and, importantly, ensure that these cells are present to induce a proinflammatory response when there is exaggerated translocation of microbes into the lamina propria.

Another major finding of this work is that PIR-B expression is highly upregulated on Th17 tissue resident memory (TRM) $CD4^+$ T cells, and the expression of this receptor can enhance the generation of this memory population. Intrinsic deletion of PIR-B in $CD4^+$ T cells resulted in the loss of accumulation of Th17 TRM cells within the GI tract and concordantly led to reduced production of pro-inflammatory cytokines and provided protection from development of $CD4^+$ T-cell dependent colitis. Th17 TRM cells rapidly act alongside innate immune signals during secondary immune responses; elevated levels of TRM $CD4^+$ T cells have been observed in colonic mucosa of IBD patients during inflammatory flares[86]. We speculate that in response to the microbial milieu, PIR-B may act as rheostat tempering Th17 TRM activation, quiescence exit, and can prevent an exaggerated proinflammatory response. Inhibitory receptor expression patterns are known to change during cellular activation and differentiation; given PIR-B recognizes microbial antigens which are present within the intestinal mucosal surface we believe this receptor is required for tight regulation of Th17 TRMs which are being activated by the same microbial content. Presumably, PIR-B serves as an additional checkpoint which must be passed before Th17 TRMs can exponentially increase proinflammatory responses, which lead to adverse disease outcomes. Our work found that PIR-B calibrates mTORC1 signaling in naïve $CD4^+$ T cells, and our in silico analysis suggests the human homologue leukocyte immunoglobulin-like receptor B3 (LILRB3) may have similar regulatory effects within memory

$CD4^+$ T cells. TRMs are like naïve $CD4^+$ T cells in that they are maintained in a state of quiescence; mTORC1 is the central regulator of quiescence exit and thus establishes whether a cell will undergo a proliferative or apoptotic response[293]. Similar to naïve $CD4^+$ T cells, we believe PIR-B suppresses mTORC1 activation in Th17 TRMs and blocking PIR-B signaling would result in heightened mTORC1 activation and lead to Th17 TRM cell death.

Finally, our work with murine colitis models and human RNAseq datasets from IBD patients established that PIR-B and LILRB3 are associated with severe disease outcomes which occur as a consequence of memory Th17 effector response. Strikingly, we linked elevated LILRB3 expression to both a subset of CD patients with severe disease and a subset of $CD4^+$ T cells that were enriched for Th17 (*Rorc*, *Rora*) and TRM (*Hobit*, *Blimp1*, *Klrg1*) transcription factors. Th17 TRM cells are found in exaggerated levels in CD patients and have been shown to be major producers of TNF-α[294]. Recent therapeutics for IBD have targeted the TRM compartment directly by impacting the recruitment of these cells to the intestine with S1PR1 agonist or by targeting the retainment of these cells in the tissue by blocking $\alpha_E\beta_7$ interactions with E-cadherin; importantly, these therapies achieved clinical remission in refractory IBD patients who are unresponsive to αTNF biologics[71,73]. We believe a LILRB3 biologic may provide another unique approach to restrain pathogenic Th17 TRM responses by limiting survival in the GI. Clinical trials that have targeted the Th17 compartment in IBD have led to divergent results; biologics against IL-17a proved to be unsuccessful in treating CD patients while biologics that have targeted IL-6 and IL-23 have improved clinical outcomes in CD[76,83,204]. Thus, we must consider the potential adverse outcomes of using an LILRB3 biologic in targeting the Th17 TRM compartment. However, our mouse-based analyses indicate that PIR-B is only expressed on a subset of Th17 TRMs; furthermore, *Pirb*$^{-/-}$ mice are capable of generating Th17

cells in vitro, and importantly, in our competitive transfer experiments, we observed that *Pirb*$^{-/-}$ CD4^{+} T cells were able to generate colonic Th17 TRMs at a reduced capacity. Targeting LILRB3 might allow for a narrow focus by specifically impacting a subset of pathogenic Th17 TRMs that respond to a limited repertoire of microbes which induce a detrimental inflammatory response in IBD but would not impact TRMs that mediate beneficial effector responses.

Cancer research has established that targeting LILRBs is a viable therapeutic approach for modulating both innate and adaptive immune inflammatory responses; preventing MHC-I interactions with LILRB1, LILRB2, or LILRB4 neutralizing antibodies significantly enhanced anti-tumor responses by suppressing inhibitory signaling and promoting activation of myeloid or natural killer cells[295-297]. Furthermore, antibody neutralization of LILRB3 prevented the development of acute myeloid leukemia (AML) by modulating T cell effector function[298]. Importantly, this work found that treatment with an αLILRB3 biologic indirectly promoted beneficial cytotoxic T cell effector responses; the biologic suppressed LILRB3 mediated survival signals in AML monocytes and impaired tolerogenic AML-T cell interactions. Our work suggests that LILRB3 promotes similar survival signals in Th17 TRMs and blocking this signal could impair detrimental proinflammatory responses mediated by this compartment. However, our previous work also revealed that PIR-B inhibits activation of mucosal macrophages and suppresses innate myeloid inflammatory responses in the development of colitis; thus, an LILRB3 biologic could exacerbate the development of myeloid driven IBD. Additional studies are needed to address the paradoxical regulatory effects mediated by LILRB3; we need to establish how LILRB3 modulates the myeloid and Th17 TRM compartment during the onset, maintenance, and exacerbation of the colitic phenotype and whether timing or approach of drug delivery can achieve a beneficial clinical response to treat IBD patients.

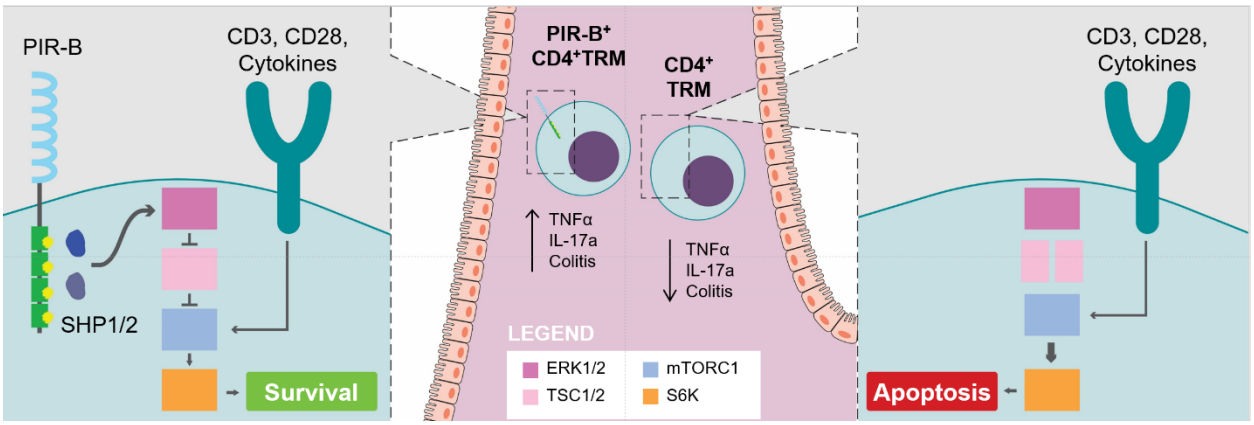

Figure 4-1 Summary of Chapter 2

This study raises important questions that should be addressed in the future, including:

- Can PIR-B be targeted therapeutically to modulate macrophage and TRM inflammatory responses and alter the course of colitis development?
- Do PIR-B's regulatory mechanisms extend to other intestinal resident immune cells, such as innate lymphoid cells?
- Is PIR-B expression on $CD4^+$ Th17 cells restricted to certain T cell clonotypes that recognize specific microbial antigens which can also bind to the inhibitory receptor?
- What is the kinetics of PIR-B expression on $CD4^+$ T cells and how does it impact effector function as the cell differentiates from a naïve cell to a memory cell?
- Is there a specific stimulus that upregulates PIR-B expression on $CD4^+$ T cells?
- Does PIR-B regulate trained immunity responses in intestinal macrophages?
- Besides LILRB3, are other LILRB's expressed on $CD4^+$ T cells, and how are their regulatory effects mediated across different $CD4^+$ T cell subtypes?

Chapter 3

With this section of the dissertation, we assessed how intestinal epithelial cells establish a strong barrier and how metabolic changes within the epithelium can negatively alter the integrity of the barrier and contribute to IBD pathogenesis. Our previous studies established a role for steroidogenic acute regulatory (StAR) protein-related lipid transfer (START) domain-containing protein 7 (STARD7) in contributing to mitochondrial fitness within the lung epithelium and barrier function[285]. The intestinal epithelium is a monolayer that provides a physical barrier between the microbial antigens present in the lumen of the GI tract and the immune compartment; the integrity of this barrier requires the maintenance of junctional proteins, which is dependent on energy derived from the mitochondria. Dysregulation of mitochondrial dynamics and energy production can negatively impact intestinal epithelial cell homeostasis and IBD pathogenesis. Phosphatidylcholine (PC) is a critical component of the mitochondrial lipid bilayers, which is important for the structural organization of the organelle and efficient ATP generation. Thus, we hypothesized STARD7 traffic of PC is critical for mitochondrial energy generation and intestinal barrier function, as well as limiting the development of colitis.

The majority of our knowledge on STARD7 has focused on one of the isoforms, STARD7-I, and its contributions to mitochondrial homeostasis. However, we know there is a truncated form of STARD7, STARD7-II, which lacks the mitochondrial targeting sequence (MTS) and is the most abundant STARD7 isoform present in the cell[242]. A recent study identified two potential ubiquitination sites on STARD7-II[299], suggesting that STARD7 traffics from the mitochondria to the cytosol for degradation. However, it is important to note that the mitochondrial processing of STARD7 does not impact the START domain, which mediates the lipid interactions. Therefore, STARD7-II is still capable of binding to PC and transporting it to

non-mitochondrial membranes. There are 15 members of the STARD family and only two of them, STARD1 and STARD7, contain an MTS and have been implicated in mitochondrial lipid transport. STARD3, STARD4, and STARD5 are cholesterol binding members of the STARD family that have redundant roles in trafficking cholesterol from the endoplasmic reticulum (ER) to endosomal compartments[142], highlighting the fact that STARD proteins have important roles in facilitating lipid transport to multiple cellular compartments, not just the mitochondria. Our own microscopy studies identified STARD7 expression localized to the plasma membrane and loss of STARD7 impacted the plasma membrane. Future work will need to elucidate the contribution of STARD7-II to non-mitochondrial organelle dynamics and whether this specific isoform can impact intestinal epithelial cell function.

In **Chapter 3**, we identified that expression of STARD7 was required for the proper mitochondrial architecture. Indeed, we saw that loss of STARD7 resulted in loss of organelle architecture, and this was associated with dysfunctional mitochondria, including altered expression of respiratory chain complexes and compromised maximal respiration. We show that STARD7-mediated defects in mitochondrial function resulted in an altered tight junction expression which was linked to a highly permeable barrier (Fig. 2). Claudins are essential tight junction proteins which couple with the actin cytoskeleton and regulate all aspects of intestinal epithelial homeostasis, including cell polarity and survival. Importantly, cytoskeleton rearrangements require energy from ATP hydrolysis, implicating STARD7 deficiencies on mitochondrial function in the maintenance of the intestinal barrier. Knockdown of STARD7 did not completely ablate mitochondrial function; this is consistent with a previous report which found loss of STARD7 only decreases mitochondrial PC composition by 60% and indicates that there are alternative routes for PC to be transferred to the mitochondria[148]. STARD2 and

STARD10 are also capable of binding to PC and facilitate transport of the lipid from the ER[142]. However, it is important to note these proteins do not contain an MTS and thus likely have a severely reduced capacity to transport PC to the mitochondria. Lipid delivery can also be achieved by vesicular trafficking via the secretory pathway, and in the absence of STARD7, we speculate PC is replenished to the mitochondrial membranes via ER-derived vesicles which transport several lipids and proteins required for mitochondrial homeostasis[300]. Collectively these studies show that STARD7 is the dominant pathway facilitating PC transport from ER to the mitochondria, proper organization of mitochondrial membranes, and optimal generation of ATP. Our work found that STARD7 mRNA expression was downregulated in IBD patients; UC patients had a 20% reduction in STARD7 relative to non IBD individuals. Given the compensatory mechanisms described above, we believe loss of STARD7 contributes as an initiating factor in development of colitis that alongside other contributing environmental and genetic factors can enhance susceptibility to development of disease. Intriguingly, our in vivo work found that STARD7 haploinsufficiency does not result in the spontaneous development of colitis; only with DSS treatment or loss of IL-10 mediated tolerance does STARD7 deficiency exacerbate the colitic phenotype. Thus, in the absence of a secondary stimulus we speculate that STARD7 mediated defects in energy production alone is not sufficient to disrupt the maintenance of intestinal homeostasis. We believe the consequences of STARD7 defects and inefficient ATP generation are most apparent under inflammatory stress conditions. Furthermore, we speculate that during inflammatory responses in IBD, there is surge in ATP demand and STARD7 deficiencies lead to a failure to fulfill the energy pressure which results in exacerbation of disease.

Using in vivo and in silico approaches, we found that STARD7 expression was inversely associated with experimental colitis and IBD severity. The enhanced colitic phenotype was due to a compromised intestinal barrier which allowed for exaggerated activation of innate and adaptive immune compartments. There may be a role for STARD7 in directly regulating the immune compartment; airway inflammatory responses in *Stard7*^{Tg} mice were driven by hyperactivated DCs, which had exaggerated expression of CD86 and MHC-II[150]. Importantly, STARD7 is readily expressed in the immune compartment with particularly high expression observed in B cells, neutrophils, and DCs[301]. Additional work is needed to decipher how STARD7 modulates the hematopoietic vs non-hematopoietic compartments within the intestine; it is possible therapeutic targeting of STARD7 could offer a synergistic approach to mucosal healing by inducing tolerogenic responses in the immune compartment and enhancing barrier function within the epithelium.

We found that treating intestinal monolayers in vitro with metformin could significantly improve barrier integrity which was directly related to enhanced expression of the tight junction proteins. Currently, metformin is approved for clinical use to treat type 2 diabetes patients where it is believed to suppress the production of glucose from the liver and reduce insulin resistance[302]. Mechanistically, metformin promotes adenosine monophosphate (AMP)-activated protein kinase (AMPK) signaling by enhancing the phosphorylation of T172 on the catalytic α subunit of the AMPK heterotrimeric complex[303]. AMPK is a serine/threonine kinase which senses the ratio of AMP to ATP and, upon activation, can promote catabolic pathways to restore cellular energy levels[304]. We identified that STARD7 expression is particularly downregulated within UC patients and speculate that metformin may prove to be a viable treatment option for these patients; metformin is currently under phase 2 clinical trials for UC patients. A

retrospective study found that UC patients who were using metformin for other indications had significantly reduced inflammatory flares compared to UC patients who were not using metformin; strikingly, there was no difference in clinical fare ups in CD patients who were taking metformin[305]. Unlike CD, UC patients have been characterized with intestinal mitochondriopathy where expression of all 13 mitochondrial encoded genes that are directly involved in ATP production were significantly reduced[244]. It is intriguing to us that STARD7 is significantly downregulated in UC patients relative to CD patients, and we believe this may be related to the mitochondria dysfunction which is observed in UC. STARD7 is known to be processed within the mitochondria, and presumptively dysfunctional mitochondria within UC patients may lead to compromised formation and export of mature STARD7, which augments regulatory pathways that impact expression of the lipid transporter. There are established feedback mechanisms between expression of nuclear-encoded proteins and expression of mitochondrial-encoded genes. For example expression of CO1, a mitochondrial-encoded subunit of respiratory Complex IV, is directly regulated by expression of nuclear-encoded COX14 and MITRAC12 proteins, which assemble the complex within the inner mitochondrial membrane[306]. An intriguing prospect is that metformin-mediated improvements to mitochondrial biogenesis could promote the expression of STARD7 and thus promote the formation of healthy

mitochondrial architecture and optimize the generation of ATP, which is required for intestinal epithelial function.

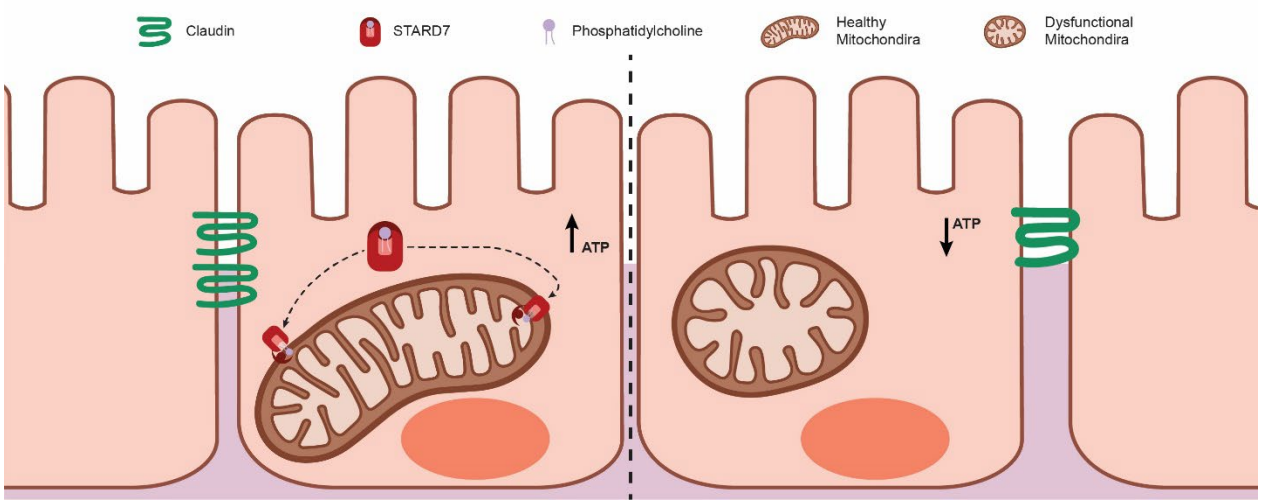

Figure 4-2 Summary of Chapter 3

This study raises important questions that should be addressed in the future, including:

- What compensatory mechanisms are present to transfer PC to the mitochondrial outer and inner membranes that help retain oxidative respiration in STARD7 deficient cells?
- Does STARD7 impact the generation of reactive oxygen species within intestinal epithelial cells and modulate apoptosis and cell turnover?
- Is there a role for STARD7 in the immune compartment within the intestinal mucosa?
- What is the function of STARD7-II in the cytosol and can it impact intestinal barrier function?
- How does STARD7 impact the different epithelial subtypes that reside within the crypt villus axis in the intestine?
- Are STARD7-mediated deficiencies related to the mitochondrial unfolding protein response that can regulate the degradation of tight junction proteins?

Final conclusions

Collectively, this dissertation advances our understanding of two regulators of intestinal homeostasis. This work describes how inhibitory receptors can regulate pathogenic T cell subsets and how lipid transport proteins are critical for the maintenance of mitochondrial function within the intestinal barrier. As discussed earlier in the dissertation, IBD is a multifactorial disease where specialized treatment approaches need to be considered for individual patients. The success of many modern clinical trials has reinforced the necessity for targeted therapeutic approaches which can modulate discrete compartments ranging from pathogenic immune subsets to enhancing the epithelium that regulates the intestinal barrier. Our work provides insight into how PIR-B promotes proinflammatory responses by Th17 TRMs and describes how STARD7 strengthens the integrity of the intestinal barrier, establishing the framework for two new therapeutic targets that can add to our arsenal of tools in treating IBD.

BIBLIOGRAPHY

1 de Souza, H. S. P. & Fiocchi, C. Immunopathogenesis of IBD: current state of the art. *Nature Reviews Gastroenterology & Hepatology* **13**, 13-27 (2016).

2 Molodecky, N. A. *et al.* Increasing incidence and prevalence of the inflammatory bowel diseases with time, based on systematic review. *Gastroenterology* **142**, 46-54.e42; quiz e30 (2012).

3 Burisch, J., Jess, T., Martinato, M. & Lakatos, P. L. The burden of inflammatory bowel disease in Europe. *J Crohns Colitis* **7**, 322-337 (2013).

4 Coward, S. *et al.* Past and Future Burden of Inflammatory Bowel Diseases Based on Modeling of Population-Based Data. *Gastroenterology* **156**, 1345-1353.e1344 (2019).

5 Lichtenstein, G. R. *et al.* Lifetime Economic Burden of Crohn's Disease and Ulcerative Colitis by Age at Diagnosis. *Clinical Gastroenterology and Hepatology* **18**, 889-897.e810 (2020).

6 Silverstein, M. D. *et al.* Clinical course and costs of care for Crohn's disease: Markov model analysis of a population-based cohort. *Gastroenterology* **117**, 49-57 (1999).

7 Mak, W. Y., Zhao, M., Ng, S. C. & Burisch, J. The epidemiology of inflammatory bowel disease: East meets west. *J Gastroenterol Hepatol* **35**, 380-389 (2020).

8 Halme, L. *et al.* Family and twin studies in inflammatory bowel disease. *World journal of gastroenterology* **12**, 3668-3672 (2006).

9 Khor, B., Gardet, A. & Xavier, R. J. Genetics and pathogenesis of inflammatory bowel disease. *Nature* **474**, 307-317 (2011).

10 Torres, J., Mehandru, S., Colombel, J.-F. & Peyrin-Biroulet, L. Crohn's disease. *The Lancet* **389**, 1741-1755 (2017).

11 Kobayashi, T. *et al.* Ulcerative colitis. *Nature Reviews Disease Primers* **6**, 74 (2020).

12 Ungaro, R., Mehandru, S., Allen, P. B., Peyrin-Biroulet, L. & Colombel, J.-F. Ulcerative colitis. *The Lancet* **389**, 1756-1770 (2017).

13 Mahid, S. S., Minor, K. S., Soto, R. E., Hornung, C. A. & Galandiuk, S. Smoking and inflammatory bowel disease: a meta-analysis. *Mayo Clin Proc* **81**, 1462-1471 (2006).

14 Harries, A. D., Baird, A. & Rhodes, J. Non-smoking: a feature of ulcerative colitis. *Br Med J (Clin Res Ed)* **284**, 706 (1982).

15 Kurina, L. M., Goldacre, M. J., Yeates, D. & Seagroatt, V. Appendicectomy, tonsillectomy, and inflammatory bowel disease: a case-control record linkage study. *J Epidemiol Community Health* **56**, 551-554 (2002).

16 Koutroubakis, I. E., Vlachonikolis, I. G. & Kouroumalis, E. A. Role of appendicitis and appendectomy in the pathogenesis of ulcerative colitis: a critical review. *Inflammatory bowel diseases* **8**, 277-286 (2002).

17 Mayer, L. & Eisenhardt, D. Lack of induction of suppressor T cells by intestinal epithelial cells from patients with inflammatory bowel disease. *J Clin Invest* **86**, 1255-1260 (1990).

18 Szigethy, E., McLafferty, L. & Goyal, A. Inflammatory bowel disease. *Child Adolesc Psychiatr Clin N Am* **19**, 301-318, ix (2010).
19 Jostins, L. *et al.* Host–microbe interactions have shaped the genetic architecture of inflammatory bowel disease. *Nature* **491**, 119-124 (2012).
20 Fisher, S. A. *et al.* Genetic determinants of ulcerative colitis include the ECM1 locus and five loci implicated in Crohn's disease. *Nat Genet* **40**, 710-712 (2008).
21 Fournier, B. M. & Parkos, C. A. The role of neutrophils during intestinal inflammation. *Mucosal Immunology* **5**, 354-366 (2012).
22 Na, Y. R., Stakenborg, M., Seok, S. H. & Matteoli, G. Macrophages in intestinal inflammation and resolution: a potential therapeutic target in IBD. *Nature Reviews Gastroenterology & Hepatology* **16**, 531-543 (2019).
23 Hsieh, C. S. *et al.* Development of TH1 CD4+ T cells through IL-12 produced by Listeria-induced macrophages. *Science* **260**, 547-549 (1993).
24 Swain, S. L., Weinberg, A. D., English, M. & Huston, G. IL-4 directs the development of Th2-like helper effectors. *J Immunol* **145**, 3796-3806 (1990).
25 Bettelli, E. *et al.* Reciprocal developmental pathways for the generation of pathogenic effector TH17 and regulatory T cells. *Nature* **441**, 235-238 (2006).
26 Zhou, L. *et al.* IL-6 programs T(H)-17 cell differentiation by promoting sequential engagement of the IL-21 and IL-23 pathways. *Nat Immunol* **8**, 967-974 (2007).
27 Bettelli, E., Korn, T. & Kuchroo, V. K. Th17: the third member of the effector T cell trilogy. *Current opinion in immunology* **19**, 652-657 (2007).
28 Duerr, R. H. *et al.* A genome-wide association study identifies IL23R as an inflammatory bowel disease gene. *Science* **314**, 1461-1463 (2006).
29 O'Shea, J. J., Lahesmaa, R., Vahedi, G., Laurence, A. & Kanno, Y. Genomic views of STAT function in CD4+ T helper cell differentiation. *Nature Reviews Immunology* **11**, 239-250 (2011).
30 Lighvani, A. A. *et al.* T-bet is rapidly induced by interferon-γ in lymphoid and myeloid cells. *Proceedings of the National Academy of Sciences* **98**, 15137-15142 (2001).
31 Burchill, M. A., Yang, J., Vogtenhuber, C., Blazar, B. R. & Farrar, M. A. IL-2 receptor beta-dependent STAT5 activation is required for the development of Foxp3+ regulatory T cells. *J Immunol* **178**, 280-290 (2007).
32 Ivanov, II *et al.* The orphan nuclear receptor RORgammat directs the differentiation program of proinflammatory IL-17+ T helper cells. *Cell* **126**, 1121-1133 (2006).
33 Yamane, H., Zhu, J. & Paul, W. E. Independent roles for IL-2 and GATA-3 in stimulating naive CD4+ T cells to generate a Th2-inducing cytokine environment. *J Exp Med* **202**, 793-804 (2005).
34 Yao, Z. *et al.* Nonredundant roles for Stat5a/b in directly regulating Foxp3. *Blood* **109**, 4368-4375 (2007).
35 Harris, T. J. *et al.* Cutting edge: An in vivo requirement for STAT3 signaling in TH17 development and TH17-dependent autoimmunity. *J Immunol* **179**, 4313-4317 (2007).
36 Fuss, I. J. *et al.* Disparate CD4+ lamina propria (LP) lymphokine secretion profiles in inflammatory bowel disease. Crohn's disease LP cells manifest increased secretion of IFN-gamma, whereas ulcerative colitis LP cells manifest increased secretion of IL-5. *J Immunol* **157**, 1261-1270 (1996).

37 Heller, F. *et al.* Interleukin-13 is the key effector Th2 cytokine in ulcerative colitis that affects epithelial tight junctions, apoptosis, and cell restitution. *Gastroenterology* **129**, 550-564 (2005).
38 Fujino, S. *et al.* Increased expression of interleukin 17 in inflammatory bowel disease. *Gut* **52**, 65-70 (2003).
39 Gerlach, K. *et al.* TH9 cells that express the transcription factor PU.1 drive T cell-mediated colitis via IL-9 receptor signaling in intestinal epithelial cells. *Nat Immunol* **15**, 676-686 (2014).
40 Leppkes, M. *et al.* RORgamma-expressing Th17 cells induce murine chronic intestinal inflammation via redundant effects of IL-17A and IL-17F. *Gastroenterology* **136**, 257-267 (2009).
41 Leung, J. M. *et al.* IL-22-producing CD4+ cells are depleted in actively inflamed colitis tissue. *Mucosal Immunology* **7**, 124-133 (2014).
42 Pickert, G. *et al.* STAT3 links IL-22 signaling in intestinal epithelial cells to mucosal wound healing. *Journal of Experimental Medicine* **206**, 1465-1472 (2009).
43 Huber, S. *et al.* IL-22BP is regulated by the inflammasome and modulates tumorigenesis in the intestine. *Nature* **491**, 259-263 (2012).
44 Brockmann, L. *et al.* Molecular and functional heterogeneity of IL-10-producing CD4+ T cells. *Nature Communications* **9**, 5457 (2018).
45 Glocker, E. O. *et al.* Inflammatory bowel disease and mutations affecting the interleukin-10 receptor. *N Engl J Med* **361**, 2033-2045 (2009).
46 Kotlarz, D. *et al.* Loss of interleukin-10 signaling and infantile inflammatory bowel disease: implications for diagnosis and therapy. *Gastroenterology* **143**, 347-355 (2012).
47 Hegazy, A. N. *et al.* Circulating and Tissue-Resident CD4(+) T Cells With Reactivity to Intestinal Microbiota Are Abundant in Healthy Individuals and Function Is Altered During Inflammation. *Gastroenterology* **153**, 1320-1337 e1316 (2017).
48 Zundler, S. *et al.* Hobit- and Blimp-1-driven CD4(+) tissue-resident memory T cells control chronic intestinal inflammation. *Nat Immunol* **20**, 288-300 (2019).
49 Bishu, S. *et al.* Citrobacter rodentium Induces Tissue-Resident Memory CD4(+) T Cells. *Infect Immun* **87** (2019).
50 Bishu, S. *et al.* CD4+ Tissue-resident Memory T Cells Expand and Are a Major Source of Mucosal Tumour Necrosis Factor alpha in Active Crohn's Disease. *J Crohns Colitis* **13**, 905-915 (2019).
51 Kumar, B. V. *et al.* Human Tissue-Resident Memory T Cells Are Defined by Core Transcriptional and Functional Signatures in Lymphoid and Mucosal Sites. *Cell reports* **20**, 2921-2934 (2017).
52 Gibbons, D. L. *et al.* Cutting Edge: Regulator of G protein signaling-1 selectively regulates gut T cell trafficking and colitic potential. *J Immunol* **187**, 2067-2071 (2011).
53 Mueller, S. N., Gebhardt, T., Carbone, F. R. & Heath, W. R. Memory T cell subsets, migration patterns, and tissue residence. *Annu Rev Immunol* **31**, 137-161 (2013).
54 Campbell, J. J. *et al.* CCR7 expression and memory T cell diversity in humans. *J Immunol* **166**, 877-884 (2001).
55 Baron, V. *et al.* The repertoires of circulating human CD8(+) central and effector memory T cell subsets are largely distinct. *Immunity* **18**, 193-204 (2003).

56 Nemoto, Y. *et al.* Long-Lived Colitogenic CD4⁺ Memory T Cells Residing Outside the Intestine Participate in the Perpetuation of Chronic Colitis. *The Journal of Immunology* **183**, 5059-5068 (2009).
57 Joller, N. *et al.* Cutting Edge: TIGIT Has T Cell-Intrinsic Inhibitory Functions. *The Journal of Immunology* **186**, 1338-1342 (2011).
58 Fuertes Marraco, S. A., Neubert, N. J., Verdeil, G. & Speiser, D. E. Inhibitory Receptors Beyond T Cell Exhaustion. *Front Immunol* **6**, 310 (2015).
59 Oakley, R. H. & Cidlowski, J. A. The biology of the glucocorticoid receptor: new signaling mechanisms in health and disease. *The Journal of allergy and clinical immunology* **132**, 1033-1044 (2013).
60 Velayos, F. S., Terdiman, J. P. & Walsh, J. M. Effect of 5-aminosalicylate use on colorectal cancer and dysplasia risk: a systematic review and metaanalysis of observational studies. *Am J Gastroenterol* **100**, 1345-1353 (2005).
61 Matsuda, S. & Koyasu, S. Mechanisms of action of cyclosporine. *Immunopharmacology* **47**, 119-125 (2000).
62 Colombel, J. F. *et al.* Infliximab, Azathioprine, or Combination Therapy for Crohn's Disease. *New England Journal of Medicine* **362**, 1383-1395 (2010).
63 Feagan, B. G. *et al.* A comparison of methotrexate with placebo for the maintenance of remission in Crohn's disease. North American Crohn's Study Group Investigators. *N Engl J Med* **342**, 1627-1632 (2000).
64 Hanauer, S. B. *et al.* Maintenance infliximab for Crohn's disease: the ACCENT I randomised trial. *Lancet* **359**, 1541-1549 (2002).
65 Present, D. H. *et al.* Infliximab for the treatment of fistulas in patients with Crohn's disease. *N Engl J Med* **340**, 1398-1405 (1999).
66 Neurath, M. F. Current and emerging therapeutic targets for IBD. *Nat Rev Gastroenterol Hepatol* **14**, 269-278 (2017).
67 Picarella, D. *et al.* Monoclonal antibodies specific for beta 7 integrin and mucosal addressin cell adhesion molecule-1 (MAdCAM-1) reduce inflammation in the colon of scid mice reconstituted with CD45RBhigh CD4+ T cells. *J Immunol* **158**, 2099-2106 (1997).
68 Sandborn, W. J. *et al.* Natalizumab Induction and Maintenance Therapy for Crohn's Disease. *New England Journal of Medicine* **353**, 1912-1925 (2005).
69 Sandborn, W. J. *et al.* Phase II evaluation of anti-MAdCAM antibody PF-00547659 in the treatment of Crohn's disease: report of the OPERA study. *Gut* **67**, 1824-1835 (2018).
70 Agace, W. W., Higgins, J. M., Sadasivan, B., Brenner, M. B. & Parker, C. M. T-lymphocyte-epithelial-cell interactions: integrin alpha(E)(CD103)beta(7), LEEP-CAM and chemokines. *Current opinion in cell biology* **12**, 563-568 (2000).
71 Zundler, S. *et al.* Blockade of αEβ7 integrin suppresses accumulation of CD8(+) and Th9 lymphocytes from patients with IBD in the inflamed gut in vivo. *Gut* **66**, 1936-1948 (2017).
72 Shiow, L. R. *et al.* CD69 acts downstream of interferon-alpha/beta to inhibit S1P1 and lymphocyte egress from lymphoid organs. *Nature* **440**, 540-544 (2006).
73 Sandborn, W. J. *et al.* Ozanimod Induction and Maintenance Treatment for Ulcerative Colitis. *New England Journal of Medicine* **374**, 1754-1762 (2016).
74 Sandborn, W. J. *et al.* Etrolizumab for the Treatment of Ulcerative Colitis and Crohn's Disease: An Overview of the Phase 3 Clinical Program. *Adv Ther* **37**, 3417-3431 (2020).

75 Danese, S. *et al.* Tralokinumab for moderate-to-severe UC: a randomised, double-blind, placebo-controlled, phase IIa study. *Gut* **64**, 243-249 (2015).
76 Hueber, W. *et al.* Secukinumab, a human anti-IL-17A monoclonal antibody, for moderate to severe Crohn's disease: unexpected results of a randomised, double-blind placebo-controlled trial. *Gut* **61**, 1693-1700 (2012).
77 Reinisch, W. *et al.* A dose escalating, placebo controlled, double blind, single dose and multidose, safety and tolerability study of fontolizumab, a humanised anti-interferon gamma antibody, in patients with moderate to severe Crohn's disease. *Gut* **55**, 1138-1144 (2006).
78 Hueber, W. *et al.* Secukinumab, a human anti-IL-17A monoclonal antibody, for moderate to severe Crohn's disease: unexpected results of a randomised, double-blind placebo-controlled trial. *Gut* **61**, 1693-1700 (2012).
79 Bettelli, E. *et al.* Reciprocal developmental pathways for the generation of pathogenic effector TH17 and regulatory T cells. *Nature* **441**, 235-238 (2006).
80 Danese, S. *et al.* Randomised trial and open-label extension study of an anti-interleukin-6 antibody in Crohn's disease (ANDANTE I and II). *Gut* **68**, 40-48 (2019).
81 Ito, H. *et al.* A pilot randomized trial of a human anti-interleukin-6 receptor monoclonal antibody in active Crohn's disease. *Gastroenterology* **126**, 989-996; discussion 947 (2004).
82 Sandborn, W. J. *et al.* Ustekinumab Induction and Maintenance Therapy in Refractory Crohn's Disease. *New England Journal of Medicine* **367**, 1519-1528 (2012).
83 Sands, B. E. *et al.* Efficacy and Safety of MEDI2070, an Antibody Against Interleukin 23, in Patients With Moderate to Severe Crohn's Disease: A Phase 2a Study. *Gastroenterology* **153**, 77-86.e76 (2017).
84 Sandborn, W. J. *et al.* Tofacitinib, an Oral Janus Kinase Inhibitor, in Active Ulcerative Colitis. *New England Journal of Medicine* **367**, 616-624 (2012).
85 Vermeire, S. *et al.* Clinical remission in patients with moderate-to-severe Crohn's disease treated with filgotinib (the FITZROY study): results from a phase 2, double-blind, randomised, placebo-controlled trial. *Lancet* **389**, 266-275 (2017).
86 Zundler, S. *et al.* Hobit- and Blimp-1-driven CD4+ tissue-resident memory T cells control chronic intestinal inflammation. *Nat Immunol* **20**, 288-300 (2019).
87 Daëron, M., Jaeger, S., Du Pasquier, L. & Vivier, E. Immunoreceptor tyrosine-based inhibition motifs: a quest in the past and future. *Immunol Rev* **224**, 11-43 (2008).
88 Hui, E. *et al.* T cell costimulatory receptor CD28 is a primary target for PD-1-mediated inhibition. *Science* **355**, 1428-1433 (2017).
89 An, H. *et al.* Phosphatase SHP-1 promotes TLR- and RIG-I-activated production of type I interferon by inhibiting the kinase IRAK1. *Nat Immunol* **9**, 542-550 (2008).
90 Billadeau, D. D. & Leibson, P. J. ITAMs versus ITIMs: striking a balance during cell regulation. *The Journal of Clinical Investigation* **109**, 161-168 (2002).
91 Ravetch, J. V. & Lanier, L. L. Immune inhibitory receptors. *Science* **290**, 84-89 (2000).
92 Barclay, A. N. & Hatherley, D. The counterbalance theory for evolution and function of paired receptors. *Immunity* **29**, 675-678 (2008).
93 Carlyle, J. R. *et al.* Evolution of the Ly49 and Nkrp1 recognition systems. *Semin Immunol* **20**, 321-330 (2008).

94 Levi-Schaffer, F. & Mandelboim, O. Inhibitory and Coactivating Receptors Recognising the Same Ligand: Immune Homeostasis Exploited by Pathogens and Tumours. *Trends Immunol* **39**, 112-122 (2018).
95 Kubagawa, H., Burrows, P. D. & Cooper, M. D. A novel pair of immunoglobulin-like receptors expressed by B cells and myeloid cells. *Proceedings of the National Academy of Sciences of the United States of America* **94**, 5261-5266 (1997).
96 Hayami, K. *et al.* Molecular cloning of a novel murine cell-surface glycoprotein homologous to killer cell inhibitory receptors. *J Biol Chem* **272**, 7320-7327 (1997).
97 Yamashita, Y. *et al.* Genomic structures and chromosomal location of p91, a novel murine regulatory receptor family. *J Biochem* **123**, 358-368 (1998).
98 Ono, M., Yuasa, T., Ra, C. & Takai, T. Stimulatory Function of Paired Immunoglobulin-like Receptor-A in Mast Cell Line by Associating with Subunits Common to Fc Receptors *. *Journal of Biological Chemistry* **274**, 30288-30296 (1999).
99 Ben Mkaddem, S., Benhamou, M. & Monteiro, R. C. Understanding Fc Receptor Involvement in Inflammatory Diseases: From Mechanisms to New Therapeutic Tools. *Front Immunol* **10**, 811 (2019).
100 Chen, C.-C., Hurez, V., Brockenbrough, J. S., Kubagawa, H. & Cooper, M. D. Paternal monoallelic expression of the paired immunoglobulin-like receptors PIR-A and PIR-B. *Proceedings of the National Academy of Sciences* **96**, 6868-6872 (1999).
101 Sloane, D. E. *et al.* Leukocyte immunoglobulin-like receptors: novel innate receptors for human basophil activation and inhibition. *Blood* **104**, 2832-2839 (2004).
102 Ujike, A. *et al.* Impaired dendritic cell maturation and increased T(H)2 responses in PIR-B(-/-) mice. *Nat Immunol* **3**, 542-548 (2002).
103 Pereira, S., Zhang, H., Takai, T. & Lowell, C. A. The inhibitory receptor PIR-B negatively regulates neutrophil and macrophage integrin signaling. *J Immunol* **173**, 5757-5765 (2004).
104 Mitsuhashi, Y. *et al.* Regulation of plasmacytoid dendritic cell responses by PIR-B. *Blood* **120**, 3256-3259 (2012).
105 Kubo, T. *et al.* Augmented TLR9-induced Btk activation in PIR-B-deficient B-1 cells provokes excessive autoantibody production and autoimmunity. *J Exp Med* **206**, 1971-1982 (2009).
106 Wang, H., Xiong, Y. & Mu, D. PirB restricts neuronal regeneration in developing rat brain following hypoxia-ischemia. *Mol Med Rep* **6**, 339-344 (2012).
107 Kubagawa, H. *et al.* Biochemical Nature and Cellular Distribution of the Paired Immunoglobulin-like Receptors, PIR-A and PIR-B. *Journal of Experimental Medicine* **189**, 309-318 (1999).
108 Ho, L. H., Uehara, T., Chen, C. C., Kubagawa, H. & Cooper, M. D. Constitutive tyrosine phosphorylation of the inhibitory paired Ig-like receptor PIR-B. *Proceedings of the National Academy of Sciences of the United States of America* **96**, 15086-15090 (1999).
109 Nakamura, A., Kobayashi, E. & Takai, T. Exacerbated graft-versus-host disease in Pirb−/− mice. *Nat Immunol* **5**, 623-629 (2004).
110 Nakayama, M. *et al.* Paired Ig-Like Receptors Bind to Bacteria and Shape TLR-Mediated Cytokine Production. *The Journal of Immunology* **178**, 4250-4259 (2007).
111 Torii, I. *et al.* PIR-B-deficient mice are susceptible to Salmonella infection. *J Immunol* **181**, 4229-4239 (2008).

112 Cai, X. *et al.* Expression of PirB protein in intact and injured optic nerve and retina of mice. *Neurochem Res* **37**, 647-654 (2012).
113 Atwal, J. K. *et al.* PirB is a Functional Receptor for Myelin Inhibitors of Axonal Regeneration. *Science* **322**, 967-970 (2008).
114 Matsushita, H. *et al.* Differential but Competitive Binding of Nogo Protein and Class I Major Histocompatibility Complex (MHCI) to the PIR-B Ectodomain Provides an Inhibition of Cells*. *Journal of Biological Chemistry* **286**, 25739-25747 (2011).
115 Kim, T. *et al.* Human LilrB2 Is a β-Amyloid Receptor and Its Murine Homolog PirB Regulates Synaptic Plasticity in an Alzheimer's Model. *Science* **341**, 1399-1404 (2013).
116 Burshtyn, D. N. & Morcos, C. The Expanding Spectrum of Ligands for Leukocyte Ig-like Receptors. *The Journal of Immunology* **196**, 947-955 (2016).
117 Takeda, K. & Nakamura, A. Regulation of immune and neural function via leukocyte Ig-like receptors. *The Journal of Biochemistry* **162**, 73-80 (2017).
118 Kim, A. *et al.* LILRB1 Blockade Enhances Bispecific T Cell Engager Antibody-Induced Tumor Cell Killing by Effector CD8(+) T Cells. *J Immunol* **203**, 1076-1087 (2019).
119 Deng, M. *et al.* Leukocyte immunoglobulin-like receptor subfamily B: therapeutic targets in cancer. *Antibody Therapeutics* **4**, 16-33 (2021).
120 Willcox, B. E., Thomas, L. M. & Bjorkman, P. J. Crystal structure of HLA-A2 bound to LIR-1, a host and viral major histocompatibility complex receptor. *Nat Immunol* **4**, 913-919 (2003).
121 Willcox, B. E. *et al.* Crystal structure of LIR-2 (ILT4) at 1.8 A: differences from LIR-1 (ILT2) in regions implicated in the binding of the Human Cytomegalovirus class I MHC homolog UL18. *BMC Struct Biol* **2**, 6 (2002).
122 Hirayasu, K. & Arase, H. Functional and genetic diversity of leukocyte immunoglobulin-like receptor and implication for disease associations. *Journal of Human Genetics* **60**, 703-708 (2015).
123 Mori, Y. *et al.* Inhibitory Immunoglobulin-Like Receptors LILRB and PIR-B Negatively Regulate Osteoclast Development. *The Journal of Immunology* **181**, 4742-4751 (2008).
124 Masuda, A., Nakamura, A., Maeda, T., Sakamoto, Y. & Takai, T. Cis binding between inhibitory receptors and MHC class I can regulate mast cell activation. *J Exp Med* **204**, 907-920 (2007).
125 Held, W. & Mariuzza, R. A. Cis interactions of immunoreceptors with MHC and non-MHC ligands. *Nature Reviews Immunology* **8**, 269-278 (2008).
126 Li, D. *et al.* Ig-Like Transcript 4 Inhibits Lipid Antigen Presentation through Direct CD1d Interaction. *The Journal of Immunology* **182**, 1033-1040 (2009).
127 Harrison, T. E. *et al.* Structural basis for RIFIN-mediated activation of LILRB1 in malaria. *Nature* **587**, 309-312 (2020).
128 Chen, Y. *et al.* Structural basis of malaria RIFIN binding by LILRB1-containing antibodies. *Nature* (2021).
129 Mori, Y. *et al.* Inhibitory immunoglobulin-like receptors LILRB and PIR-B negatively regulate osteoclast development. *J Immunol* **181**, 4742-4751 (2008).
130 Karo-Atar, D., Moshkovits, I., Eickelberg, O., Königshoff, M. & Munitz, A. Paired immunoglobulin-like receptor-B inhibits pulmonary fibrosis by suppressing profibrogenic properties of alveolar macrophages. *Am J Respir Cell Mol Biol* **48**, 456-464 (2013).

131 Yeboah, M. *et al.* LILRB3 (ILT5) is a myeloid cell checkpoint that elicits profound immunomodulation. *JCI Insight* **5** (2020).
132 Rudolph, M. G., Stanfield, R. L. & Wilson, I. A. How TCRs bind MHCs, peptides, and coreceptors. *Annu Rev Immunol* **24**, 419-466 (2006).
133 Leavy, O. A mismatch that works. *Nature Reviews Immunology* **8**, 321-321 (2008).
134 Dai, H. *et al.* PIRs mediate innate myeloid cell memory to nonself MHC molecules. *Science* **368**, 1122-1127 (2020).
135 Arnott, I. D. R., Ho, G.-T., Nimmo, E. R. & Satsangi, J. Toll-like receptor 4 gene in IBD: further evidence for genetic heterogeneity in Europe. *Gut* **54**, 308-309 (2005).
136 MacDonald, T. T., Monteleone, I., Fantini, M. C. & Monteleone, G. Regulation of Homeostasis and Inflammation in the Intestine. *Gastroenterology* **140**, 1768-1775 (2011).
137 Keubler, L. M., Buettner, M., Häger, C. & Bleich, A. A Multihit Model: Colitis Lessons from the Interleukin-10-deficient Mouse. *Inflammatory bowel diseases* **21**, 1967-1975 (2015).
138 Ghia, J.-E. *et al.* Role of M-CSF-dependent macrophages in colitis is driven by the nature of the inflammatory stimulus. *American Journal of Physiology-Gastrointestinal and Liver Physiology* **294**, G770-G777 (2008).
139 Marshall, D., Cameron, J., Lightwood, D. & Lawson, A. D. Blockade of colony stimulating factor-1 (CSF-I) leads to inhibition of DSS-induced colitis. *Inflammatory bowel diseases* **13**, 219-224 (2007).
140 Pereira, S., Zhang, H., Takai, T. & Lowell, C. A. The Inhibitory Receptor PIR-B Negatively Regulates Neutrophil and Macrophage Integrin Signaling. *The Journal of Immunology* **173**, 5757-5765 (2004).
141 Munitz, A. *et al.* Paired immunoglobulin-like receptor B (PIR-B) negatively regulates macrophage activation in experimental colitis. *Gastroenterology* **139**, 530-541 (2010).
142 Clark, B. J. The START-domain proteins in intracellular lipid transport and beyond. *Mol Cell Endocrinol* **504**, 110704 (2020).
143 Kanno, K., Wu, M. K., Scapa, E. F., Roderick, S. L. & Cohen, D. E. Structure and function of phosphatidylcholine transfer protein (PC-TP)/StarD2. *Biochimica et Biophysica Acta (BBA) - Molecular and Cell Biology of Lipids* **1771**, 654-662 (2007).
144 Olayioye, M. A. *et al.* StarD10, a START Domain Protein Overexpressed in Breast Cancer, Functions as a Phospholipid Transfer Protein*. *Journal of Biological Chemistry* **280**, 27436-27442 (2005).
145 Bell, R. M., Ballas, L. M. & Coleman, R. A. Lipid topogenesis. *Journal of Lipid Research* **22**, 391-403 (1981).
146 Durand, S., Angeletti, S. & Genti-Raimondi, S. GTT1/StarD7, a Novel Phosphatidylcholine Transfer Protein-like Highly Expressed in Gestational Trophoblastic Tumour:: Cloning and Characterization. *Placenta* **25**, 37-44 (2004).
147 Horibata, Y. & Sugimoto, H. StarD7 Mediates the Intracellular Trafficking of Phosphatidylcholine to Mitochondria*. *Journal of Biological Chemistry* **285**, 7358-7365 (2010).
148 Saita, S. *et al.* PARL partitions the lipid transfer protein STARD7 between the cytosol and mitochondria. *Embo j* **37** (2018).
149 Horibata, Y. *et al.* StarD7 Protein Deficiency Adversely Affects the Phosphatidylcholine Composition, Respiratory Activity, and Cristae Structure of Mitochondria. *J Biol Chem* **291**, 24880-24891 (2016).

150 Yang, L. *et al.* Haploinsufficiency for Stard7 Is Associated with Enhanced Allergic Responses in Lung and Skin. *The Journal of Immunology* **194**, 5635-5643 (2015).
151 Kaser, A., Zeissig, S. & Blumberg, R. S. Inflammatory bowel disease. *Annu Rev Immunol* **28**, 573-621 (2010).
152 Mahida, Y. R., Patel, S., Gionchetti, P., Vaux, D. & Jewell, D. P. Macrophage subpopulations in lamina propria of normal and inflamed colon and terminal ileum. *Gut* **30**, 826-834 (1989).
153 Marks, D. J. & Segal, A. W. Innate immunity in inflammatory bowel disease: a disease hypothesis. *J Pathol* **214**, 260-266 (2008).
154 Neurath, M. F. *et al.* The transcription factor T-bet regulates mucosal T cell activation in experimental colitis and Crohn's disease. *J Exp Med* **195**, 1129-1143 (2002).
155 Heller, F., Fuss, I. J., Nieuwenhuis, E. E., Blumberg, R. S. & Strober, W. Oxazolone colitis, a Th2 colitis model resembling ulcerative colitis, is mediated by IL-13-producing NK-T cells. *Immunity* **17**, 629-638 (2002).
156 Ahern, P. P. *et al.* Interleukin-23 drives intestinal inflammation through direct activity on T cells. *Immunity* **33**, 279-288 (2010).
157 Peters, C. P., Mjösberg, J. M., Bernink, J. H. & Spits, H. Innate lymphoid cells in inflammatory bowel diseases. *Immunol Lett* **172**, 124-131 (2016).
158 Geremia, A. *et al.* IL-23-responsive innate lymphoid cells are increased in inflammatory bowel disease. *J Exp Med* **208**, 1127-1133 (2011).
159 Mangan, P. R. *et al.* Transforming growth factor-beta induces development of the T(H)17 lineage. *Nature* **441**, 231-234 (2006).
160 McGeachy, M. J. *et al.* The interleukin 23 receptor is essential for the terminal differentiation of interleukin 17-producing effector T helper cells in vivo. *Nat Immunol* **10**, 314-324 (2009).
161 Bettelli, E., Korn, T. & Kuchroo, V. K. Th17: the third member of the effector T cell trilogy. *Current opinion in immunology* **19**, 652-657 (2007).
162 Wiekowski, M. T. *et al.* Ubiquitous transgenic expression of the IL-23 subunit p19 induces multiorgan inflammation, runting, infertility, and premature death. *J Immunol* **166**, 7563-7570 (2001).
163 Yen, D. *et al.* IL-23 is essential for T cell-mediated colitis and promotes inflammation via IL-17 and IL-6. *J Clin Invest* **116**, 1310-1316 (2006).
164 Kullberg, M. C. *et al.* IL-23 plays a key role in Helicobacter hepaticus-induced T cell-dependent colitis. *J Exp Med* **203**, 2485-2494 (2006).
165 Hue, S. *et al.* Interleukin-23 drives innate and T cell-mediated intestinal inflammation. *J Exp Med* **203**, 2473-2483 (2006).
166 Elson, C. O. *et al.* Monoclonal anti-interleukin 23 reverses active colitis in a T cell-mediated model in mice. *Gastroenterology* **132**, 2359-2370 (2007).
167 Kubagawa, H. *et al.* Biochemical nature and cellular distribution of the paired immunoglobulin-like receptors, PIR-A and PIR-B. *J Exp Med* **189**, 309-318 (1999).
168 Long, E. O. Regulation of immune responses through inhibitory receptors. *Annu Rev Immunol* **17**, 875-904 (1999).
169 Masuda, A., Nakamura, A., Maeda, T., Sakamoto, Y. & Takai, T. Cis binding between inhibitory receptors and MHC class I can regulate mast cell activation. *J Exp Med* **204**, 907-920 (2007).

170 Nakayama, M. *et al.* Paired Ig-like receptors bind to bacteria and shape TLR-mediated cytokine production. *J Immunol* **178**, 4250-4259 (2007).
171 Arita, K. *et al.* Transcriptional activation of the Pirb gene in B cells by PU.1 and Runx3. *J Immunol* **186**, 7050-7059 (2011).
172 Takai, T. A Novel Recognition System for MHC Class I Molecules Constituted by PIR. *Adv Immunol* **88**, 161-192 (2005).
173 Nakayama, M. *et al.* Inhibitory receptor paired Ig-like receptor B is exploited by Staphylococcus aureus for virulence. *J Immunol* **189**, 5903-5911 (2012).
174 Torii, I. *et al.* PIR-B-deficient mice are susceptible to Salmonella infection. *J Immunol* **181**, 4229-4239 (2008).
175 Munitz, A. *et al.* Paired immunoglobulin-like receptor B (PIR-B) negatively regulates macrophage activation in experimental colitis. *Gastroenterology* **139**, 530-541 (2010).
176 Musch, M. W. *et al.* T cell activation causes diarrhea by increasing intestinal permeability and inhibiting epithelial Na+/K+-ATPase. *J Clin Invest* **110**, 1739-1747 (2002).
177 Miura, N. *et al.* Anti-CD3 induces bi-phasic apoptosis in murine intestinal epithelial cells: possible involvement of the Fas/Fas ligand system in different T cell compartments. *Int Immunol* **17**, 513-522 (2005).
178 Powrie, F. *et al.* Inhibition of Th1 responses prevents inflammatory bowel disease in scid mice reconstituted with CD45RBhi CD4+ T cells. *Immunity* **1**, 553-562 (1994).
179 Mottet, C., Uhlig, H. H. & Powrie, F. Cutting edge: cure of colitis by CD4+CD25+ regulatory T cells. *J Immunol* **170**, 3939-3943 (2003).
180 Chi, H. Regulation and function of mTOR signalling in T cell fate decisions. *Nat Rev Immunol* **12**, 325-338 (2012).
181 Kurebayashi, Y. *et al.* PI3K-Akt-mTORC1-S6K1/2 axis controls Th17 differentiation by regulating Gfi1 expression and nuclear translocation of RORgamma. *Cell Rep* **1**, 360-373 (2012).
182 Inoki, K., Li, Y., Zhu, T., Wu, J. & Guan, K. L. TSC2 is phosphorylated and inhibited by Akt and suppresses mTOR signalling. *Nat Cell Biol* **4**, 648-657 (2002).
183 Zhang, Y. *et al.* Rheb is a direct target of the tuberous sclerosis tumour suppressor proteins. *Nat Cell Biol* **5**, 578-581 (2003).
184 Tee, A. R., Manning, B. D., Roux, P. P., Cantley, L. C. & Blenis, J. Tuberous sclerosis complex gene products, Tuberin and Hamartin, control mTOR signaling by acting as a GTPase-activating protein complex toward Rheb. *Curr Biol* **13**, 1259-1268 (2003).
185 Castel, P. *et al.* PDK1-SGK1 Signaling Sustains AKT-Independent mTORC1 Activation and Confers Resistance to PI3Kalpha Inhibition. *Cancer Cell* **30**, 229-242 (2016).
186 Inoki, K. *et al.* TSC2 integrates Wnt and energy signals via a coordinated phosphorylation by AMPK and GSK3 to regulate cell growth. *Cell* **126**, 955-968 (2006).
187 Dibble, C. C. & Cantley, L. C. Regulation of mTORC1 by PI3K signaling. *Trends Cell Biol* **25**, 545-555 (2015).
188 Kopf, H., de la Rosa, G. M., Howard, O. M. & Chen, X. Rapamycin inhibits differentiation of Th17 cells and promotes generation of FoxP3+ T regulatory cells. *Int Immunopharmacol* **7**, 1819-1824 (2007).
189 Nagai, S., Kurebayashi, Y. & Koyasu, S. Role of PI3K/Akt and mTOR complexes in Th17 cell differentiation. *Ann N Y Acad Sci* **1280**, 30-34 (2013).

190 Amezcua Vesely, M. C. *et al.* Effector TH17 Cells Give Rise to Long-Lived TRM Cells that Are Essential for an Immediate Response against Bacterial Infection. *Cell* **178**, 1176-1188 e1115 (2019).
191 Haberman, Y. *et al.* Pediatric Crohn disease patients exhibit specific ileal transcriptome and microbiome signature. *J Clin Invest* **124**, 3617-3633 (2014).
192 Allez, M. *et al.* Long term outcome of patients with active Crohn's disease exhibiting extensive and deep ulcerations at colonoscopy. *Am J Gastroenterol* **97**, 947-953 (2002).
193 Ligumsky, M., Simon, P. L., Karmeli, F. & Rachmilewitz, D. Role of interleukin 1 in inflammatory bowel disease--enhanced production during active disease. *Gut* **31**, 686-689 (1990).
194 Bunn, S. K. *et al.* Fecal calprotectin: validation as a noninvasive measure of bowel inflammation in childhood inflammatory bowel disease. *J Pediatr Gastroenterol Nutr* **33**, 14-22 (2001).
195 Feng, T. *et al.* Th17 cells induce colitis and promote Th1 cell responses through IL-17 induction of innate IL-12 and IL-23 production. *J Immunol* **186**, 6313-6318 (2011).
196 Rachitskaya, A. V. *et al.* Cutting edge: NKT cells constitutively express IL-23 receptor and RORgammat and rapidly produce IL-17 upon receptor ligation in an IL-6-independent fashion. *J Immunol* **180**, 5167-5171 (2008).
197 Villanova, F. *et al.* Characterization of innate lymphoid cells in human skin and blood demonstrates increase of NKp44+ ILC3 in psoriasis. *J Invest Dermatol* **134**, 984-991 (2014).
198 Lockhart, E., Green, A. M. & Flynn, J. L. IL-17 production is dominated by gammadelta T cells rather than CD4 T cells during Mycobacterium tuberculosis infection. *J Immunol* **177**, 4662-4669 (2006).
199 Park, H. *et al.* A distinct lineage of CD4 T cells regulates tissue inflammation by producing interleukin 17. *Nat Immunol* **6**, 1133-1141 (2005).
200 Sellon, R. K. *et al.* Resident enteric bacteria are necessary for development of spontaneous colitis and immune system activation in interleukin-10-deficient mice. *Infect Immun* **66**, 5224-5231 (1998).
201 Whibley, N. & Gaffen, S. L. Gut-Busters: IL-17 Ain't Afraid of No IL-23. *Immunity* **43**, 620-622 (2015).
202 O'Connor, W., Jr. *et al.* A protective function for interleukin 17A in T cell-mediated intestinal inflammation. *Nat Immunol* **10**, 603-609 (2009).
203 Targan, S. R. *et al.* A Randomized, Double-Blind, Placebo-Controlled Phase 2 Study of Brodalumab in Patients With Moderate-to-Severe Crohn's Disease. *Am J Gastroenterol* **111**, 1599-1607 (2016).
204 Danese, S. *et al.* Randomised trial and open-label extension study of an anti-interleukin-6 antibody in Crohn's disease (ANDANTE I and II). *Gut* **68**, 40-48 (2019).
205 Sandborn, W. J. *et al.* Efficacy and Safety of Mirikizumab in a Randomized Phase 2 Study of Patients With Ulcerative Colitis. *Gastroenterology* **158**, 537-549.e510 (2020).
206 Withers, D. R. *et al.* Transient inhibition of ROR-γt therapeutically limits intestinal inflammation by reducing TH17 cells and preserving group 3 innate lymphoid cells. *Nature medicine* **22**, 319-323 (2016).
207 Yoshida, H. *et al.* The cis-Regulatory Atlas of the Mouse Immune System. *Cell* **176**, 897-912.e820 (2019).

208 Chapman, N. M. & Chi, H. Hallmarks of T-cell Exit from Quiescence. *Cancer Immunol Res* **6**, 502-508 (2018).
209 Delgoffe, G. M. *et al.* The kinase mTOR regulates the differentiation of helper T cells through the selective activation of signaling by mTORC1 and mTORC2. *Nat Immunol* **12**, 295-303 (2011).
210 Delgoffe, G. M. *et al.* The mTOR kinase differentially regulates effector and regulatory T cell lineage commitment. *Immunity* **30**, 832-844 (2009).
211 Sasaki, C. Y. *et al.* p70S6K1 in the TORC1 pathway is essential for the differentiation of Th17 Cells, but not Th1, Th2, or Treg cells in mice. *Eur J Immunol* **46**, 212-222 (2016).
212 Yang, K., Neale, G., Green, D. R., He, W. & Chi, H. The tumor suppressor Tsc1 enforces quiescence of naive T cells to promote immune homeostasis and function. *Nat Immunol* **12**, 888-897 (2011).
213 Blery, M. *et al.* The paired Ig-like receptor PIR-B is an inhibitory receptor that recruits the protein-tyrosine phosphatase SHP-1. *Proc Natl Acad Sci U S A* **95**, 2446-2451 (1998).
214 Lee, K. M. *et al.* Molecular basis of T cell inactivation by CTLA-4. *Science* **282**, 2263-2266 (1998).
215 Chemnitz, J. M., Parry, R. V., Nichols, K. E., June, C. H. & Riley, J. L. SHP-1 and SHP-2 associate with immunoreceptor tyrosine-based switch motif of programmed death 1 upon primary human T cell stimulation, but only receptor ligation prevents T cell activation. *J Immunol* **173**, 945-954 (2004).
216 Salmond, R. J., Huyer, G., Kotsoni, A., Clements, L. & Alexander, D. R. The src homology 2 domain-containing tyrosine phosphatase 2 regulates primary T-dependent immune responses and Th cell differentiation. *J Immunol* **175**, 6498-6508 (2005).
217 Wang, J. *et al.* Inhibition of SHP2 ameliorates the pathogenesis of systemic lupus erythematosus. *J Clin Invest* **126**, 2077-2092 (2016).
218 Johnnidis, J. B. *et al.* Inhibitory signaling sustains a distinct early memory CD8(+) T cell precursor that is resistant to DNA damage. *Sci Immunol* **6** (2021).
219 Kok, L. *et al.* A committed tissue-resident memory T cell precursor within the circulating CD8+ effector T cell pool. *J Exp Med* **217** (2020).
220 Scheinin, T., Butler, D. M., Salway, F., Scallon, B. & Feldmann, M. Validation of the interleukin-10 knockout mouse model of colitis: antitumour necrosis factor-antibodies suppress the progression of colitis. *Clinical and experimental immunology* **133**, 38-43 (2003).
221 Berg, D. J. *et al.* Enterocolitis and colon cancer in interleukin-10-deficient mice are associated with aberrant cytokine production and CD4(+) TH1-like responses. *The Journal of Clinical Investigation* **98**, 1010-1020 (1996).
222 Finkelman, F., Morris, S., Orekhova, T. & Sehy, D. The in vivo cytokine capture assay for measurement of cytokine production in the mouse. *Curr Protoc Immunol* **Chapter 6**, Unit 6 28 (2003).
223 Kim, K. H. & Sederstrom, J. M. Assaying Cell Cycle Status Using Flow Cytometry. *Curr Protoc Mol Biol* **111**, 28 26 21-28 26 11 (2015).
224 Ge, S. X., Son, E. W. & Yao, R. iDEP: an integrated web application for differential expression and pathway analysis of RNA-Seq data. *BMC Bioinformatics* **19**, 534 (2018).
225 Gentleman, R. C. *et al.* Bioconductor: open software development for computational biology and bioinformatics. *Genome Biol* **5**, R80 (2004).

226 Zenkova D. KV, S. R., Artyomov M., Sergushichev A. Phantasus: visual and interactive gene expression analysis. (2018).
227 Roda, G. *et al.* Crohn's disease. *Nature Reviews Disease Primers* **6**, 22 (2020).
228 de Souza, H. S. P., Fiocchi, C. & Iliopoulos, D. The IBD interactome: an integrated view of aetiology, pathogenesis and therapy. *Nat Rev Gastroenterol Hepatol* **14**, 739-749 (2017).
229 Neurath, M. F. Cytokines in inflammatory bowel disease. *Nat Rev Immunol* **14**, 329-342 (2014).
230 McCole, D. F. IBD candidate genes and intestinal barrier regulation. *Inflammatory bowel diseases* **20**, 1829-1849 (2014).
231 de Lange, K. M. *et al.* Genome-wide association study implicates immune activation of multiple integrin genes in inflammatory bowel disease. *Nat Genet* **49**, 256-261 (2017).
232 Barker, N. & Clevers, H. Leucine-rich repeat-containing G-protein-coupled receptors as markers of adult stem cells. *Gastroenterology* **138**, 1681-1696 (2010).
233 Barker, N. Adult intestinal stem cells: critical drivers of epithelial homeostasis and regeneration. *Nat Rev Mol Cell Biol* **15**, 19-33 (2014).
234 Kameyama, J.-I., Narui, H., Inui, M. & Sato, T. Energy Level in Large Intestinal Mucosa in Patients with Ulcerative Colitis. *The Tohoku Journal of Experimental Medicine* **143**, 253-254 (1984).
235 Roediger, W. E. The colonic epithelium in ulcerative colitis: an energy-deficiency disease? *Lancet* **2**, 712-715 (1980).
236 Heller, S. *et al.* Reduced mitochondrial activity in colonocytes facilitates AMPKα2-dependent inflammation. *FASEB journal : official publication of the Federation of American Societies for Experimental Biology* **31**, 2013-2025 (2017).
237 Delpre, G., Avidor, I., Steinherz, R., Kadish, U. & Ben-Bassat, M. Ultrastructural abnormalities in endoscopically and histologically normal and involved colon in ulcerative colitis. *Am J Gastroenterol* **84**, 1038-1046 (1989).
238 Osman, C., Voelker, D. R. & Langer, T. Making heads or tails of phospholipids in mitochondria. *The Journal of cell biology* **192**, 7-16 (2011).
239 Vance, J. E. Phospholipid synthesis and transport in mammalian cells. *Traffic* **16**, 1-18 (2015).
240 Lev, S. Nonvesicular lipid transfer from the endoplasmic reticulum. *Cold Spring Harbor perspectives in biology* **4** (2012).
241 Alpy, F. & Tomasetto, C. Give lipids a START: the StAR-related lipid transfer (START) domain in mammals. *J Cell Sci* **118**, 2791-2801 (2005).
242 Horibata, Y. & Sugimoto, H. StarD7 mediates the intracellular trafficking of phosphatidylcholine to mitochondria. *J Biol Chem* **285**, 7358-7365 (2010).
243 Horibata, Y. *et al.* Identification of the N-terminal transmembrane domain of StarD7 and its importance for mitochondrial outer membrane localization and phosphatidylcholine transfer. *Sci Rep* **7**, 8793 (2017).
244 Haberman, Y. *et al.* Ulcerative colitis mucosal transcriptomes reveal mitochondriopathy and personalized mechanisms underlying disease severity and treatment response. *Nat Commun* **10**, 38 (2019).
245 Uhlén, M. *et al.* Tissue-based map of the human proteome. *Science* **347**, 1260419 (2015).
246 Smillie, C. S. *et al.* Intra- and Inter-cellular Rewiring of the Human Colon during Ulcerative Colitis. *Cell* **178**, 714-730.e722 (2019).

247 Crakes, K. R. *et al.* PPARα-targeted mitochondrial bioenergetics mediate repair of intestinal barriers at the host–microbe intersection during SIV infection. *Proceedings of the National Academy of Sciences* **116**, 24819-24829 (2019).
248 JanssenDuijghuijsen, L. M. *et al.* Mitochondrial ATP Depletion Disrupts Caco-2 Monolayer Integrity and Internalizes Claudin 7. *Frontiers in Physiology* **8** (2017).
249 Borisova, M. A. *et al.* Mucin-2 knockout is a model of intercellular junction defects, mitochondrial damage and ATP depletion in the intestinal epithelium. *Scientific Reports* **10**, 21135 (2020).
250 Lin, J. *et al.* Transcriptional co-activator PGC-1 alpha drives the formation of slow-twitch muscle fibres. *Nature* **418**, 797-801 (2002).
251 Toyama, E. Q. *et al.* Metabolism. AMP-activated protein kinase mediates mitochondrial fission in response to energy stress. *Science* **351**, 275-281 (2016).
252 Zhang, L., Li, J., Young, L. H. & Caplan, M. J. AMP-activated protein kinase regulates the assembly of epithelial tight junctions. *Proceedings of the National Academy of Sciences* **103**, 17272-17277 (2006).
253 Zheng, B. & Cantley, L. C. Regulation of epithelial tight junction assembly and disassembly by AMP-activated protein kinase. *Proceedings of the National Academy of Sciences* **104**, 819-822 (2007).
254 Berg, D. J. *et al.* Enterocolitis and colon cancer in interleukin-10-deficient mice are associated with aberrant cytokine production and CD4(+) TH1-like responses. *J Clin Invest* **98**, 1010-1020 (1996).
255 Schuler, M.-H., Di Bartolomeo, F., Mårtensson, C. U., Daum, G. & Becker, T. Phosphatidylcholine Affects Inner Membrane Protein Translocases of Mitochondria. *J Biol Chem* **291**, 18718-18729 (2016).
256 Brandt, U. Energy converting NADH:quinone oxidoreductase (complex I). *Annu Rev Biochem* **75**, 69-92 (2006).
257 Sazanov, L. A. A giant molecular proton pump: structure and mechanism of respiratory complex I. *Nature Reviews Molecular Cell Biology* **16**, 375-388 (2015).
258 Cogliati, S., Enriquez, J. A. & Scorrano, L. Mitochondrial Cristae: Where Beauty Meets Functionality. *Trends in Biochemical Sciences* **41**, 261-273 (2016).
259 Pérez, E., Bourguet, W., Gronemeyer, H. & de Lera, A. R. Modulation of RXR function through ligand design. *Biochimica et Biophysica Acta (BBA) - Molecular and Cell Biology of Lipids* **1821**, 57-69 (2012).
260 Bougarne, N. *et al.* Molecular Actions of PPARα in Lipid Metabolism and Inflammation. *Endocrine Reviews* **39**, 760-802 (2018).
261 Levine, T. Short-range intracellular trafficking of small molecules across endoplasmic reticulum junctions. *Trends in Cell Biology* **14**, 483-490 (2004).
262 Giamogante, F., Barazzuol, L., Brini, M. & Calì, T. ER-Mitochondria Contact Sites Reporters: Strengths and Weaknesses of the Available Approaches. *Int J Mol Sci* **21**, 8157 (2020).
263 Zhu, L. *et al.* Claudin Family Participates in the Pathogenesis of Inflammatory Bowel Diseases and Colitis-Associated Colorectal Cancer. *Front Immunol* **10**, 1441-1441 (2019).
264 Prasad, S. *et al.* Inflammatory processes have differential effects on claudins 2, 3 and 4 in colonic epithelial cells. *Lab Invest* **85**, 1139-1162 (2005).

265 Weber, C. R., Nalle, S. C., Tretiakova, M., Rubin, D. T. & Turner, J. R. Claudin-1 and claudin-2 expression is elevated in inflammatory bowel disease and may contribute to early neoplastic transformation. *Lab Invest* **88**, 1110-1120 (2008).
266 Amrouche-Mekkioui, I. & Djerdjouri, B. N-acetylcysteine improves redox status, mitochondrial dysfunction, mucin-depleted crypts and epithelial hyperplasia in dextran sulfate sodium-induced oxidative colitis in mice. *Eur J Pharmacol* **691**, 209-217 (2012).
267 Santhanam, S. *et al.* Mitochondrial electron transport chain complex dysfunction in the colonic mucosa in ulcerative colitis. *Inflammatory bowel diseases* **18**, 2158-2168 (2012).
268 Cunningham, K. E. *et al.* Peroxisome Proliferator-activated Receptor-γ Coactivator 1-α (PGC1α) Protects against Experimental Murine Colitis. *J Biol Chem* **291**, 10184-10200 (2016).
269 Chang, C.-R. & Blackstone, C. Dynamic regulation of mitochondrial fission through modification of the dynamin-related protein Drp1. *Ann N Y Acad Sci* **1201**, 34-39 (2010).
270 Mancini, N. L. *et al.* Perturbed Mitochondrial Dynamics Is a Novel Feature of Colitis That Can Be Targeted to Lessen Disease. *Cellular and Molecular Gastroenterology and Hepatology* **10**, 287-307 (2020).
271 D'Errico, I. *et al.* Peroxisome proliferator-activated receptor-gamma coactivator 1-alpha (PGC1alpha) is a metabolic regulator of intestinal epithelial cell fate. *Proceedings of the National Academy of Sciences of the United States of America* **108**, 6603-6608 (2011).
272 Ehehalt, R. *et al.* Phosphatidylcholine and lysophosphatidylcholine in intestinal mucus of ulcerative colitis patients. A quantitative approach by nanoElectrospray-tandem mass spectrometry. *Scand J Gastroenterol* **39**, 737-742 (2004).
273 Stremmel, W. *et al.* Retarded release phosphatidylcholine benefits patients with chronic active ulcerative colitis. *Gut* **54**, 966-971 (2005).
274 Stremmel, W. *et al.* Delayed release phosphatidylcholine in chronic-active ulcerative colitis: a randomized, double-blinded, dose finding study. *J Clin Gastroenterol* **44**, e101-107 (2010).
275 Violette, M. I., Madan, P. & Watson, A. J. Na+/K+-ATPase regulates tight junction formation and function during mouse preimplantation development. *Developmental Biology* **289**, 406-419 (2006).
276 Rajasekaran, S. A. *et al.* Na,K-ATPase activity is required for formation of tight junctions, desmosomes, and induction of polarity in epithelial cells. *Molecular biology of the cell* **12**, 3717-3732 (2001).
277 Shen, L., Weber, C. R. & Turner, J. R. The tight junction protein complex undergoes rapid and continuous molecular remodeling at steady state. *The Journal of cell biology* **181**, 683-695 (2008).
278 Citi, S. The mechanobiology of tight junctions. *Biophysical reviews* **11**, 783-793 (2019).
279 Otera, H. *et al.* Mff is an essential factor for mitochondrial recruitment of Drp1 during mitochondrial fission in mammalian cells. *The Journal of cell biology* **191**, 1141-1158 (2010).
280 Egan, D. F. *et al.* Phosphorylation of ULK1 (hATG1) by AMP-activated protein kinase connects energy sensing to mitophagy. *Science* **331**, 456-461 (2011).
281 Chen, L. *et al.* Activating AMPK to Restore Tight Junction Assembly in Intestinal Epithelium and to Attenuate Experimental Colitis by Metformin. *Front Pharmacol* **9**, 761 (2018).

282 Deng, J. *et al.* Metformin protects against intestinal barrier dysfunction via AMPKα1-dependent inhibition of JNK signalling activation. *J Cell Mol Med* **22**, 546-557 (2018).
283 Xue, Y., Zhang, H., Sun, X. & Zhu, M.-J. Metformin Improves Ileal Epithelial Barrier Function in Interleukin-10 Deficient Mice. *PloS one* **11**, e0168670-e0168670 (2016).
284 Sun, X., Yang, Q., Rogers, C. J., Du, M. & Zhu, M. J. AMPK improves gut epithelial differentiation and barrier function via regulating Cdx2 expression. *Cell Death Differ* **24**, 819-831 (2017).
285 Yang, L. *et al.* The Phosphatidylcholine Transfer Protein Stard7 is Required for Mitochondrial and Epithelial Cell Homeostasis. *Scientific Reports* **7**, 46416 (2017).
286 McQuin, C. *et al.* CellProfiler 3.0: Next-generation image processing for biology. *PLOS Biology* **16**, e2005970 (2018).
287 Schneider, C. A., Rasband, W. S. & Eliceiri, K. W. NIH Image to ImageJ: 25 years of image analysis. *Nature Methods* **9**, 671-675 (2012).
288 Gentleman, R. C. *et al.* Bioconductor: open software development for computational biology and bioinformatics. *Genome Biology* **5**, R80 (2004).
289 Ivanov, II *et al.* Induction of intestinal Th17 cells by segmented filamentous bacteria. *Cell* **139**, 485-498 (2009).
290 Iwakura, Y., Ishigame, H., Saijo, S. & Nakae, S. Functional specialization of interleukin-17 family members. *Immunity* **34**, 149-162 (2011).
291 Pickert, G. *et al.* STAT3 links IL-22 signaling in intestinal epithelial cells to mucosal wound healing. *J Exp Med* **206**, 1465-1472 (2009).
292 Kleinschek, M. A. *et al.* Circulating and gut-resident human Th17 cells express CD161 and promote intestinal inflammation. *J Exp Med* **206**, 525-534 (2009).
293 Jones, R. G. & Pearce, E. J. MenTORing Immunity: mTOR Signaling in the Development and Function of Tissue-Resident Immune Cells. *Immunity* **46**, 730-742 (2017).
294 Bishu, S. *et al.* CD4+ Tissue-resident Memory T Cells Expand and Are a Major Source of Mucosal Tumour Necrosis Factor α in Active Crohn's Disease. *J Crohns Colitis* **13**, 905-915 (2019).
295 Barkal, A. A. *et al.* Engagement of MHC class I by the inhibitory receptor LILRB1 suppresses macrophages and is a target of cancer immunotherapy. *Nat Immunol* **19**, 76-84 (2018).
296 Chen, H. M. *et al.* Blocking immunoinhibitory receptor LILRB2 reprograms tumor-associated myeloid cells and promotes antitumor immunity. *J Clin Invest* **128**, 5647-5662 (2018).
297 Deng, M. *et al.* LILRB4 signalling in leukaemia cells mediates T cell suppression and tumour infiltration. *Nature* **562**, 605-609 (2018).
298 Wu, G. *et al.* LILRB3 supports acute myeloid leukemia development and regulates T-cell antitumor immune responses through the TRAF2–cFLIP–NF-κB signaling axis. *Nature Cancer* **2**, 1170-1184 (2021).
299 Flores-Martin, J., Rena, V., Angeletti, S., Panzetta-Dutari, G. M. & Genti-Raimondi, S. The Lipid Transfer Protein StarD7: Structure, Function, and Regulation. *Int J Mol Sci* **14**, 6170-6186 (2013).
300 Chen, P.-L. *et al.* Vesicular transport mediates the uptake of cytoplasmic proteins into mitochondria in Drosophila melanogaster. *Nature Communications* **11**, 2592 (2020).

301 Benoist, C., Lanier, L., Merad, M., Mathis, D. & The Immunological Genome, P. Consortium biology in immunology: the perspective from the Immunological Genome Project. *Nature Reviews Immunology* **12**, 734-740 (2012).
302 Hundal, R. S. *et al.* Mechanism by which metformin reduces glucose production in type 2 diabetes. *Diabetes* **49**, 2063-2069 (2000).
303 Hardie, D. G., Ross, F. A. & Hawley, S. A. AMPK: a nutrient and energy sensor that maintains energy homeostasis. *Nature Reviews Molecular Cell Biology* **13**, 251-262 (2012).
304 Kahn, B. B., Alquier, T., Carling, D. & Hardie, D. G. AMP-activated protein kinase: Ancient energy gauge provides clues to modern understanding of metabolism. *Cell Metab* **1**, 15-25 (2005).
305 Ali, F. *et al.* S3194 Metformin: A Therapeutic Adjunct for Patients With Inflammatory Bowel Disease? *Official journal of the American College of Gastroenterology | ACG* **115** (2020).
306 Mick, David U. *et al.* MITRAC Links Mitochondrial Protein Translocation to Respiratory-Chain Assembly and Translational Regulation. *Cell* **151**, 1528-1541 (2012).